AD-784 132

MODEL 301 HLH/ATC (HEAVY LIFT HELICOPTER/ADVANCED TECHNOLOGY COMPONENT) TRANSMISSION NOISE REDUCTION PROGRAM

R. Hartman, et al

Boeing Vertol Company

Prepared for:

Army Air Mobility Research and Development Laboratory

May 1974

EUSTIS DIRECTORATE POSITION STATEMENT

The results of the effort reported herein show that significant noise reductions can be attained through the use of the analytical techniques presented in this report.

This directorate concurs with the conclusions presented herein.

The technical monitor for this effort was Mr. Wayne A. Hudgins, Heavy Lift Helicopter Project Office, Systems Support Division.

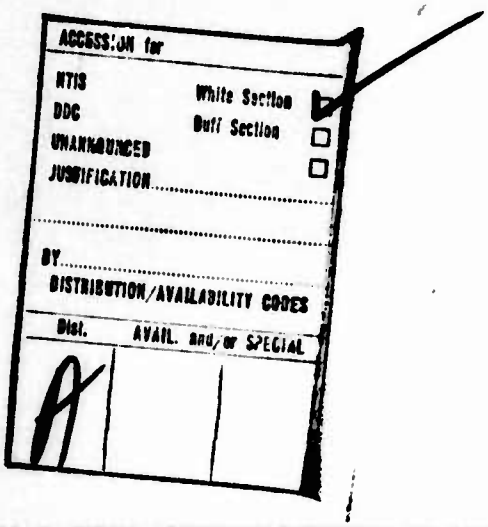

Unclassified

SECURITY CLASSIFICATION OF THIS PAGE (When Data Entered)

REPORT DOCUMENTATION PAGE		READ INSTRUCTIONS BEFORE COMPLETING FORM
1. REPORT NUMBER USAAMRDL-TR-74-58	2. GOVT ACCESSION NO.	3. RECIPIENT'S CATALOG NUMBER AD 784132
4. TITLE (and Subtitle) MODEL 301 HLH/ATC TRANSMISSION NOISE REDUCTION PROGRAM		5. TYPE OF REPORT & PERIOD COVERED Final Report 6. PERFORMING ORG. REPORT NUMBER
7. AUTHOR(s) R. Hartman R. Badgley		8. CONTRACT OR GRANT NUMBER(s) Contract DAAJ01-71-C-0840(P40)
9. PERFORMING ORGANIZATION NAME AND ADDRESS The Boeing Vertol Company Vertol Division - Boeing Center P.O. Box 16858 Philadelphia, Pa. 19142		10. PROGRAM ELEMENT, PROJECT, TASK AREA & WORK UNIT NUMBERS
11. CONTROLLING OFFICE NAME AND ADDRESS U. S. Army Aviation Systems Command P.O. Box 209, Main Office St. Louis, Mo. 63166		12. REPORT DATE May 1974 13. NUMBER OF PAGES 176
14. MONITORING AGENCY NAME & ADDRESS(if different from Controlling Office) Eustis Directorate U. S. Army Air Mobility R&D Laboratory Fort Eustis, Va. 23604		15. SECURITY CLASS. (of this report) Unclassified 15a. DECLASSIFICATION/DOWNGRADING SCHEDULE

16. DISTRIBUTION STATEMENT (of this Report)

Approved for public release; distribution unlimited.

17. DISTRIBUTION STATEMENT (of the abstract entered in Block 20, if different from Report)

18. SUPPLEMENTARY NOTES

19. KEY WORDS (Continue on reverse side if necessary and identify by block number)

Helicopters
Transmissions (Mechanics)
Noise
Noise Reduction
Mechanics
Aircraft Noise

20. ABSTRACT (Continue on reverse side if necessary and identify by block number)

This report presents the results of a transmission noise reduction program performed jointly by the Boeing Vertol Company and Mechanical Technology Incorporated. The emphasis of this program is to reduce transmission noise at its source. The program included a dynamic test of a CH-47C helicopter transmission with internal instrumentation to measure strains, displacements, and accelerations of rotating components and external instrumentation to measure case acceleration and noise levels. Test results were used to

DD FORM 1 JAN 73 1473 EDITION OF 1 NOV 65 IS OBSOLETE

Unclassified

SECURITY CLASSIFICATION OF THIS PAGE (When Data Entered)

Block 20 - continued

verify prediction methodology which in turn was used to analyze the dynamic response of the Heavy Lift Helicopter (HLH) transmission components. All objectives of this program were successfully met. As a result of this program, the HLH should meet its interior noise specification with a quieter transmission with increased reliability. A preliminary design study indicates that the increased weight of the transmission components can be traded off for the reduced weight of the acoustic treatment.

PREFACE

The work reported herein was performed by the Boeing Vertol acoustic staff, in consultation with Dr. Robert Badgley of Mechanical Technology Incorporated, who prepared the section entitled "Predictions and Measurements of Torsional Vibration and Noise Levels". The program was accomplished under the technical cognizance of Mr. Wayne Hudgins of the Eustis Directorate, USAAMRDL staff.

TABLE OF CONTENTS

TABLE OF CONTENTS (Continued)

TABLE OF CONTENTS (continued)

LIST OF ILLUSTRATIONS

LIST OF ILLUSTRATIONS (continued)

LIST OF ILLUSTRATIONS (continued)

LIST OF ILLUSTRATIONS (Continued)

LIST OF TABLES

INTRODUCTION

The internal noise levels for military helicopter crew and cabin areas are specified in MIL-A-8806. The major contributor to the ambient noise level in these areas is the structure-borne and airborne noise generated by the helicopter transmissions, and significant acoustical treatment is required in order to meet the Mil Spec requirements. Today's operational aircraft employ noise control techniques which include one or more of several concepts including skin damping and limp material blanketing to reduce fuselage radiated or structure-borne noise, and high-density rigid sound barriers or source enclosures to reduce the airborne noise. Reduction of the airborne noise by the use of enclosures is considered to be effective, but the actual noise attenuation that can be achieved is dependent upon the completeness of the enclosure or, in the other sense, the lack of completeness due to seams, access doors, and perimeter joints. Consequently, the noise reduction limitation in the speech frequency range with typical acoustical enclosures and seals is about 25 dB, with up to 35 dB obtainable through use of improved seal configurations.[1,2] Further reductions in noise level up to 50 to 60 dB can be achieved with fume-tight enclosures, such as employed in some commercial helicopters and in some commercial transport aircraft engine installations operating today. To date, fume-type enclosures have not been employed on military helicopters since the noise levels of even the largest transmissions in service today can be reduced to Mil Spec levels without the complexity and weight penalty associated with fume-tight enclosures. However, with the advent of the Heavy Lift Helicopter, whose transmission rating is greater than any of today's operational helicopter transmissions, a reduction of over 50 dB in the speech range at the most critical crew area location may be required, necessitating a fume-type enclosure or new concepts in noise reduction.

---

[1] H. Sternfeld, R. H. Spencer, and E. G. Schaeffer, STUDY TO ESTABLISH REALISTIC ACOUSTIC DESIGN CRITERIA FOR FUTURE ARMY AIRCRAFT, Vertol Division, The Boeing Company, TREC TR 61-72, U. S. Army Transportation Research Command, Fort Eustis, Virginia, June 1961.

[2] H. Sternfeld, J. Schairer, and R. Spencer, AN INVESTIGATION OF HELICOPTER TRANSMISSION NOISE REDUCTION BY VIBRATION ABSORBERS AND DAMPING, Vertol Division, The Boeing Company, USAAMRDL TR 72-34, U. S. Army Air Mobility Research and Development Laboratory, Fort Eustis, Virginia, August 1972.

Two new approaches in helicopter transmission noise control aimed at reducing acoustical energy at the source are being investigated in the Heavy Lift Helicopter Advanced Technology Component Development Program. These approaches are:

1) Reduce transmission case vibrations by coating with attenuation material.

2) Reduce transmission gear shaft deflections at the bearings and avoid resonances by control of dynamic response through stiffness, mass, and inertia distribution.

Tests of coating materials applicable to transmission case damping have been conducted.[3] Gear shaft deflections and their effect on case deflections and noise production are the subject of an analysis and test program reported herein.

Controlling the dynamic response of the transmission is a desirable approach to noise reduction since reducing deflections at the bearings and avoiding resonances also inherently increase bearing lives and improve transmission reliability. To this end, both Mechanical Technology Incorporated (M.T.I.) of Latham, New York, and Boeing-Vertol have developed methodologies for analyzing the dynamic response of the internal shafting and ring gear.

The noise-producing mechanism has been investigated by Dr. Robert Badgley of M.T.I. under contracts funded by USAAMRDL.[4,5] The hypothesis offered by Dr. Badgley is that noise is generated by the transmission case as a result of nonuniform transfer of torque from pinion to gear due to tooth profile errors or to

---

[3]E. G. Schaeffer and E. Shadburn, TEST RESULTS REPORT - HLH/ATC EVALUATION OF TRANSMISSION NOISE ATTENUATION MATERIALS, The Boeing Company, Vertol Division, Report T301-10176-1, December 1972.

[4]R. H. Badgley and I. Laskin, PROGRAM FOR HELICOPTER GEARBOX NOISE PREDICTION AND REDUCTION, Mechanical Technology Incorporated, USAAVLABS TR 70-12, U. S. Army Aviation Materiel Laboratories, Fort Eustis, Virginia, March 1970, AD 869 822.

[5]R. H. Badgley and T. Chiang, INVESTIGATION OF GEARBOX DESIGN MODIFICATIONS FOR REDUCING HELICOPTER GEARBOX NOISE, Mechanical Technology Incorporated, USAAMRDL TR 72-6, U. S. Army Air Mobility Research and Development Laboratory, Fort Eustis, Virginia, March 1972.

the elastic deformation of gear teeth under load. This non-uniform transfer of torque produces a dynamic force at the gear mesh frequency, and its multiples, resulting in a coupled torsion/lateral vibration response of the gear shaft. The lateral vibration (or bending) produces displacements at the bearings which in turn cause the case to vibrate, thus producing noise. This noise-producing mechanism is diagrammed in Figure 1.

Since neither the M.T.I. nor the Vertol analysis had been experimentally verified, a dynamic test of a CH-47C forward transmission was conducted in the Boeing-Vertol closed-loop test stand[6] to provide test data for correlation. The transmission was instrumented internally to measure strains, displacements, and accelerations of rotating components, and externally to measure case acceleration and noise levels. This data was successfully obtained and correlated with predicted results.

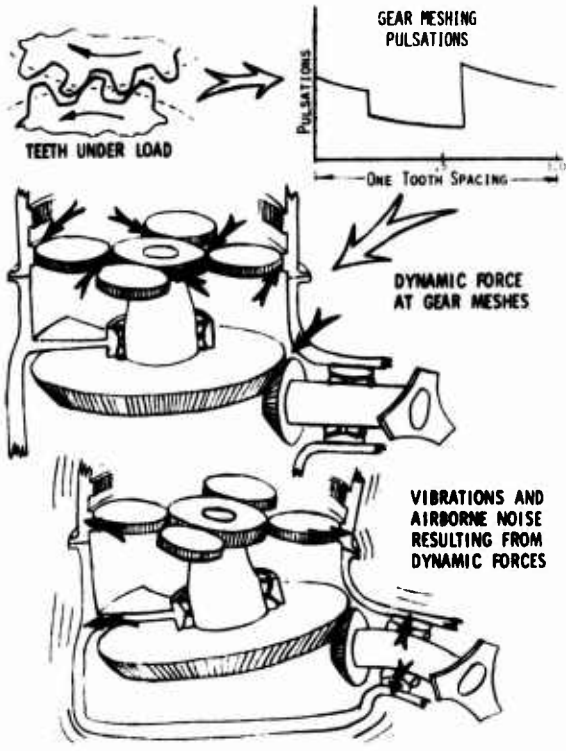

Figure 1. Source of Transmission Noise.

As a result of this test program, the mechanism of noise generation has been experimentally verified. Figure 2 traces the propagation of the first-stage sun gear mesh frequency (sun frequency) torsional excitation through the transmission to the microphone, and Figure 3 traces the bevel gear mesh frequency (bevel frequency) torsional excitation. The dynamic torsion and bending response are seen in Figure 4. The dynamic bending is seen superimposed on the one/rev steady bending. The number of peaks per revolution confirms that the response is at the gear mesh frequency.

With the successful correlation of the analytical programs, a usable design tool has been developed. A simplified flow chart of this design tool is seen in Figure 5. The M.T.I.

---

[6]H. Sternfeld, TEST PLAN - MODEL 301 HLH/ATC TRANSMISSION NOISE REDUCTION PROGRAM, The Boeing Company, Vertol Division Report D301-10091-1, January 1972.

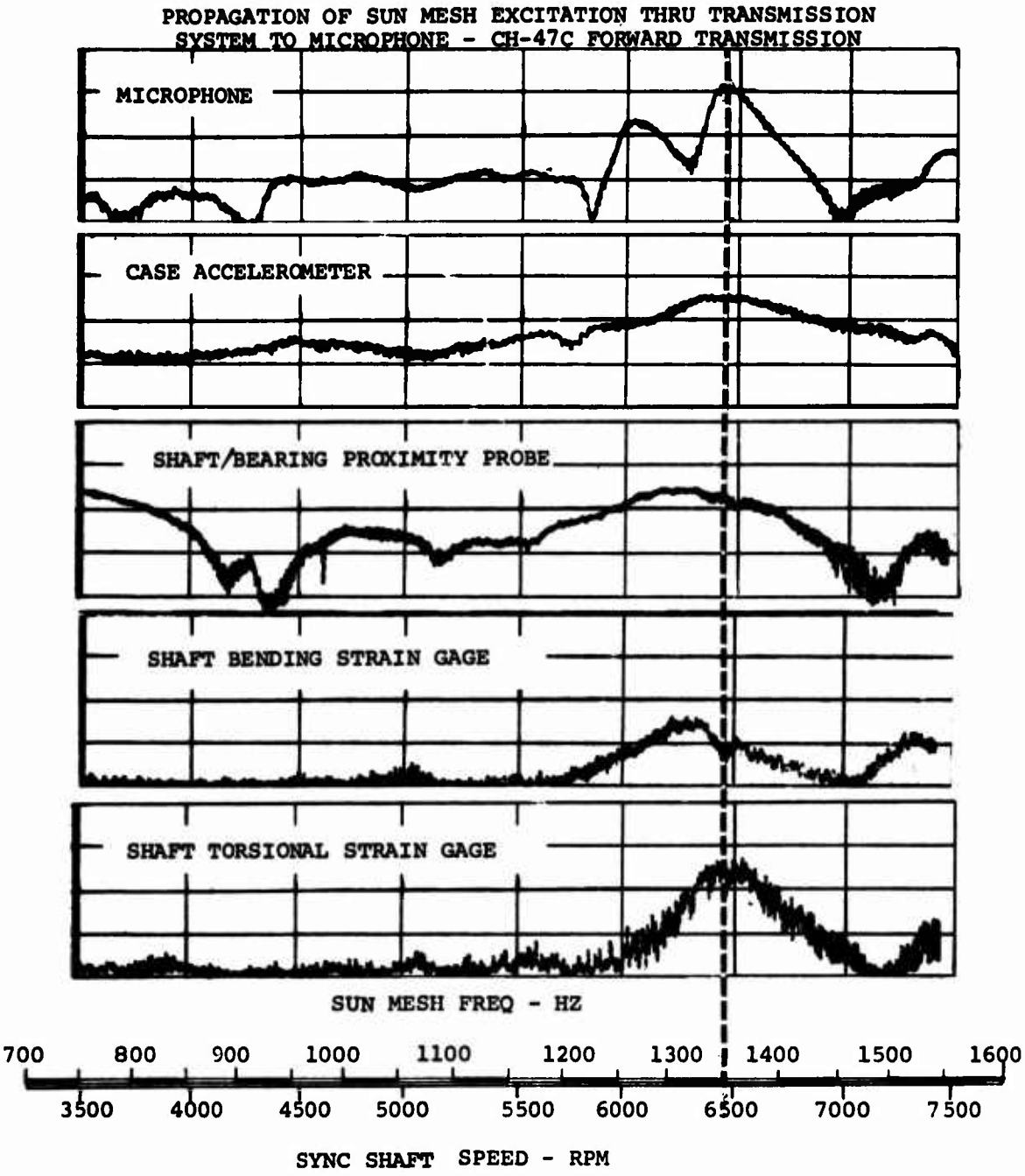

Figure 2. Propagation of Sun Mesh Excitation.

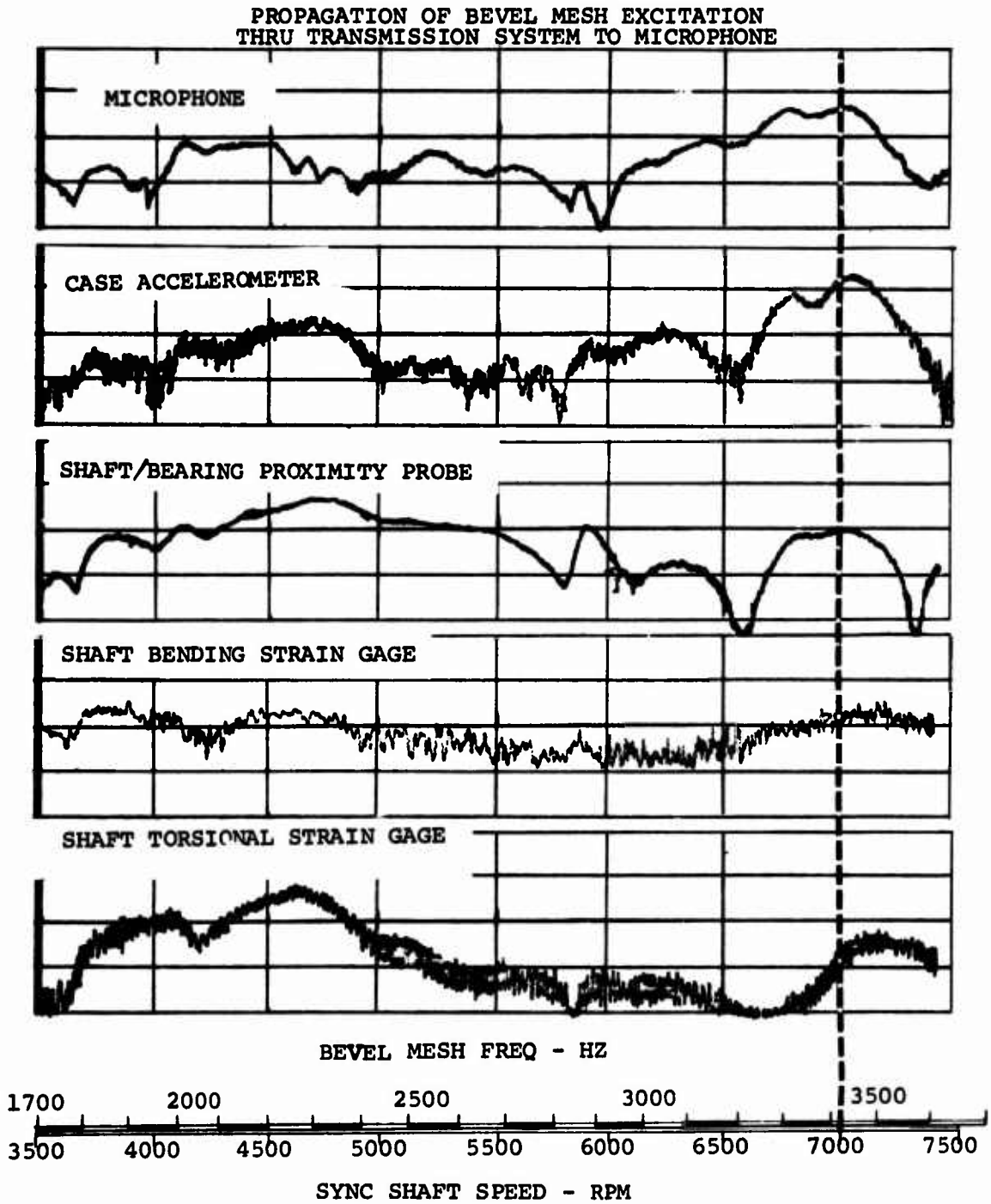

Figure 3. Propagation of Bevel Mesh Excitation.

PARTIAL WAVEFORM OF
TORSIONAL GAGE ON SPIRAL
BEVEL/SUN GEAR SHAFT

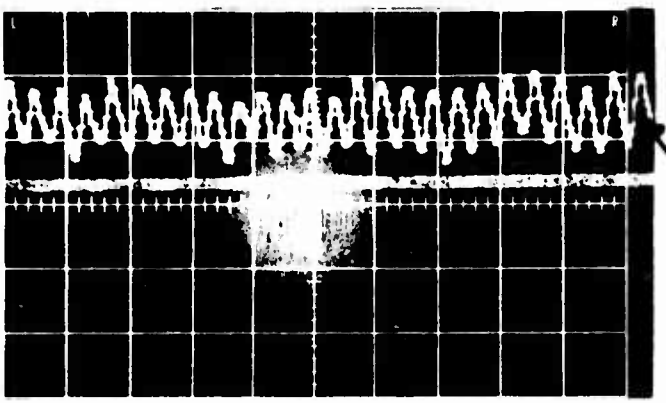

DYNAMIC MOMENT AT
BEVEL MESH FREQUENCY
SUPERIMPOSED ON
STEADY TORSION

PARTIAL WAVEFORM OF
BENDING GAGE ON SPIRAL
BEVEL/SUN GEAR SHAFT

ONE HALF REV

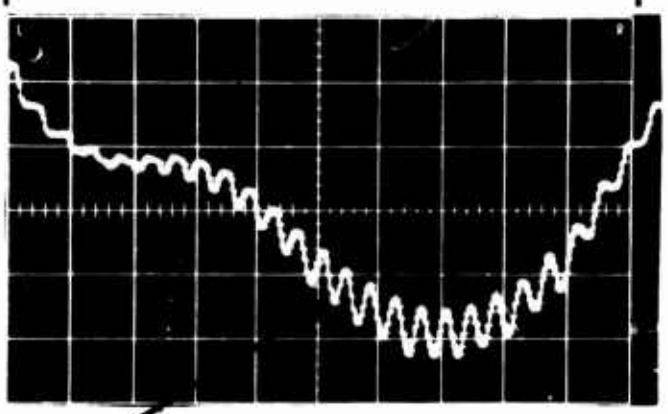

DYNAMIC FORCE AT BEVEL MESH FREQUENCY SUPERIMPOSED ON STEADY ONE PER REV BENDING FORCE. (25.5 PEAKS/ .5 REV = 51 TEETH OF BEVEL GEAR)

Figure 4. Demonstration of Dynamic Tooth Mesh Excitation.

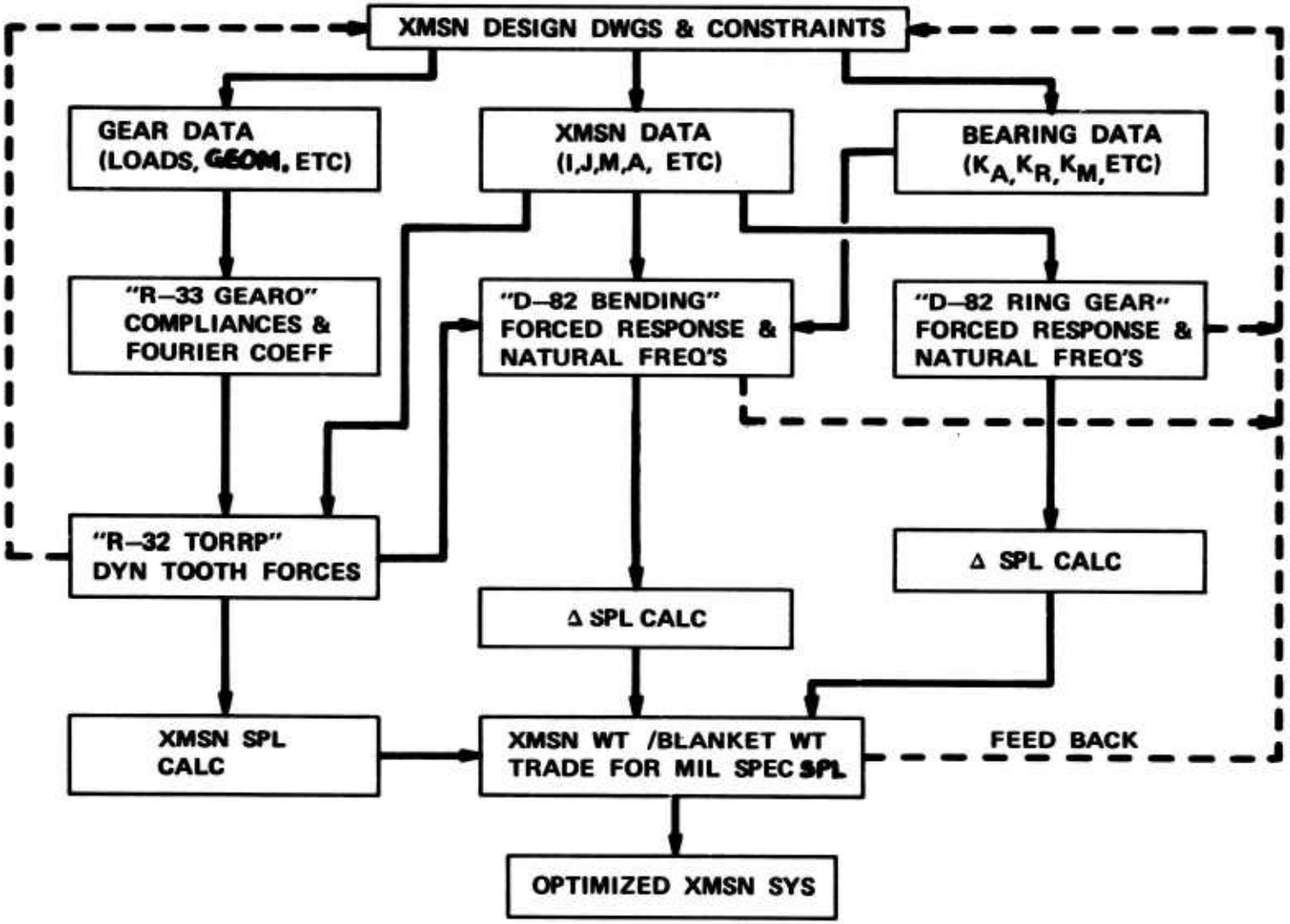

Figure 5. Flow Chart, Transmission Noise Reduction Methodology.

computer programs (GEARO and TORRP) are used to predict the gear mesh compliance, excitation amplitude, dynamic tooth forces and the sound pressure level (SPL) of the transmission. The Boeing-Vertol ring gear analysis and shaft bending analysis (D-82) are used to analyze the damped force response (DFR) of the transmission components and to perform parametric studies leading to design modifications of the gear shafts and ring gear.

An application of this design tool to the HLH transmission is shown in Figure 6. Here the improved damped force response (resulting from the change in internal diameter) of the HLH bevel gear, responding to the sun mesh frequency, is shown compared to the damped force response of the baseline gear shaft. The reduced displacements at the bearings, in addition to the improved ring gear response, are predicted to result in a total noise level reduction of 17 dB at the critical bevel mesh frequency. Another 10 dB reduction is predicted from transmission case coatings based on the results of Reference 3. This means that only a 27-dB reduction would be required from an acoustical enclosure to achieve a predicted 54-dB reduction required at the bevel mesh frequency in the

Heavy Lift Helicopter crew area (refer to Figure 63). This reduction is attainable without a fume-tight acoustical enclosure. Preliminary weight studies comparing the combined weight of the modification and acoustic treatment with the total weight of a fume-tight enclosure suggest that a lower weight penalty is associated with the modifications. In addition, the reduced transmission shaft deflection will result in increased bearing life, and the use of a nonfume-tight enclosure reduces complexity and minimizes maintenance requirements.

The modified gear shafts and ring gear will be manufactured as part of the HLH/ATC Program in addition to the baseline gear shafts and ring gear. This will provide experimental validation of the effect of the design modifications and external noise, and form the basis for definition of the acoustical treatment for the HLH.

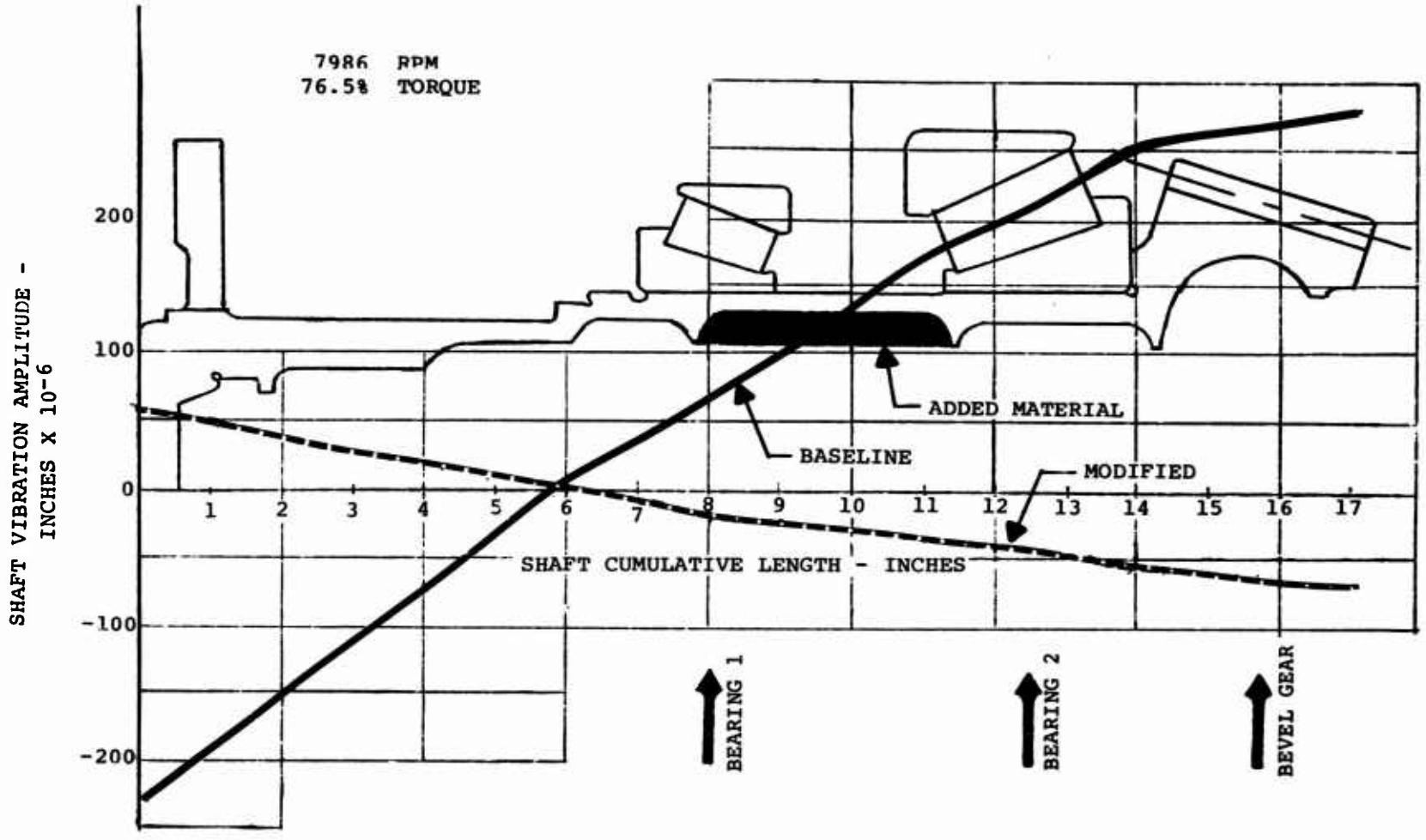

Figure 6. Effect of Modification on HLH Bevel Gear Response to Sun Frequency.

TEST OBJECTIVE

The primary objective of the noise reduction program for the HLH/ATC was to experimentally verify existing computer programs for the prediction of noise-related transmission component high-frequency vibration characteristics, thereby providing a method of designing noise-reducing features into the HLH drive system to aid in providing an environment not exceeding limits of MIL-A-8806A, Tables 1, 2, and 4.

This objective was successfully accomplished, and in the course of so doing, a large data base has been established for future reference.

GENERAL DISCUSSION

Prior to the analysis of the test results, a general discussion of helicopter transmissions, gears, shafts, bearings, housings, and dynamic response of components may provide insight into the mechanics and dynamics of this highly complex dynamic system.

Transmission and Components

Transmission - On large tandem helicopters such as the CH-47 and the HLH, the drive system typically has three primary transmissions:

Forward transmission
Combiner transmission (or mix box)
Aft transmission

Due to the location of the forward transmission, it usually sets the interior noise levels in the cockpit, crew chief, and cabin areas. A CH-47C forward transmission is shown in Figure 7. This transmission is similar in essentials to transmissions in many other helicopters, including that designed for the HLH. As a result, most of the following discussion is applicable for other helicopter transmissions in addition to Boeing Vertol transmissions.

Gear Geometry and Load Sharing - Gears are used to transmit motion and power at constant angular velocity. However, the elastic bending of the gear teeth under load and, in addition, errors in tooth profile and spacing result in short periods of nonuniform motion which superimposes an incremental dynamic or vibrating load on the transmitted load at the gear mesh frequency. These dynamic forces have been identified as the excitation force which ultimately vibrates the case, thereby producing noise.

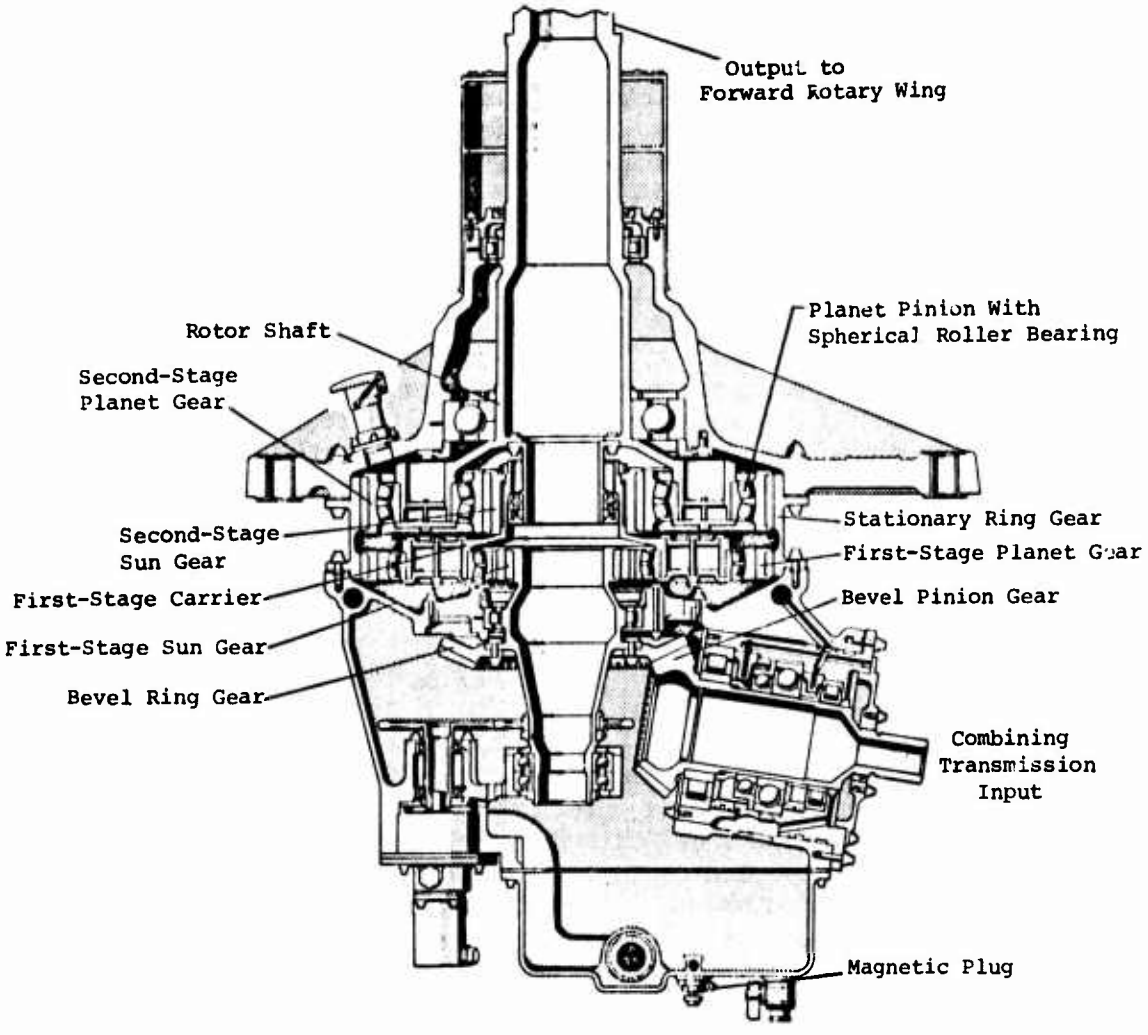

Figure 7. CH-47 Forward Transmission.

The load sharing of spur gear teeth during the cycle-of-engagement is dependent upon the contact ratio (M_p). Gears with a contact ratio between 1.0 and 2.0 share the load among two pairs of teeth during the entrance and exit phases of the cycle-of-engagement, while only one pair of teeth carries all the load during the remaining phase. As the contact ratio approaches 2.0, the one-pair load sharing zone is reduced with an accompanying increase in the two-pair load-sharing zone. For high-contact-ratio tooth designs ($M_p > 2$), such as used in the planet stages of the HLH transmission, the maximum tooth load occurs at a position in the immediate vicinity of the pitch circle where three pairs of teeth all share a portion of the transmitted load.[7] The meshing of a pair of high-contact-ratio gears is seen in Figure 8. By contrast, for contact ratios under 2, the maximum tooth load occurs high up on the tooth at the position of high single-tooth contact where only one pair of teeth is carrying all the load (see Figure 9).

The forward and aft transmissions of the HLH/ATC incorporate high-contact gearing in the planet stages. The involute profile of the gear tooth has been modified to reduce dynamic loads.

A pulsation curve, calculated by M.T.I., for a low-contact-ratio gear mesh is shown in Figure 10a. An estimate of a corresponding curve for a high-contact gear mesh is shown in Figure 10b. The pulsation curve for the low-contact-ratio gear mesh demonstrates the rapid buildup of load as one tooth picks up the load formerly shared by two teeth. The pulsation curve for the high-contact gear mesh shows the load being shared by either two or three teeth, with the maximum load being shared among three teeth. This results in a reduced pulse amplitude for the high-contact gear mesh.

Shafts - Shafts behave much like a beam supported by springs (i.e., the bearings on which they are supported). As such, the shafts have natural rigid bending and torsional modes which will respond when excited at their critical frequencies.

The primary shafts of interest with respect to transmission noise are the spiral bevel pinion shaft (bevel gear) and the spiral bevel/sun gear shaft (sun gear), as these shafts are supported by the case. These shafts were shown in Figure 7 for the CH-47C forward transmission.

---

[7] J. Alberti and A. Lemanski, INVESTIGATION OF INCREASED LOAD CAPACITY OF SPUR AND HELICAL GEARS WITH INCREASED CONTACT RATIO, The Boeing Company, Vertol Division, Report D210-10190-1, October 1970.

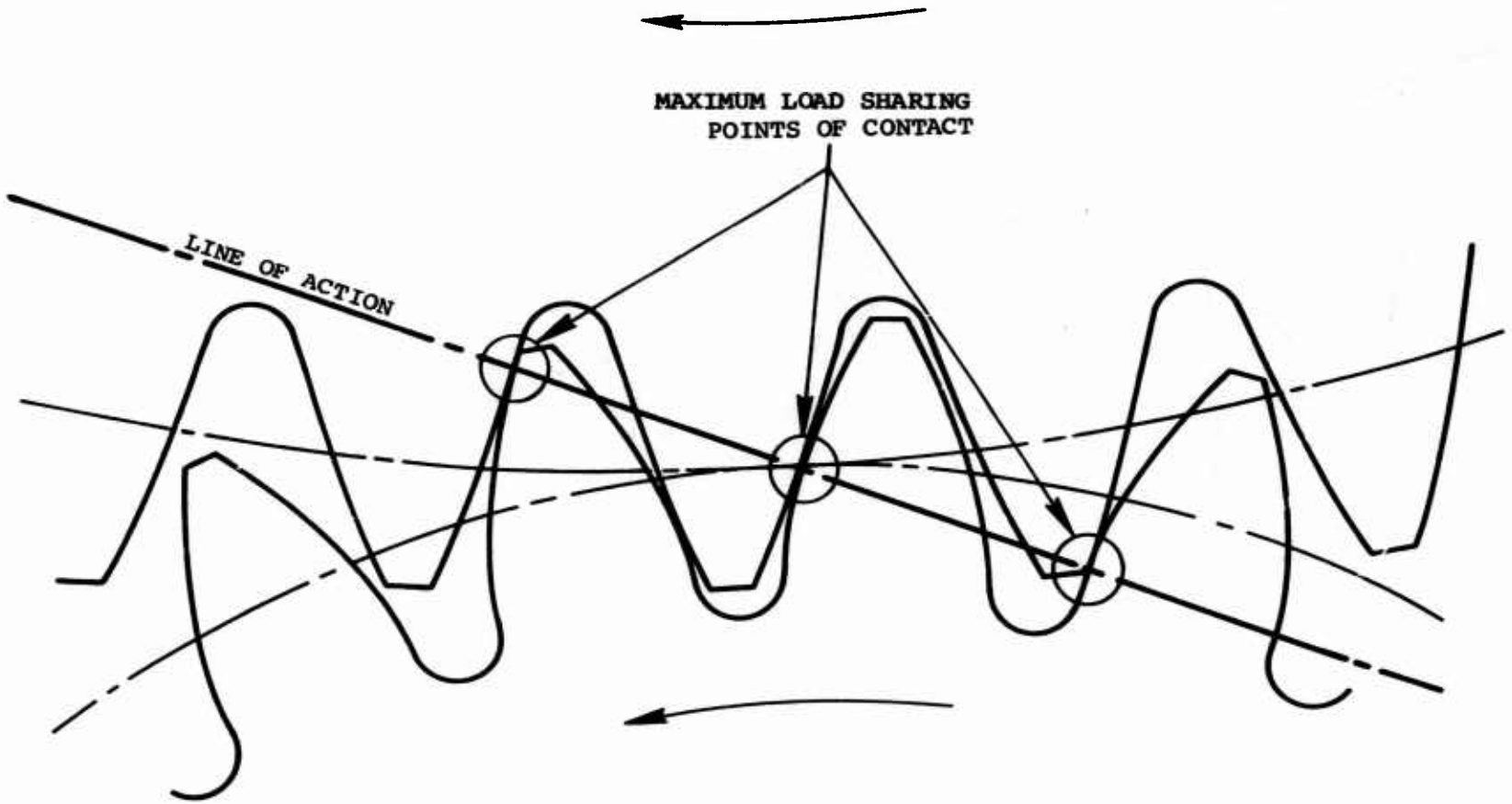

Figure 8. High-Contact-Ratio Gears.

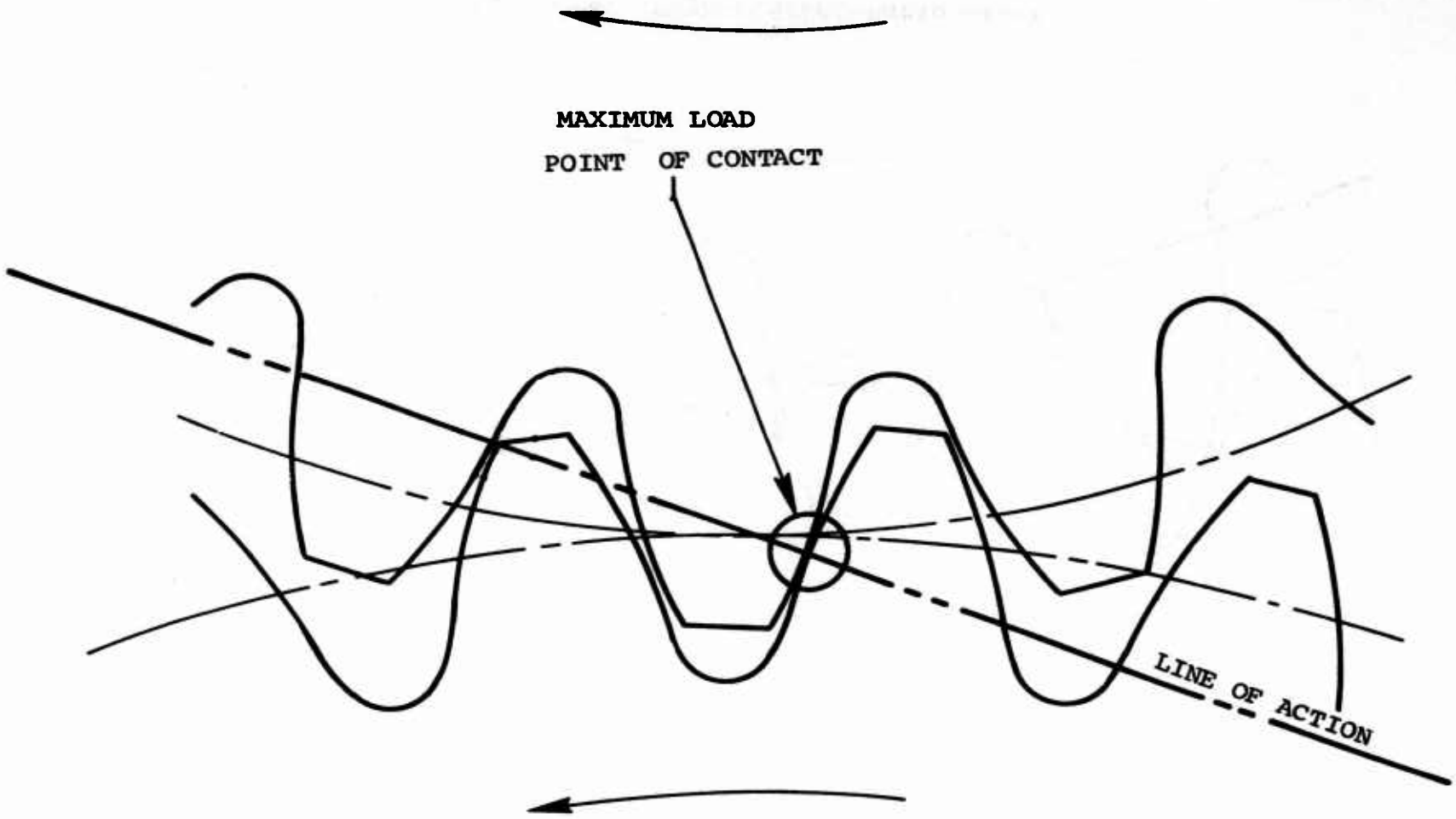

Figure 9. Standard Involute Gears.

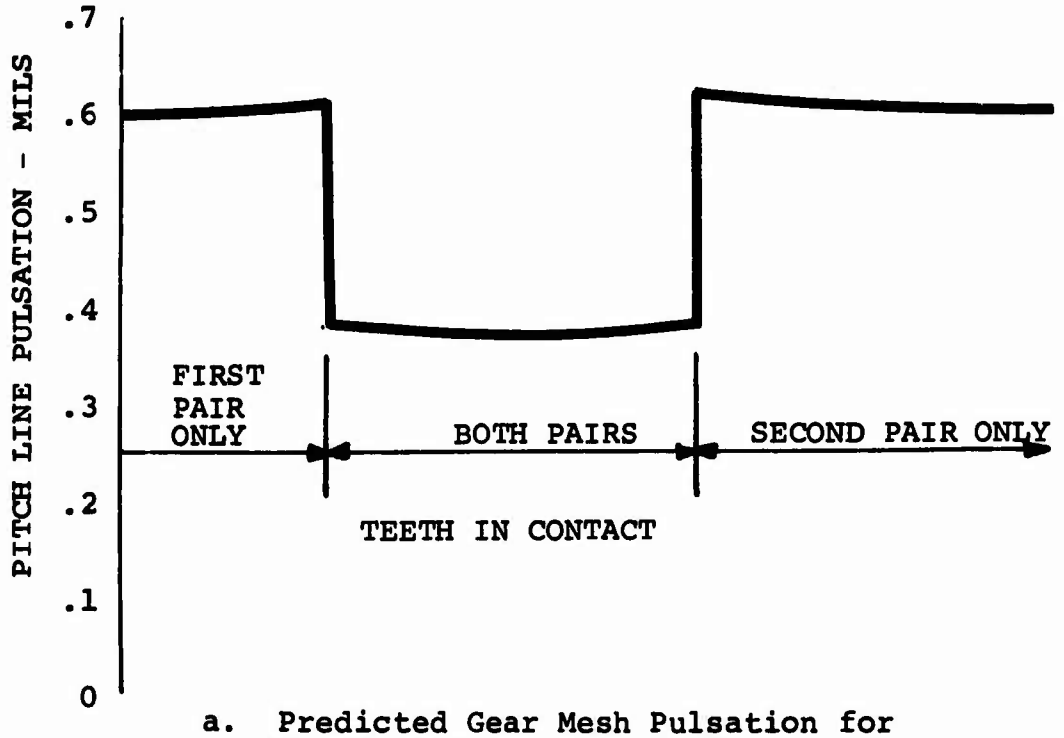

a. Predicted Gear Mesh Pulsation for Standard-Contact-Ratio Gear

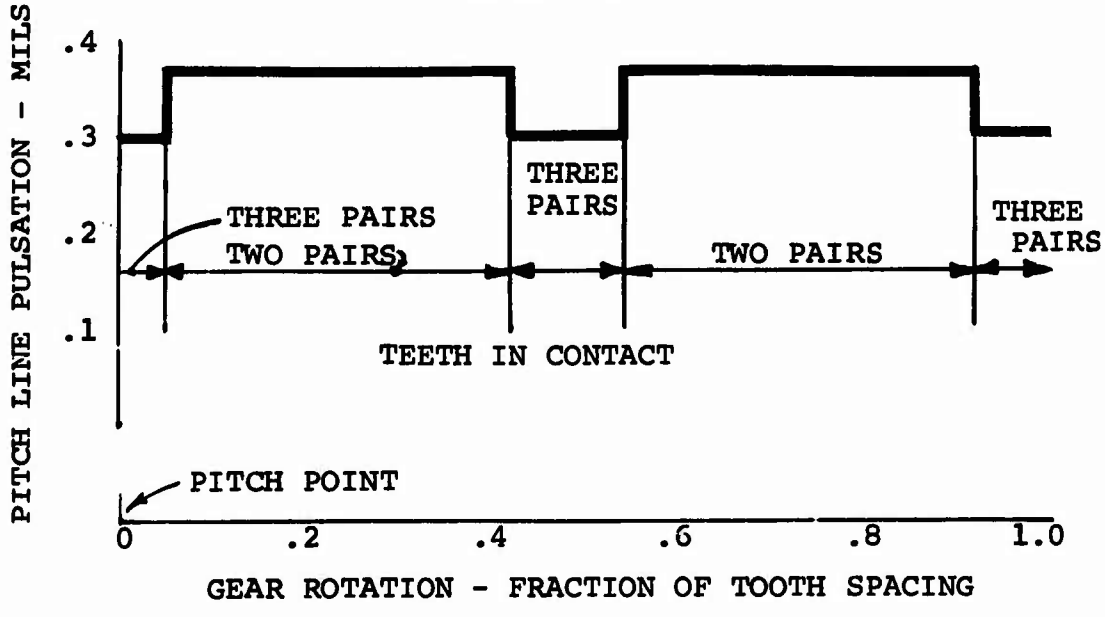

b. Estimated Equivalent Gear Mesh Pulsation for High-Contact-Ratio Gear

Figure 10. Gear Mesh Pulsation Curves.

Bearings - In supporting shafts, bearings must react the steady and dynamic loads generated by the gears. Since any load supported by a bearing must be transmitted through the roller elements, the contact with the races necessarily takes place over a very small surface area. The roller elements, being elastic, deform and allow relative radial motion between inner and outer races. As the roller element deforms, more contact area is provided due to the round shape of the element. Therefore, these deformations are nonlinear. In this way a bearing may be considered as a nonlinear spring support. However, the change in displacements due to the dynamic loads is usually small compared to the steady loads. This allows us to consider the bearing stiffness as linear about the mean steady load stiffness. Consider a bearing supporting a shaft; a steady load results from the transfer of torque from pinion to gear. This load results in the shaft centerline being displaced from the centerline of the outer race of the bearing. As a result of this displacement, the bearing stiffness is increased in the direction of displacement relative to the stiffness at right angles to the displacement. Therefore, the bearing stiffness is not symmetrical. Thus, when bearings are modeled as a pair of linear springs, the spring in the direction of the load is stiffer than the spring at right angles to it. This is one way in which torque affects the dynamic response of the shafts. As the torque is increased, the tangential tooth load is increased, which displaces the shaft centerline and changes the effective stiffness of the bearings.

Transmission Housings - Helicopter transmission housings are cast or forged of magnesium or aluminum. The case performs the primary functions of providing structural support for bearings, transmitting loads from the rotor shaft to the airframe, retaining lubricants within the transmission, and sealing critical transmission components from the environment.

Essentially, the external housing of the transmission consists of four separate sections: the upper support housing, the ring gear, the midsection or case, and the sump. All of these sections vibrate under all operating conditions and produce audible sound. The ring gear casing has been determined to be a very effective noise generator. Because of this, considerable interest has been generated in predicting its dynamic response. The symmetrical design of the ring gear makes it easier to analyze than the other parts of the housing. Due to the complex geometry of the other case components, no analytical investigation of these parts has

been undertaken. However, a finite element approach to computer modeling of these components could lead to a design configuration which will minimize the radiated noise.

In the absence of an analytical approach, an effective and more practical approach to reducing the case radiated noise has been the application of damping materials to the case. This is the topic of another study reported in Reference 3.

Dynamic Response

Dynamic Response of Shafts - As mentioned in the section entitled "Shafts", shafts supported by bearings behave much like beams supported by springs. The dynamic tooth forces generated by the gear mesh frequencies will excite this system. Should there be a critical shaft frequency near the gear mesh frequency, the resulting shaft response can become quite large. The amplitude is limited by the damping present in the system. If this forced response (or mode shape) has large displacements at the bearing locations, these displacements will propagate through the bearings, forcing the transmission case to vibrate. The case vibration (at the mesh frequencies) produces the audible sound.

There are two items which should be considered here: one is that not all critical frequencies will result in high noise levels (if, for example, all the bearings were located at nodes, there would be no excitation propagated across the bearings to the case); second, operation of the shaft between critical frequencies does not insure that the transmission will be quiet. The neighboring critical frequencies (higher and lower) will be excited with possibly undesirable mode shapes. Therefore, avoiding resonances, although desirable from a reliability point of view, does not necessarily result in minimum noise transmission.

What is important in regard to noise reduction is the reduction of displacements at the bearing locations. This can be done in several ways:

1. Relocate the bearings
2. Change shaft stiffness distribution
3. Change shaft mass distribution
4. Change bearing stiffness
5. Reduce dynamic tooth forces

All of the above are rather straightforward design changes and can be incorporated into the design. However, bearing size, internal geometry and location are influenced by other considerations. This tends to restrict outside diameters

of shafts and thereby limits practical design changes to varying inside diameters to change mass and stiffness distributions. Experience with this program has indicated that considerable power over the forced response can be achieved by varying the mass distribution. This will be discussed in more detail later in this report.

Reduction in tooth force is approached in several ways. Since dynamic tooth forces are associated with the transmission system torsional response, avoidance of a system torsional resonance will greatly reduce these forces. System torsional resonances are associated with gear tooth compliances. That is, the gear teeth behave somewhat as springs in a dynamic system. Since the elastic compliance is a function of tooth thickness, which in turn is a function of contact ratio, these resonances can sometimes be shifted by varying the contact ratio. Because of this, high contact ratios are not necessarily better than low contact ratios with regard to noise. Although the high contact ratios reduce the pulse amplitude, if this ratio places the operating condition near a system torsional resonance, the results could be very detrimental.

A second approach is to modify the involute profile of the tooth. If the tooth can be modified to produce true conjugate action under load, the dynamic excitation will be eliminated and only steady bending will remain. Complete elimination is not practical due to machining errors, tooth spacing errors, runout, and varying load levels.

Thirdly, if a system torsional resonance is determined to be related to a critical torsional mode of one of the gear shafts, a stiffness or inertia change to that shaft could result in shifting this resonance away from the operating condition.

Dynamic Response of Transmission System - In actual transmissions, the dynamic response of the shafts is highly complex. The dynamic system torsional excitations induce a coupled bending response in the shafts. This coupled torsion/bending response is coupled from gear shaft to gear shaft. The planet gears of the lower stage planetary system further complicate the system by restricting the motion of the sun gear.

Finally, there are several gear mesh frequencies present in the system, and response to all these frequencies must be analyzed. Without the aid of a computer, an analysis of such a dynamic system would not be possible. But, having the computer as a design tool, this system has been success-

fully modeled. As a result of this program, a method has been developed which should be of considerable value in controlling transmission noise at its source.

DESCRIPTION OF TEST PROGRAM

The following test program was performed in order to obtain experimental data required to verify or modify existing transmission noise reduction methodologies.

Test Setup

Transmission - The transmission used in this program was a CH-47C forward rotor transmission (shown in Figure 7). This transmission is very similar in essentials to the HLH transmission.

Test Stand - The transmission was run in the Boeing Vertol closed-loop test stand (see Figure 11). This stand employs four components to close the torque loop. First, a set of helical gears increases the output or rotor shaft speed to input or synchronization shaft speed. A torque device connects this gear shaft to a bevel gearbox. The bevel gearbox closes the loop to the input shaft of the transmission and also connects to a variable speed clutch and an electric motor which drives the system. This closed-loop test stand provides the capability of running a transmission over its full design torque and speed range under controlled conditions.

Acoustic Enclosure - The transmission test stand was equipped with an acoustic enclosure to allow for the partitioningg of the transmission into separate zones, as well as to minimize noise reflected from the test cell walls. With this enclosure it was possible to isolate the sump, case, and the ring gear and upper cover. This enclosure is shown in Figure 12 with the installed partitions for each test indicated in the table. The acoustic blanketing used for the enclosure was 1-inch lined Soundmat LF-1 (foam-lead-foam). The inside was lined with neoprene-coated nylon and the outside with vinyl-coated glass cloth.

Shaker Installation - To allow for frequency sweeps of the nonrotating transmission, a 50-pound M.B. Electronics shaker (Model PM-50) was connected to the sync shaft via an arm attached to the Thomas coupling. The frequency was controlled by a B&K oscillator (Type 1024) which provided a constant shaking force throughout the frequency range. A photograph of the shaker installation and the compressor is seen in Figure 13.

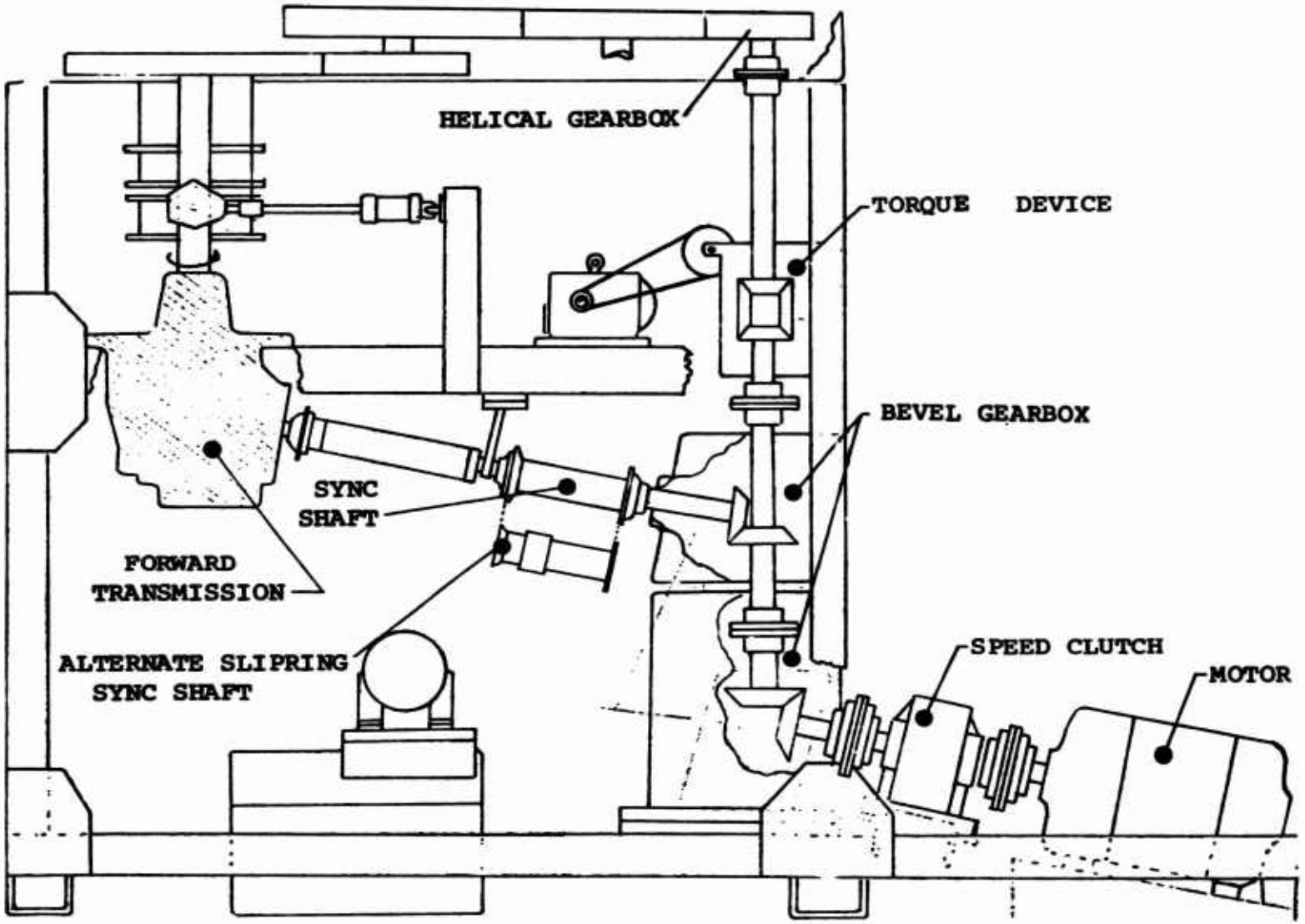

Figure 11. Closed-Loop Test Stand.

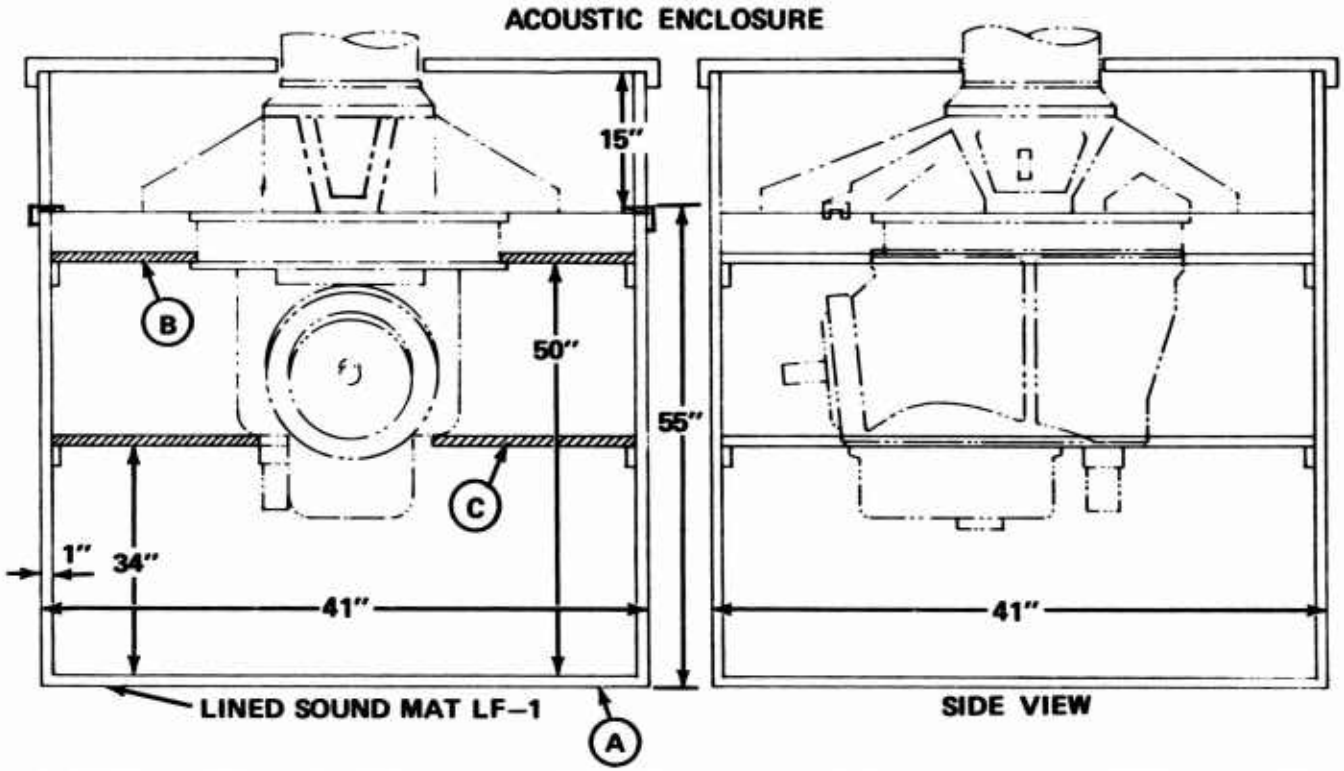

ENCLOSURE NO.	CONFIGURATION
NONE	NO ENCLOSURES USED
1	A, OUTSIDE ENCLOSURE ONLY
2	A + B, OUTSIDE ENCLOSURE WITH PANEL B ADDED
3	A + B + C, OUTSIDE ENCLOSURE WITH PANELS B & C ADDED

Figure 12. Acoustic Enclosure.

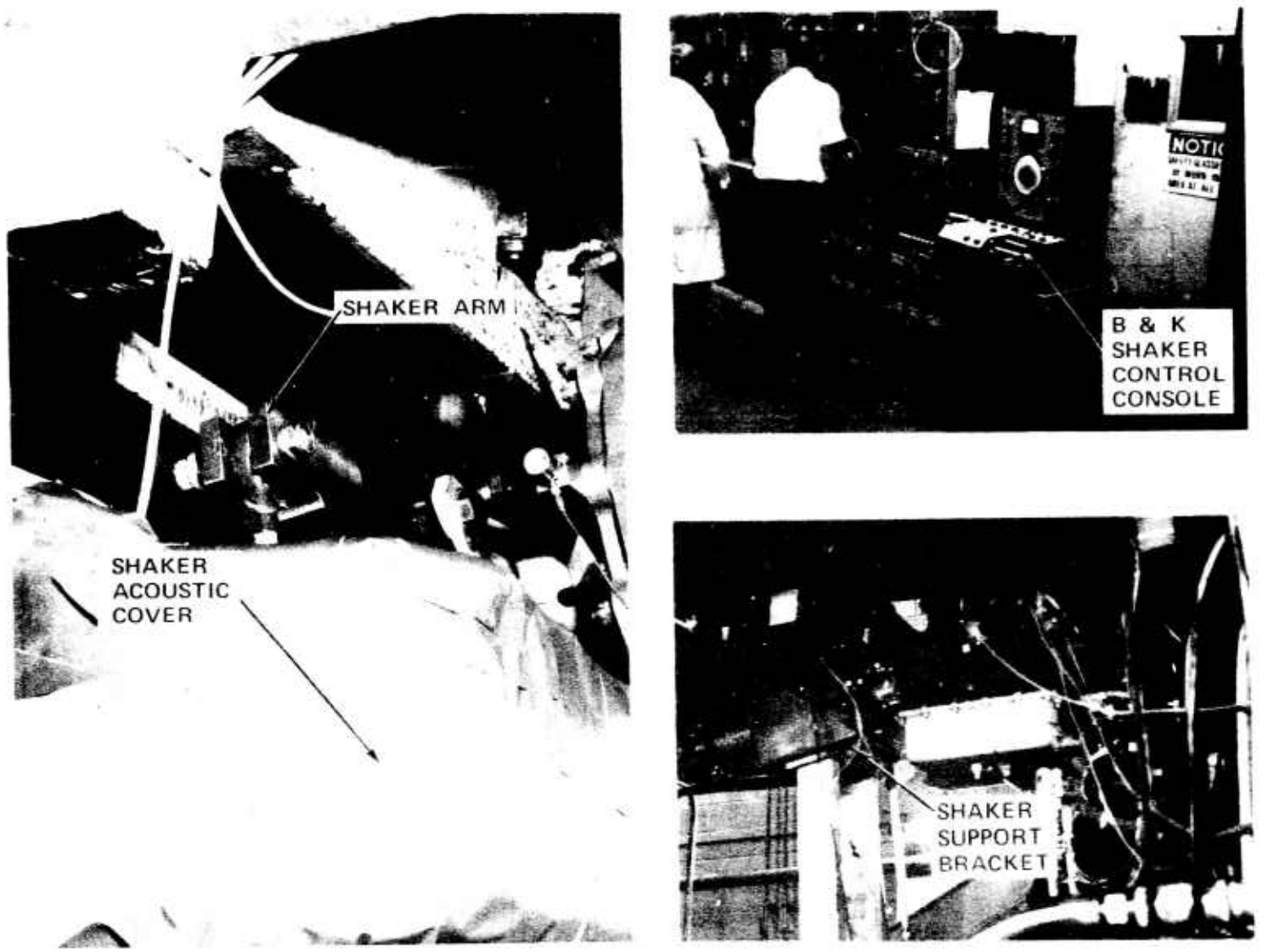

Figure 13. Shaker Installation.

Data Acquisition

System Description - A 53-channel data acquisition system was designed and built to measure accelerations, speeds, strains, torques, and lateral shaft motions of the CH-47C forward transmission. Housed in a three-bay movable console, this unit was completely portable and self-contained with respect to sensor conditioning, signal programming, and data recording. A photograph of this console is seen in Figure 14; a block diagram depicting the flow of data from sensor to tapes is seen in Figure 15.

Specifically, the data system was comprised of nine subsystems taking data both internally and externally from the transmission. The designations given to the subsystems explain their functions and are as follows:

1. Case Acceleration (see Figure 22)
2. Shaft Torque and Shaft Bending - Strain Gage Bridges (see Figure 16)
3. Shaft Proximity (see Figure 16)
4. Proximity Probe Acceleration (see Figure 16)
5. Radiated Noise (see Figure 24)
6. Shaft Speed
7. Shaft Mounted Rotating Acceleration (see Figure 16)
8. Data Programming (see Appendix A)
9. Data Recording (see Figure 15)

Internal Instrumentation - The general arrangement of the internal instrumentation is shown in Figure 16. On each of the two shafts of interest - spiral bevel pinion gear shaft (bevel gear), and spiral bevel/lower stage sun gear shaft (sun gear) - four-arm active bending and torque strain gage bridges were mounted to detect alternating shaft torque and shaft bending. Rotary transformers (S. Himmelstein and Company Models 2-16, 3-08) were used to transmit this data from the rotating system to the stationary system. The bridge conditioning used was a Natel Engineering Company, Inc. Model 2088-X Carrier Amplifier System built to the specifications required by the test. Frequency response of the unit was ± 1 dB from DC to 10 kHz. Gage locations are seen in Figure 17 for the bevel gear and in Figure 18 for the sun gear. The selection of these locations was based upon pretest predictions of maximum shaft vibration amplitudes.

The shaft proximity subsystem was used to detect lateral shaft motion of the spiral bevel pinion and sun gear shafts. Proximity probes were positioned in pairs at two locations on each shaft, the probes in each pair being 90 degrees apart.

Figure 14. Instrumentation and Control Console.

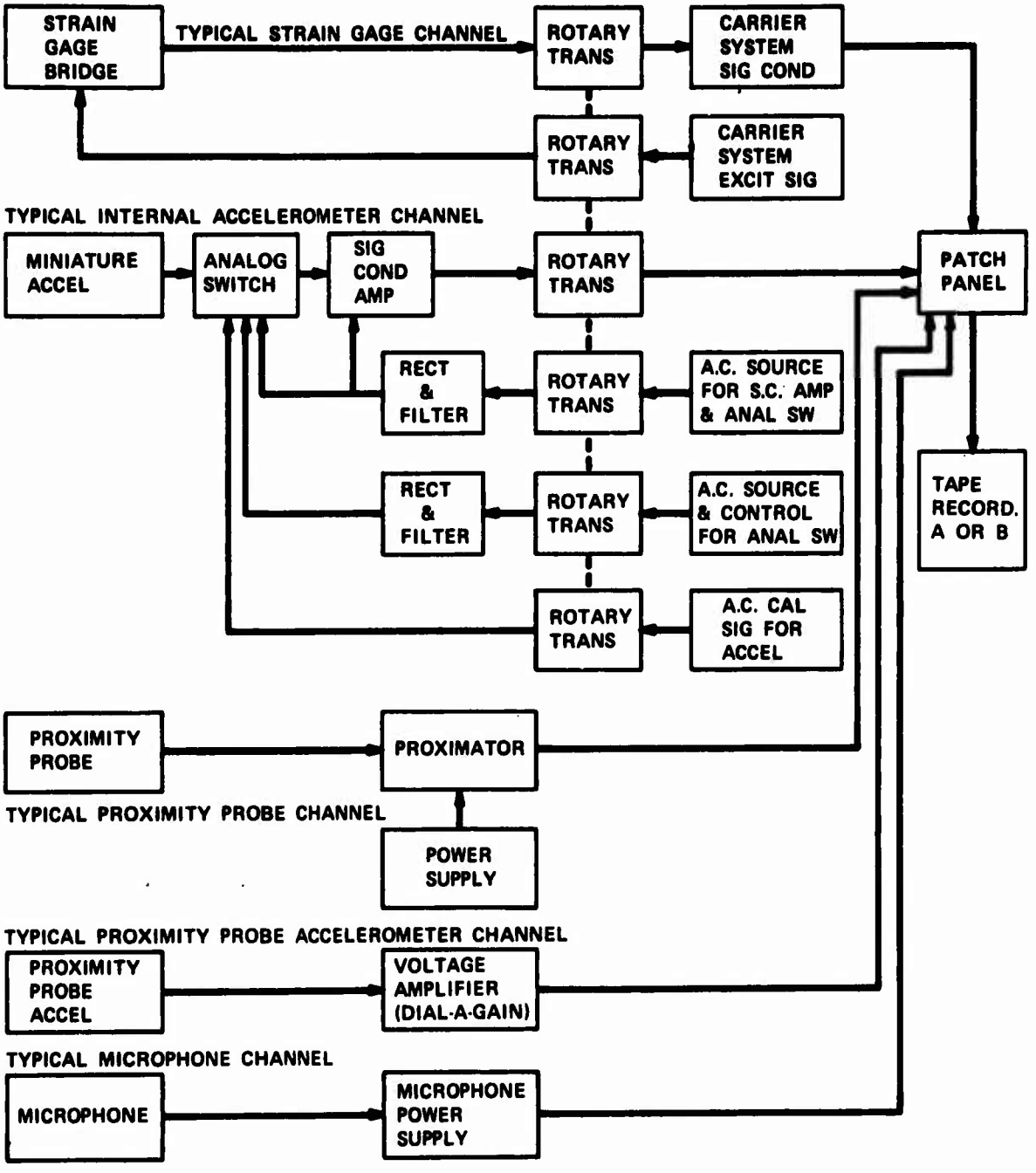

Figure 15. Instrumentation Block Diagram.

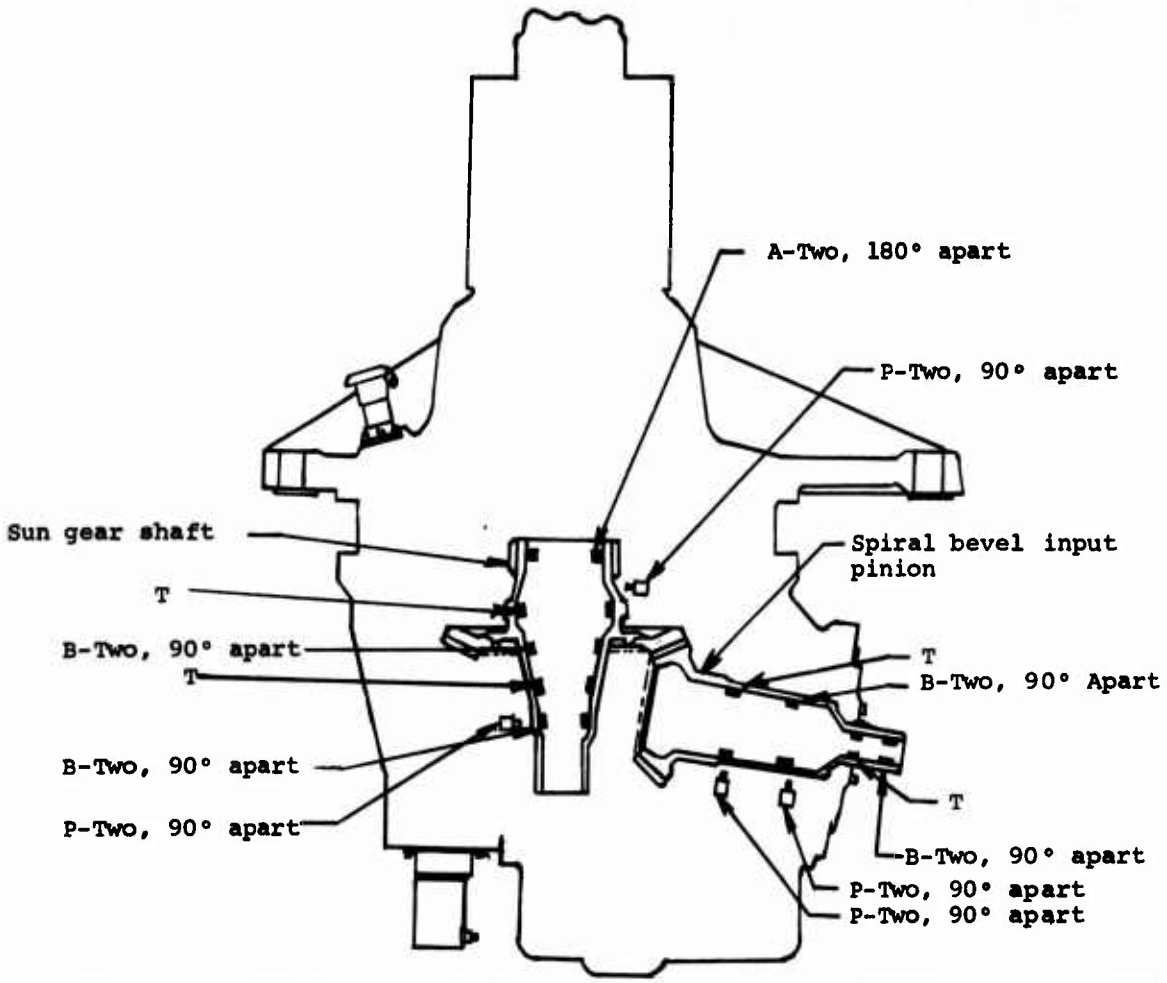

TYPE SENSOR	CODE	INSTALLATION FIGURE NO.
Torsional Strain Gage	T	17 & 18
Bending Strain Gage	B	17 & 18
Proximity Probe With Accelerometer	P	19 & 20
Rotary Accelerometer	A	21

Figure 16. Internal Instrumentation Location.

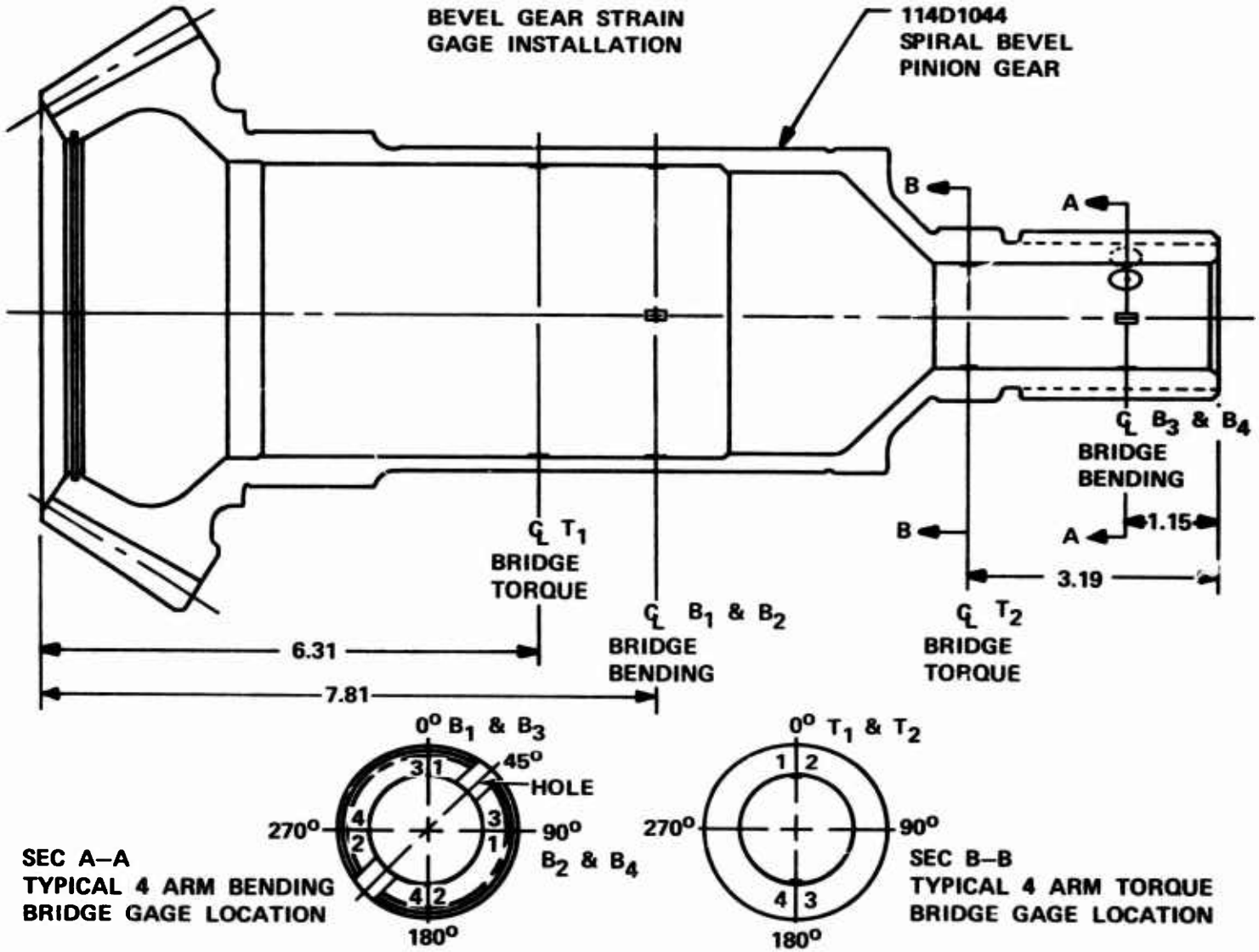

Figure 17. Bevel Gear Strain Gage Installation.

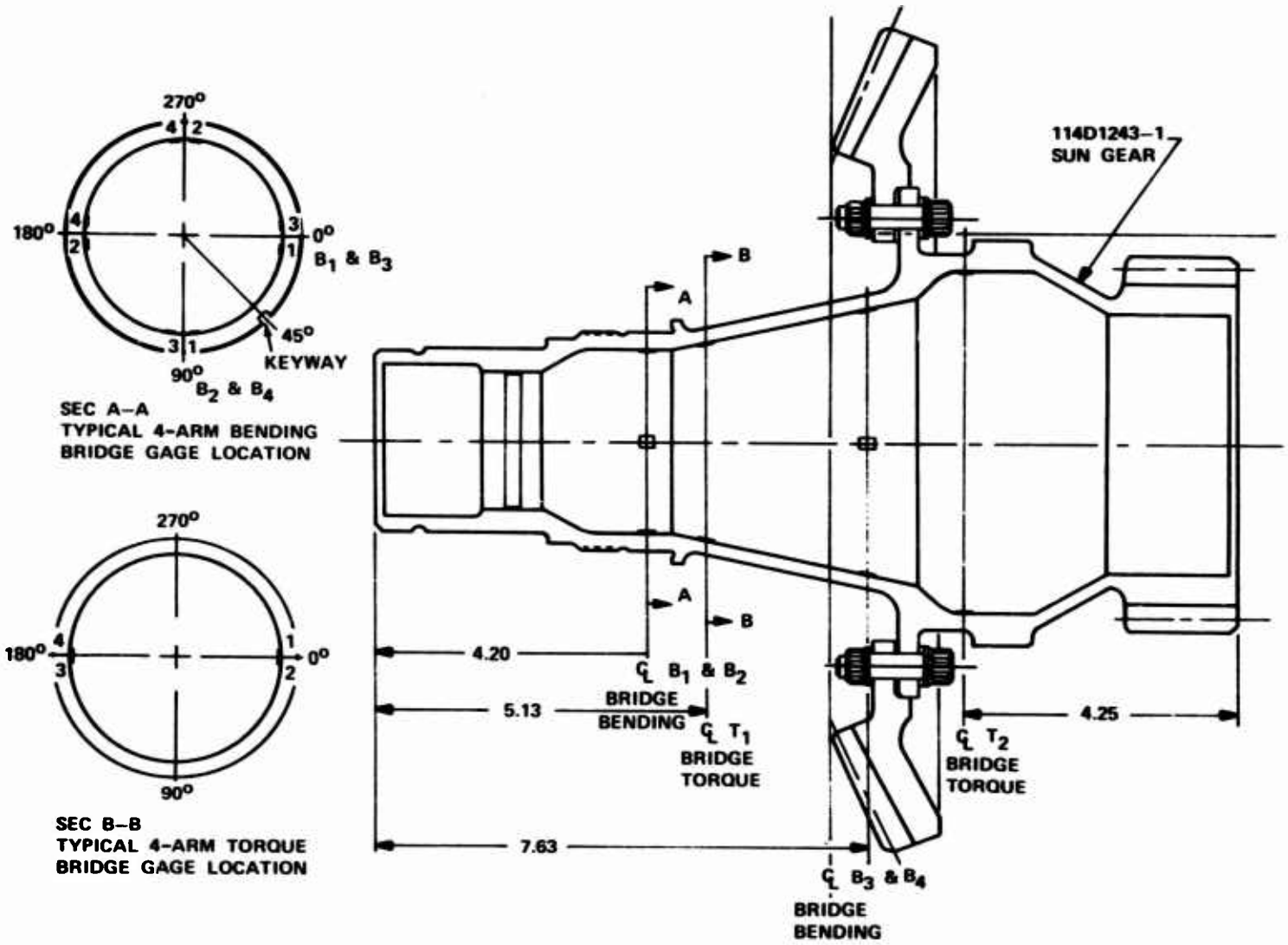

Figure 18. Sun Gear Strain Gage Installation.

The subsystem was comprised of eight Bently-Nevada proximity probes (Model 306L36) conditioned by eight Bently-Nevada proximators (Model 3500), eight 500-Hz cutoff high-pass filters and a rack of Beckman (Model C-44) amplifiers equipped with variable bandwidth low-pass filters. The eight probe channels were calibrated each using a material similar to the material to be sensed in the transmission.

As a means of checking the absolute displacement of the proximity probes, the proximity probe accelerations were also recorded. Eight Endevco Model 222B microminiature accelerometers conditioned by Unholtz-Dickie Model 610 RMG3 cathode follower amplifiers were chosen for this purpose. The Model 222B accelerometers were selected on the basis of frequency response within +2.5% to 6000 Hz for the temperature range encountered, size, and weight. The unit measures .250 inch x .375 inch and weighs .5 gram. Locations of probes and probe accelerometers are seen in Figure 19 for the bevel gear and in Figure 20 for the sun gear.

The acceleration of the sun gear shaft was detected by using two shaft-mounted rotating accelerometers. This method used two Endevco Model 22 Picomin accelerometers amplified by two Vector NMA-20 miniature amplifiers mounted within the sun gear shaft. Power for the amplifiers (DC) was developed on the shaft by a miniature power supply excited by a 10-kHz AC signal. Connection of the signal leads from the amplifiers, and power leads to the power supply, to the stationary acquisition system from the rotating gear was made by means of a rotary transformer (S. Himmelstein and Co. Model 2-16). On-shaft calibration checks were made during the test by means of a National Semiconductor Model NH1400F analog switch. The switch was connected to the MMA-20 amplifier and was excited via rotary transformer by a front panel mounted console control. The entire instrumentation package was mounted circumferentially within the sun gear shaft and was covered with Viton PLV-2002 coating as a protection against the MIL-L-23699 transmission fluid. This system and installation are seen in Figure 21.

External Instrumentation - Case acceleration was detected by Endevco Model 2213C, 2224B, and 2235C accelerometers which were conditioned by Unholtz-Dickie 610-RMG3 (Dial-A-Gain) cathode follower amplification. The frequency response of this subsystem was determined to be flat within ±2% to 5000 Hz for the temperature range encountered. Twelve accelerometers were installed throughout the test program. The accelerometers were stud mounted to aluminum blocks which were either epoxied to the case or secured to existing

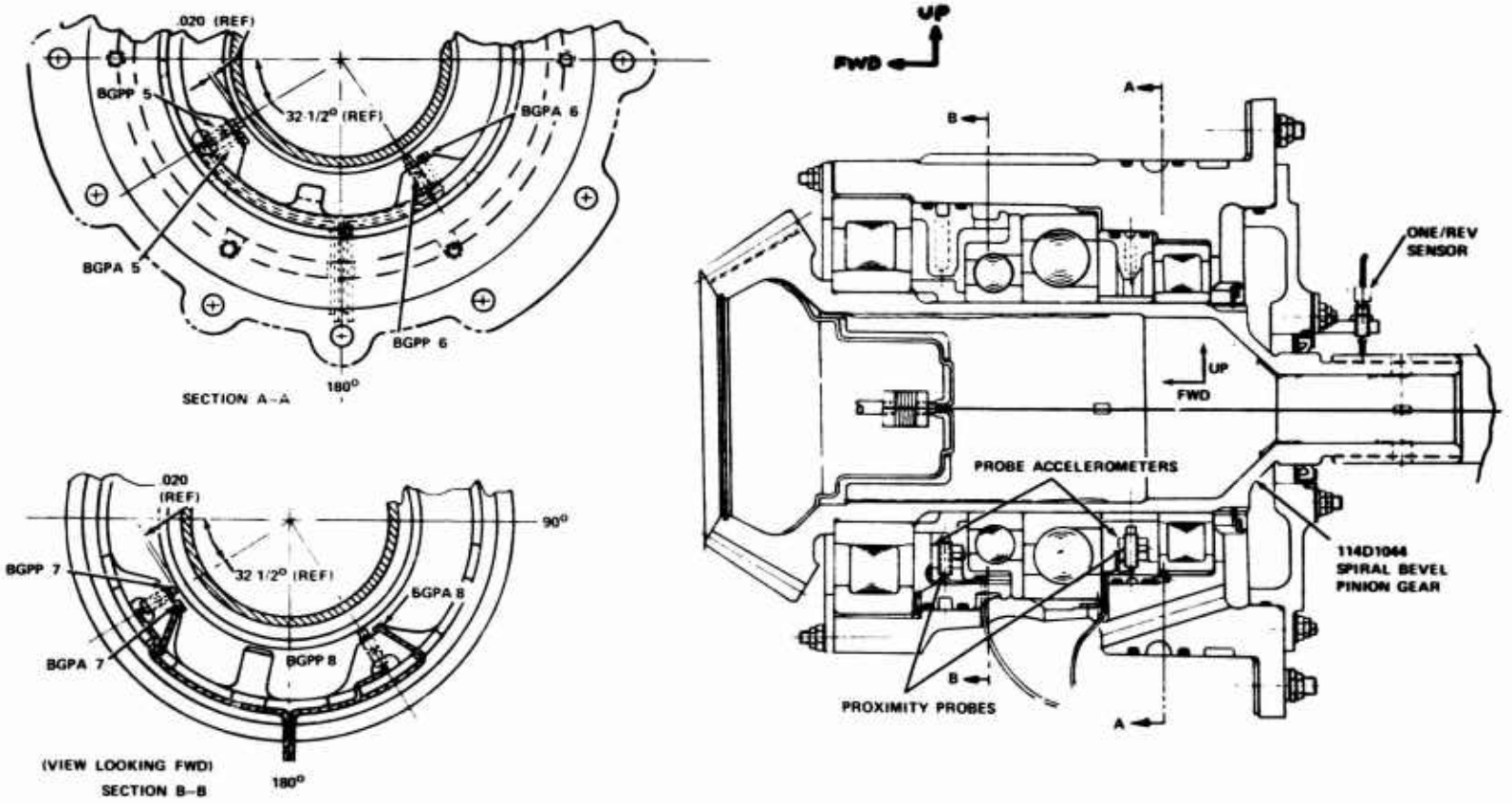

Figure 19. Proximity Probes and Accelerometers Installation - Bevel Gear.

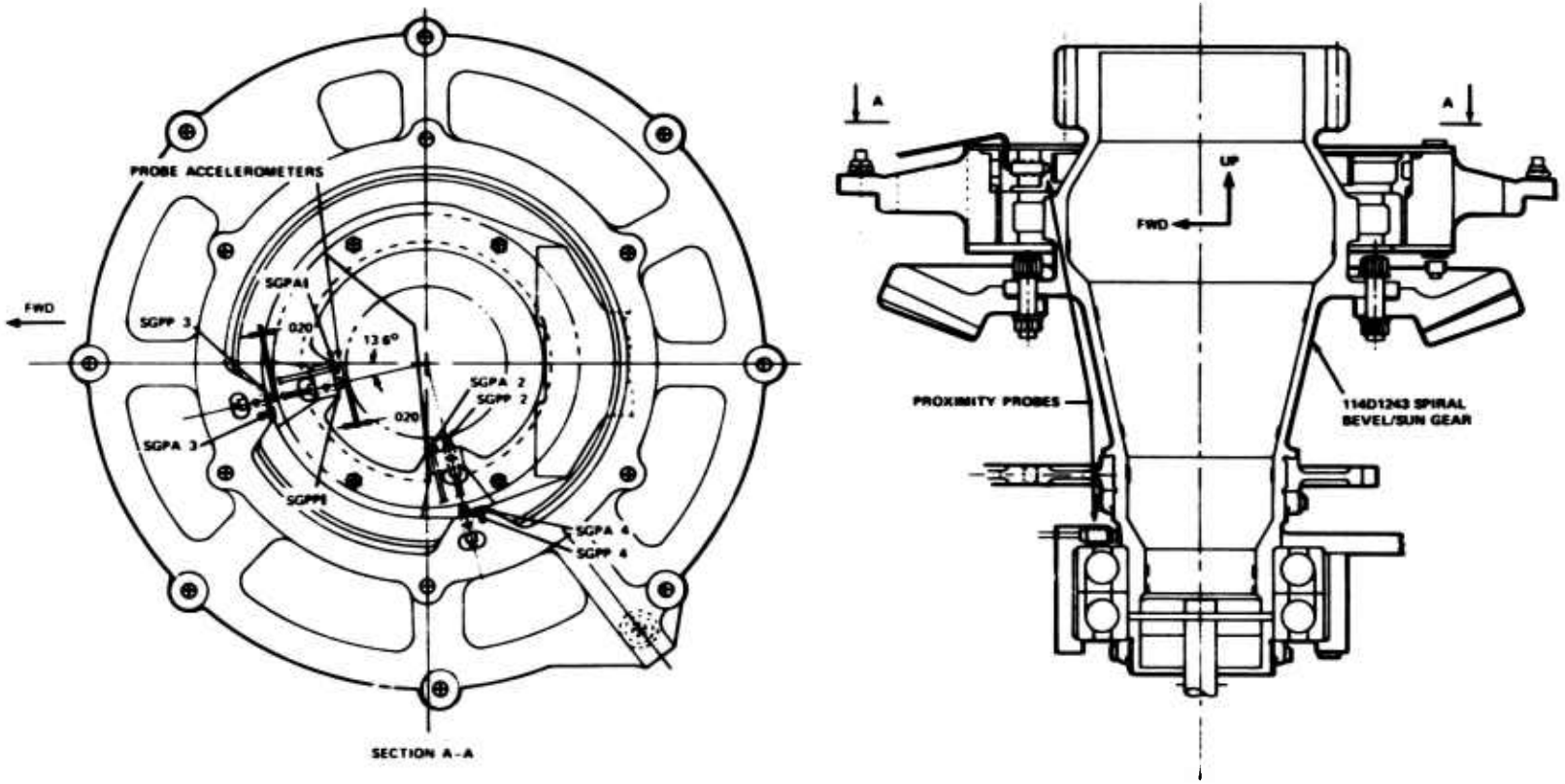

Figure 20. Proximity Probes and Accelerometers Installation - Sun Gear.

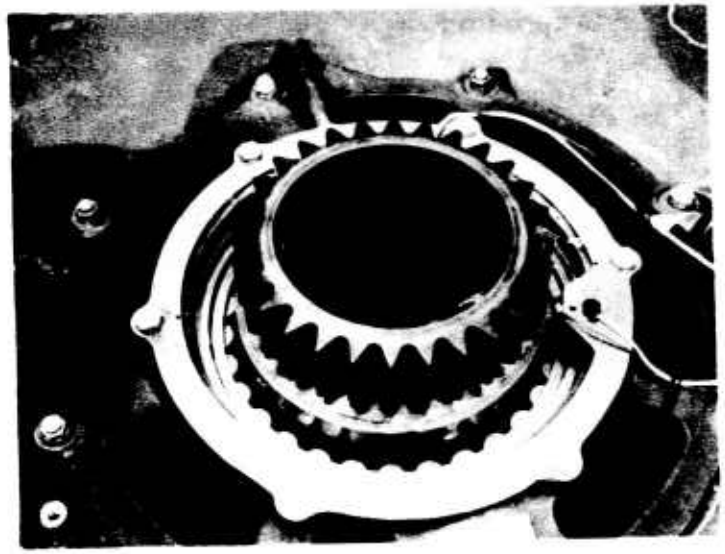

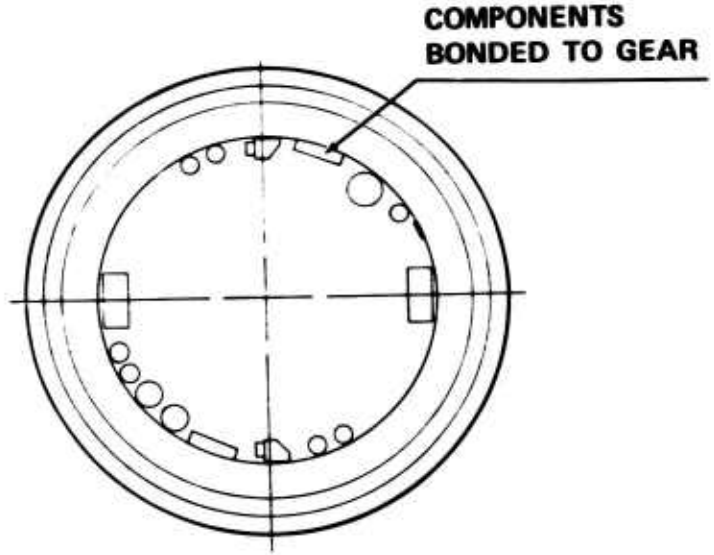

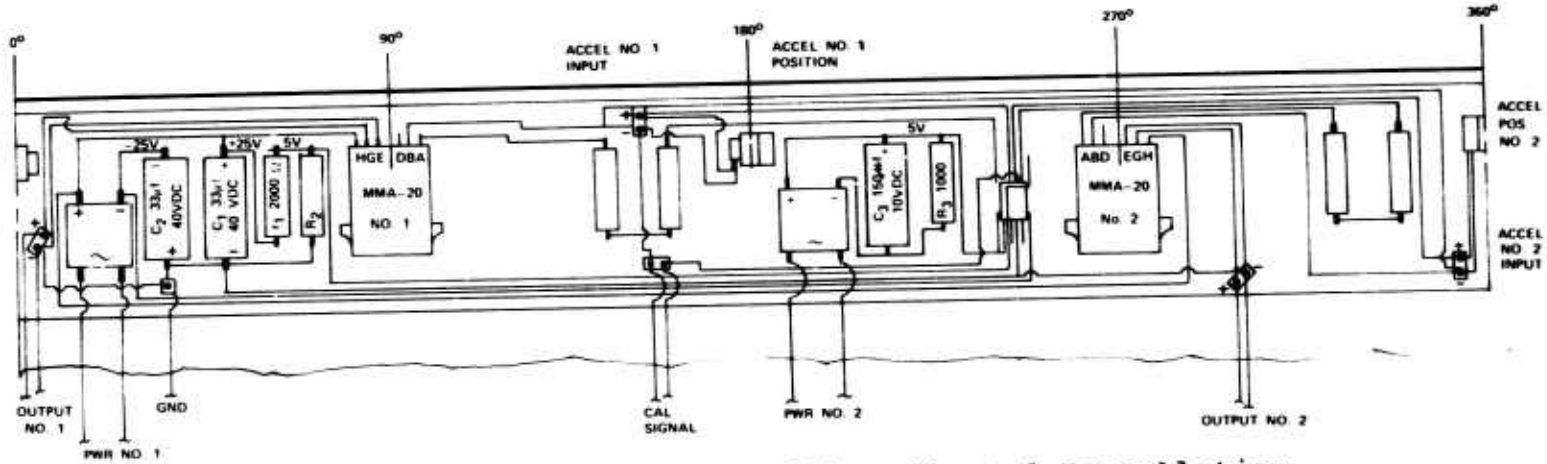

Figure 21. Rotary Accelerometers Schematic and Installation.

case hardware. Accelerometer locations varied from one test to another. The locations for each test are seen in Figure 22. A photograph of a typical installation is seen in Figure 23.

Audible case vibration, or radiated noise, was detected by six Bruel and Kjaer (B&K) Model 4131 microphones powered by six B&K Model 2801 microphone power supplies. The B&K system was chosen for temperature stability, frequency response (20 Hz to 18 kHz), and sound pressure level sensitivity (15 dB to 146 dB). The microphones were employed as portable sensors during the period of testing; their location adjacent to the transmission was dependent upon the specific test requirement. Six microphones were installed throughout the test program. The microphones either were supported by a stand or were string mounted near the side of the case. The microphones were loosely covered with a very thin plastic bag to protect them from transmission oil. Prior experience indicated that the frequency response is not appreciably affected. The microphone locations for each test are seen in Figure 24. A photograph of a typical installation is seen in Figure 25.

Shaft speed was indicated by pulse trains produced by Electro Products Laboratories magnetic pickups (Model 3055-A). Three pulse trains were generated: two by a single shaft perturbation on both the bevel gear and the sun gear which produced one/rev signals, and the third by a 60-tooth gear on the sync shaft for a 60/rev signal of the quality required for data analysis.

Data Programming - A data programming system was designed to enable any combination of the 53 data channels to be recorded 26 channels at a time. In general, combinations were either selected to allow for tracking the propagation of a particular signal through the transmission to the case or to group common sensors. These groupings were referred to a sequence schedule which allows for time phasing of signals by providing logical groupings for each data point. A complete set of sequence schedules used for each test phase is included in Appendix A. To accomplish this sequencing the programming was performed by means of an AMP Inc. Model 695070-1 patch panel and two five-position twelve-pole rotary switches. Specifically, the instrumentation systems outputs were wired to one side of the patch panel. The other side was wired to the five-position switches, 120 channels in five groups of 12 per switch. Interconnection of the two sides of the patch panel programmed the switches whose outputs were connected to two tape recorders, respectively.

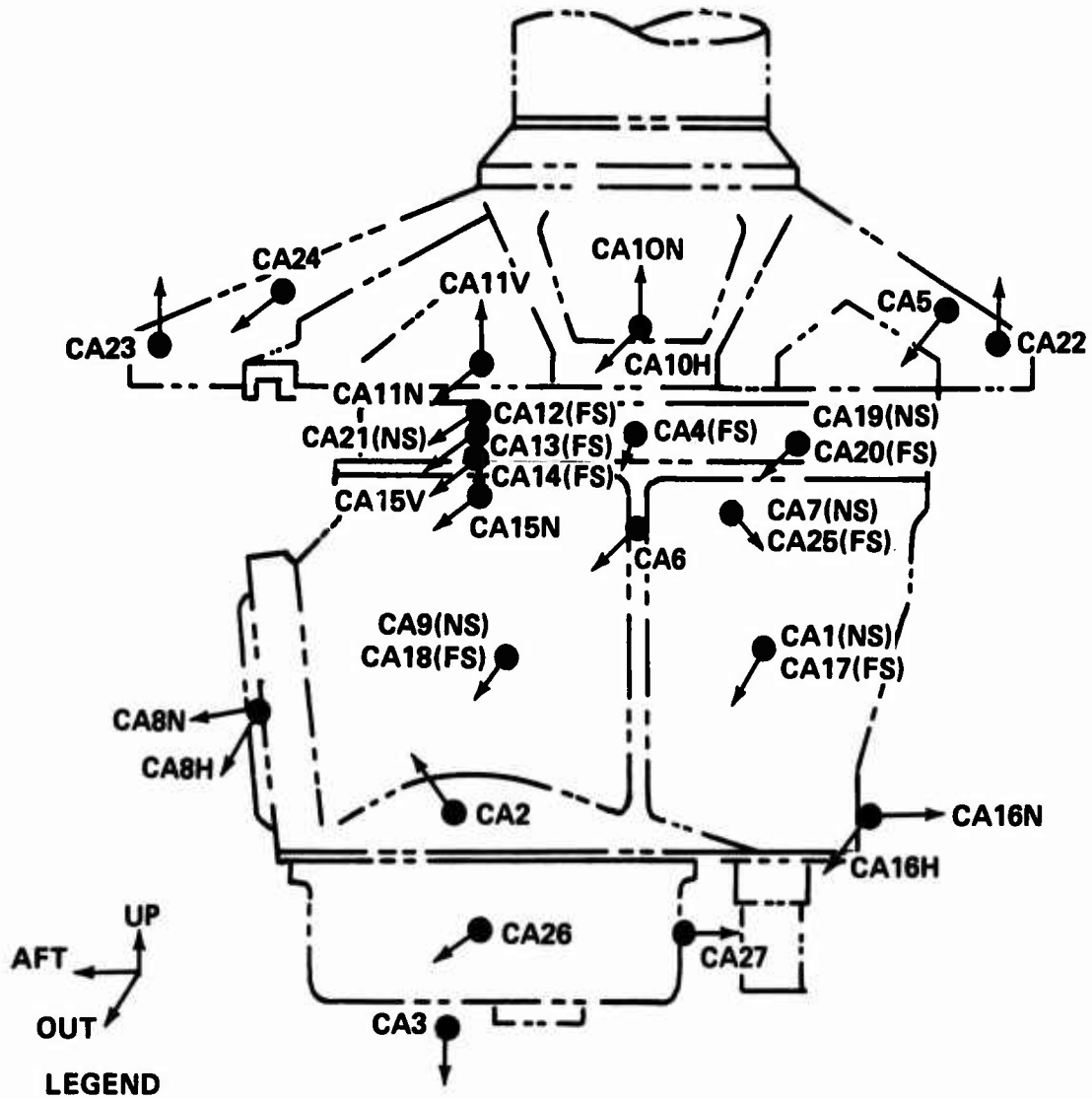

LEGEND

NOTES: (1) UNLESS OTHERWISE SPECIFIED, ALL ACCELEROMETERS ARE INSTALLED NORMAL TO MOUNTING SURFACE

(2) NS MEANS NEAR SIDE, FS MEANS FAR SIDE

CONFIG	INSTALLED ACCEL LOCATIONS
1	1, 3, 4, 8N, 9, 16N, 11N, 12, 13, 14, 15N, 17
2	5, 6, 7, 10N, 11N, 12, 13, 14, 15N, 19, 20, 21
3	5, 7, 10H, 10N, 11V, 11N, 13, 15V, 15N, 22, 23, 24
4	2, 3, 7. 8H, 16H, 16N, 17, 18, 25, 26, 27

Figure 22. Accelerometer Installation.

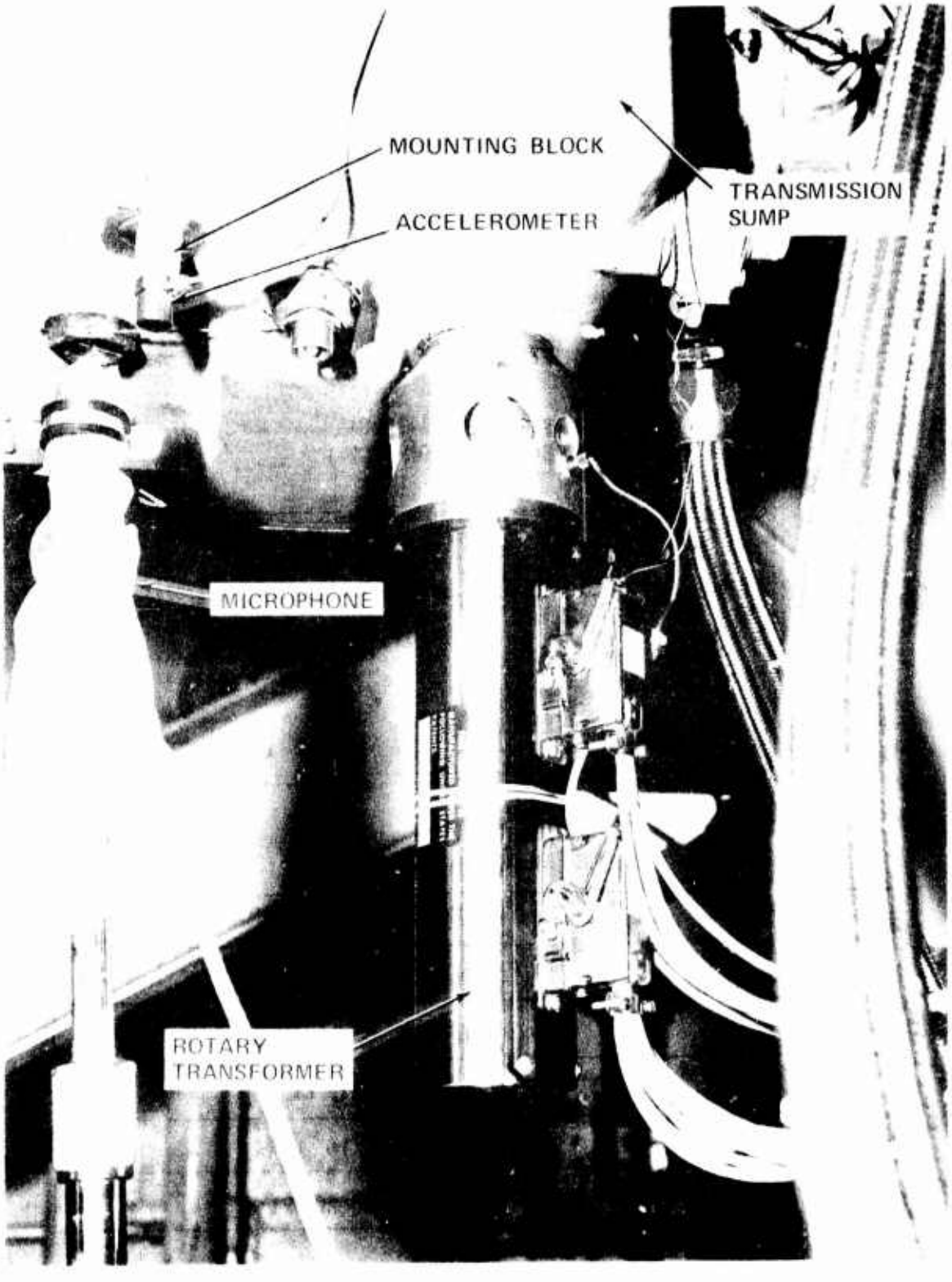

Figure 23. Typical Accelerometer Installation.

MICROPHONE INSTALLATION

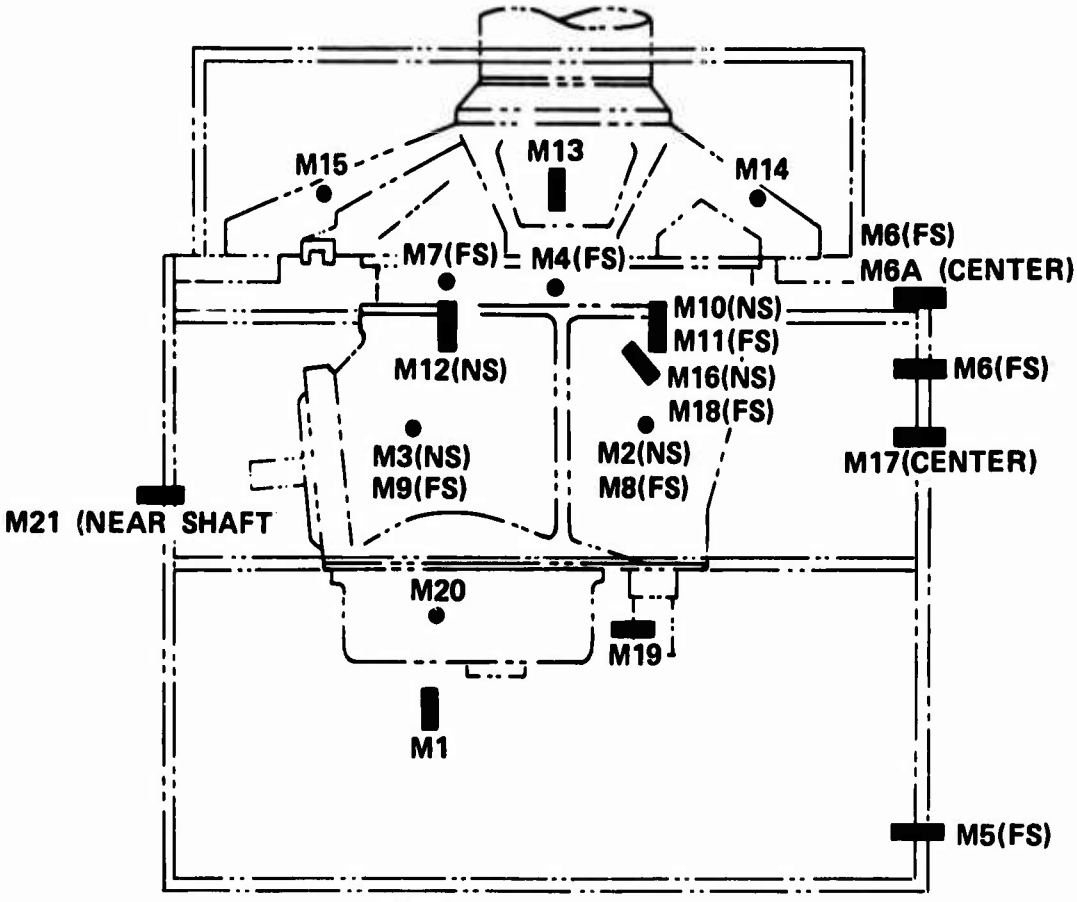

NOTE:
FS MEANS FAR SIDE
NS MEANS NEAR SIDE

CONFIG	INSTALLED MICROPHONE LOCATIONS
1	1, 2, 3, 4, 8, 9
2	1, 2, 3, 4, 5, 6A
3	5, 6, 7, 10, 11, 13
4	1, 5, 14, 15, 16, 17
5	1, 16, 18, 19, 20, 21

Figure 24. Microphone Installation.

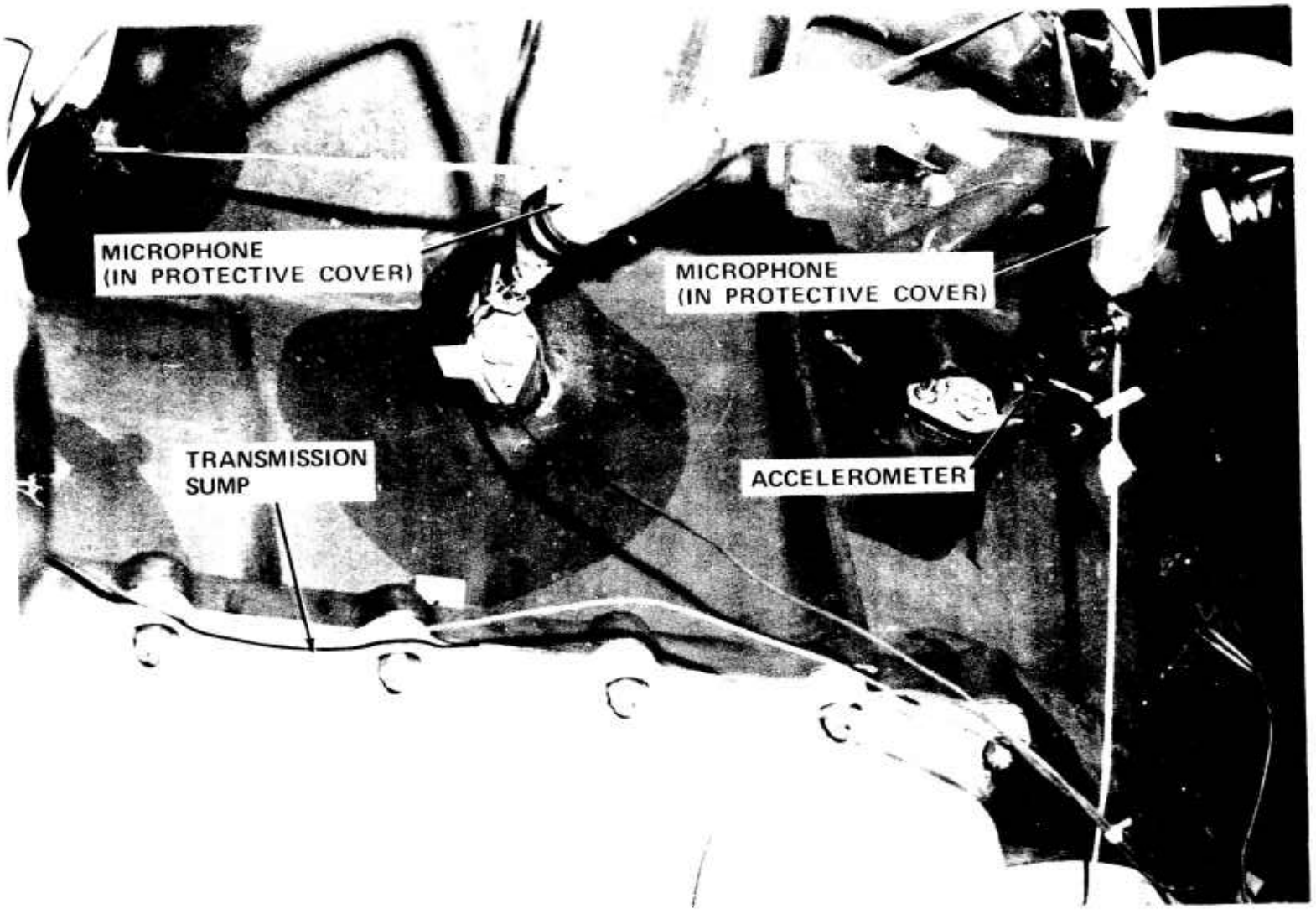

Figure 25. Typical Microphone Installation.

Data Recording - Data recording was accomplished by two 14-channel magnetic tape recorders: a Sangamo Electric Model 3500 and an Ampex Model AR-200. The machines were controlled simultaneously by a front panel control, and their inputs were supplied by the five-position rotary switches. A tape speed of 30 IPS and FM recording techniques were used to obtain a data bandwidth of 10 kHz. Tracks 13 and 14 on each machine were used for transmission input shaft RPM and voice identification, respectively.

System Operation - All systems operated perfectly for the duration of the first dynamic test program. The rotating accelerometers were rendered inoperable after the initial dynamic test run, and the strain gage bridges failed individually as the test progressed. Since all internal data was recorded during the first dynamic test, no data was lost as a result of these failures. The patch panel was repatched for each of the four dynamic tests per the respective test requirement.

System Calibration - A complete listing of sensor sensitivities for each test is included in Appendix B. A complete set of calibration curves and discussion is included in Reference 8.

Test Procedure

Test Configuration - The test data was obtained for the configurations listed in Table 1.

Test Conditions - For each of the above configurations, data were taken at each of the five torques tabulated in Table 2.

1. Shake Test - For the shake test, frequency sweeps were performed for each torque for each of four shake test sequences (four sweeps per five torques). In addition, stabilized data points were obtained for the gear mesh frequencies.

2. Dynamic Tests - For the dynamic tests, acceleration and deceleration sweeps were performed for each torque for each sequence (two sweeps x five sequences x five torques). In addition, for the first dynamic test, a minimum of 18 stabilized rpm data points were obtained for each torque for each sequence (18 rpm's x five sequences x five torques). For

---

[8]A. D'Agostini, DRIVE SYSTEM NOISE REDUCTION DATA ACQUISITION SYSTEM, Boeing-Vertol Test Memorandum Report TMR 1362, 30 August 1972.

TABLE 1. TEST CONFIGURATIONS

TEST NUMBER	ENCLOSURE CONFIGURATION (see Fig. 12)	MICROPHONE LOCATION (see Fig. 24)	ACCELEROMETER LOCATION (see Fig. 22)	SEQUENCE SCHEDULE (see App. A)	TEST FUNCTION
Shake Test	None	1	1	1-4 A&B (Calib.Bd.)	Nonrotating dataa
Dynamic Test 1	1	2	1	1-5 A&B	Internal data and signal propagation
Dynamic Test 2	2	3	2	103-104 A&B	Ring gear and upper case survey
Dynamic Test 3	3	4	3	101-102 A&B	Main case survey
Dynamic Test 4	3	5	4	201-202 A&B	Lower case and sump survey (lift, drag investigation)

TABLE 2. TEST TORQUES

PERCENT	INCH-POUNDS AT OUTPUT SHAFT
40	$.42 \times 10^6$
60	$.64 \times 10^6$
80	$.85 \times 10^6$
90	$.96 \times 10^6$
100	1.06×10^6

the remaining three dynamic tests, ten stabilized rpm data points were obtained for each torque for each sequence (10 rpm's x two sequences x five torques x three tests). Finally, for the fourth dynamic test, additional rpm sweep data and stabilized rpm data points were obtained to evaluate the effects of lift and drag on transmission noise. it is estimated that over 25,000 channel data points were recorded during this test period. A detailed run log with tape log cross reference is included in Appendix C.

Test Operation - Testing was accomplished in the following manner. Prior to running for data, the transmission was warmed up for a minimum of 30 minutes at 7460 rpm. During this period the transmission was operated for approximately 10 minutes at 10 percent torque and then increased to 100 percent torque until transmission oil temperatures and pressure had stabilized. Once the transmission was stabilized, the torque was set to the appropriate level and allowed to stabilize, during which time the data system was balanced. "E" cals and "R" cals were recorded prior to each test and repeated at the beginning of each new tape reel. A typical dynamic test consisted of constant torque deceleration sweeps followed by acceleration sweeps, repeated for each sequence. The nominal sweep rate was two minutes for a sweep from 3000 to 7500 rpm (input shaft). On-line observation of sweep data determined which stabilized data rpm's should be recorded. These stabilized data points were then recorded for each sequence. Stabilized data was recorded for 30 seconds, which would allow for a 256 spectrum average during data analysis. Tape speed for recording of data was 30 inches per second.

Data Analysis

Stabilized Data - In order to properly interpret transmission noise data, narrowband analysis techniques are required. The data obtained on this program were analyzed using a Federal Scientific UA-6 Ubiquitous Spectrum Analyzer (Figure 26). This analyzer was used in a mode which gives a constant bandwidth of 10 Hz over the range of 0 to 5000 Hz. To facilitate interpretation of results, the horizontal axis (normally shown as frequency) has been identified in terms of the gear mesh frequencies and their harmonics. Since the frequencies are a function of rotation speed, it was necessary to provide for frequency tracking in order to hold the peaks in a fixed horizontal position (as determined by normal operational speed). An example of this is seen in Figure 26a.

Speed Sweeps - Another method of looking at the data was to track a mesh frequency as the speed of the transmission was changed. The UA-6 analyzer was used as a tracking filter for

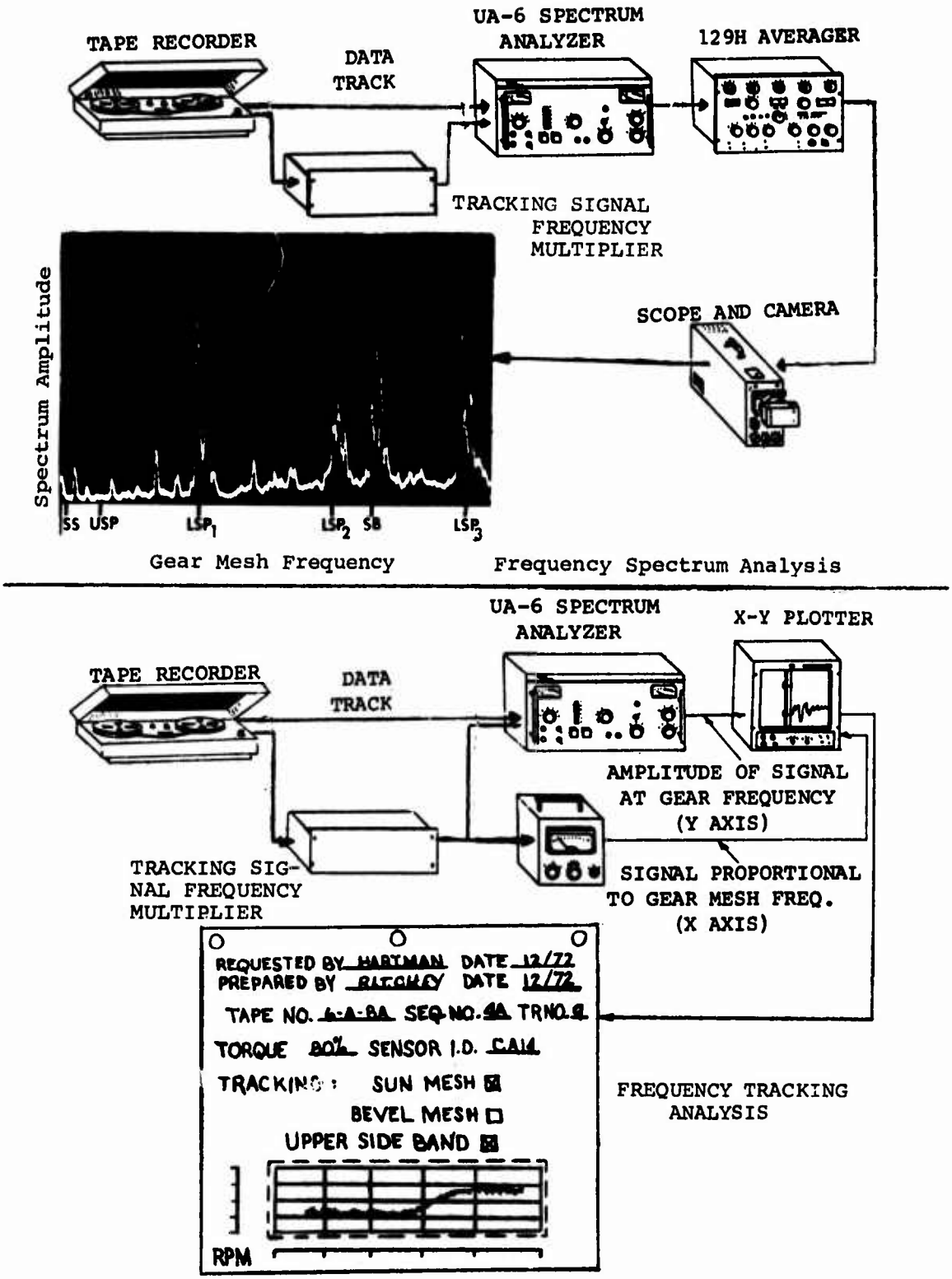

Figure 26. Frequency Spectrum and Tracking Analysis.

this purpose. The output was plotted on the vertical axis, and the tracking frequency was plotted on the horizontal axis (see Figure 26). Figure 27 shows a typical plot produced with this method. In addition, several full spectra for points on the curve are shown. This illustrates how the sweep data was reduced.

PREDICTIONS AND MEASUREMENTS OF TORSIONAL VIBRATION AND NOISE LEVELS

Analytical Prediction Procedures

The mesh frequency vibrations which occur in geared power trains are often complex phenomena. As discussed briefly in the General Discussion portion of this document, these vibrations are superimposed upon the steady-state rotation of the train and may be composed of several components at mesh frequencies or their integer multiples. Moreover, they may exist as coupled lateral-torsional-axial modes, with any or all of the coupled motions occurring in each drive train component.

Because of the difficulty in programming a complete analytical solution to this problem, gearbox vibration (noise) prediction and reduction technology has been developed in stages of increasing complexity. To date, the following major assumptions have been made:

1. The excitations produced in the several gear meshes are not influenced by drive train vibrations;

2. Excitations produced in the several gear meshes act separately to produce torsional responses in the drive train, with resulting dynamic tooth forces;

3. The dynamic tooth forces produce lateral, combined lateral-torsional, or combined lateral-torsional-axial vibrations, depending upon the complexity of the dynamic model; and

4. The dynamic tooth forces and gear mesh excitations may be combined empirically to yield noise level predictions.

It was the desire to test these assumptions, and particularly the analyses and computer programs which resulted from them which led to the test results reported herein.

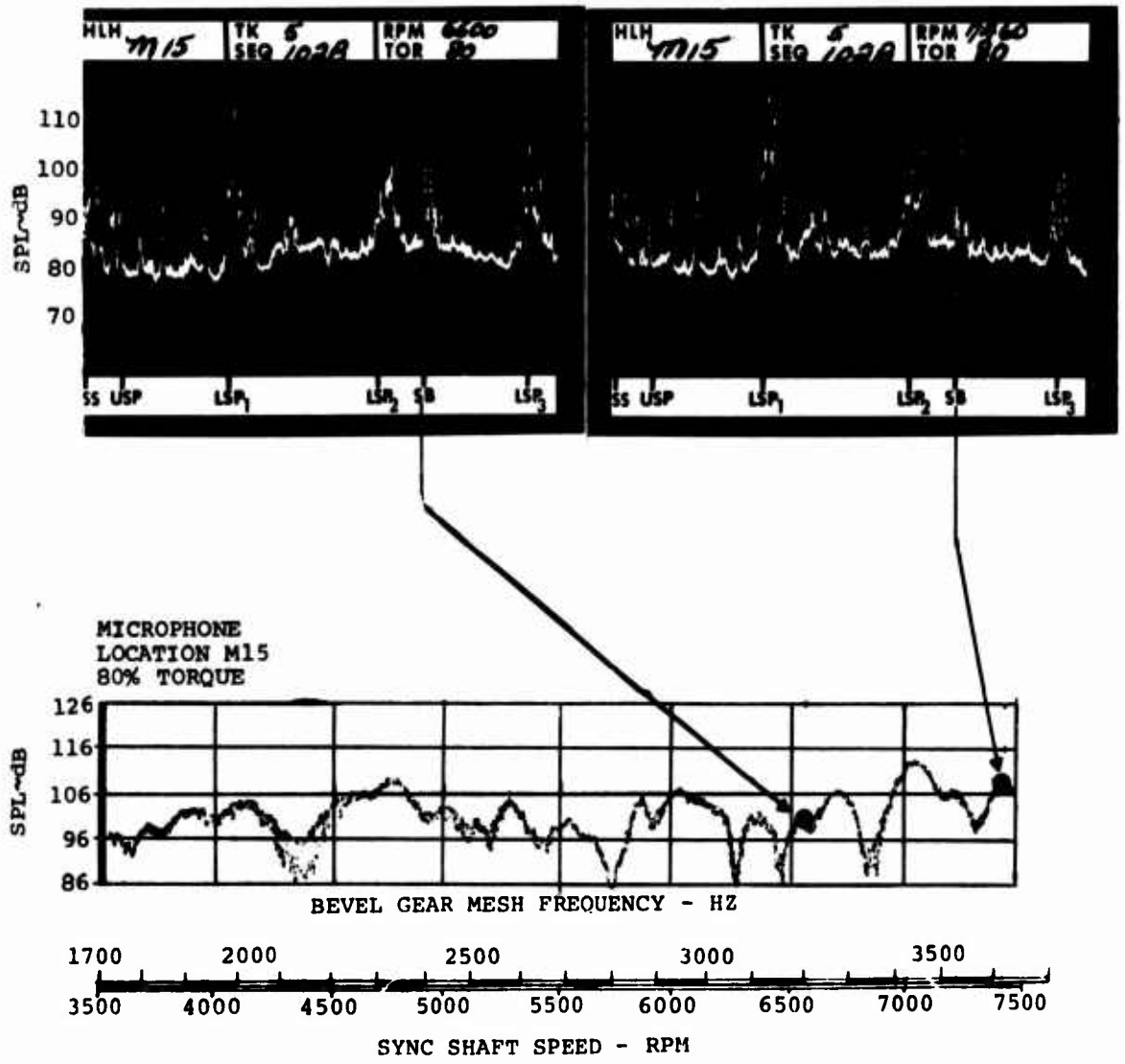

Figure 27. Example of Sweep and Spectra.

Gear Mesh Excitation Predictions (GEARO) - A detailed analytical procedure has been reported in Reference 2 for calculating the dynamic excitations produced in gear meshes as a result of the mesh properties. These excitations, which are essentially deviations of the gear body from smooth rotation, are due to mismatches or errors of tooth profiles, tooth location errors, or elastic deformation of the tooth or tooth surfaces. The excitations are considerably different from sinusoidal in nature, thereby producing disturbance components at the mesh frequency and its integer multiples.

The analytical procedure has been developed for spur gears under the assumption that one or two pairs of teeth are in contact, on the average, and that each pair of meshing teeth is exactly the same as each other pair of meshing teeth. This procedure is currently limited to standard contact ratios. An approximate method has been developed to treat helical and spiral bevel meshes.

Torsional Response Predictions (TORRP) - The torsional vibration responses produced in geared drive trains as a result of gear-mesh-produced excitations may be calculated by means of an analytical procedure.[9] An extended version of this procedure was reported in Reference 4.

The computer program in which the torsional response analysis is implemented permits a rather large and complex torsional dynamic model to be considered, including torsional branches, planetary reductions, and simple gear meshes. Dynamic excitations at the gear mesh locations are of the sinusoidally varying angular position type. Calculated output consists of angular amplitudes, phase angles, and dynamic torques for each element of the torsional model and resulting dynamic tooth forces at each mesh in the system.

Lateral-Torsional-Axial Response Predictions - A prediction of lateral (and occasionally axial) response of the gear carrying drive train element is a major objective in any gearbox noise prediction analysis, since this is the motion which produces casing vibrations and noise. The manner in which this prediction is made will depend upon the complexity and capabilities of analytical methods which the investigator may bring to the problem, and upon

---

[9] I. Laskin, F. K. Orcutt, and E. E. Shipley, ANALYSIS OF NOISE GENERATED BY UH-1 HELICOPTER TRANSMISSION, Mechanical Technology Incorporated, USAAVLABS TR 68-41, U. S. Army Aviation Materiel Laboratories, Fort Eustis, Virginia, June 1967, AD 675457.

the dynamics of the system under study. A rigorous solution would take the tooth excitation amplitudes as inputs and produce coupled lateral-torsional-axial vibration amplitudes as results.

To date the analytical capability for performing this complete solution has not existed, and it has proven necessary to treat the lateral response after gear tooth dynamic forces have been obtained by a torsional response analysis. Two basic calculation sequences have been used to date:

A) A finite element system dynamics approach (D-82) in which the shaft-bearing system is represented by a series of springs and masses, each of which can have up to six degrees of freedom; and

B) A shaft-bearing system dynamics approach in which the gear-carrying shaft is represented by a series of finite cylindrical beam elements having rotation, but which are limited to lateral or coupled lateral-torsional vibration.

In each of these sequences the system is forced by dynamic forces resulting from the intermediate torsional response analysis. Approach A has the advantage of permitting coupling of vibrations between adjacent shafts across gear meshes, an important system effect, whereas Approach B considers the shaft rotation aspects more exactly. The finite element system dynamics approach used for the subsequent HLH noise redesign study is discussed in more detail in the section of this report entitled "Damped Forced Response (D-82)".

Empirical Noise Level Predictions (SPL) - A detailed analytical noise level prediction was reported in Reference 9 and implemented in a computer program in Reference 4. This analysis accepts gear mesh pitchline excitations and gear tooth dynamic forces as input quantities for each individual harmonic of each mesh. The acoustic energy corresponding to each such frequency is then calculated by multiplying together the excitation and dynamic force and summing the results within each frequency band of interest. The basis for this analysis is the assumption that a small but predictable fraction (α) of the dynamic power train energy appears as acoustic energy.

Analytical Modeling for Calculations - A considerable amount of the detailed system modeling performed prior to making the gearbox vibration and noise calculations is reported in detail

in References 4, 10, 11, and 12, particularly in the case of the gear mesh excitation calculations. The torsional response calculations, on the other hand, required extensive system remodeling beyond that reported in those references since the earlier dynamic models were based upon gearbox components as they existed in a flight-quality gearbox. The tested gearbox, on the other hand, had a number of modifications incorporated into it, the most significant of which were shaft changes designed to permit rotating strain gage and accelerometer signals to be conducted to the outside.

Modeling for Gear Mesh Excitation Calculations - Reference 10 presents design details of the gears contained in a CH-47 gearbox. The test gearbox was assumed to have gears of the same design, with tooth profiles identical to the "average" profiles described in Reference 10. Details of the gear designs and of the assumed profiles may be found on pages 22, 50, and 51, and 60 through 62 of Reference 10. (It should be noted that design tooth load levels in the present analysis are considerably higher than those for which the results reported in Reference 10 were obtained since the horsepower levels used in the calculations in Reference 10 were considerably below those corresponding to the torques at which the present gearbox tests were conducted.)

Modeling for Torsional Response Calculations - A drawing of the closed-loop test stand is shown in Figure 11. From this figure it is apparent that the tested gearbox is part of a torque loop with a major branch consisting of the driving motor and speed clutch. A detailed torsional model of this system was prepared for use in the torsional response calculations.

---

[10] R. H. Badgley and T. Chiang, REDUCTION OF VIBRATION AND NOISE GENERATED BY PLANETARY RING GEARS IN HELICOPTER AIRCRAFT TRANSMISSIONS, ASME Paper Number 72-PTG-11, Presented at ASME Mechanisms Conference and International Symposium on Gearing and Transmissions, San Francisco, California, 8-12 October 1972.

[11] R. H. Badgley, GEARBOX DYNAMICS - THE KEY TO UNDERSTANDING AND REDUCING ACOUSTIC-FREQUENCY ENERGY IN GEARED POWER TRAINS, Presented at the Meeting of the Aerospace Gearing Committee of the American Gear Manufacturers Association, Cleveland, Ohio, 17-18 January 1972.

[12] R. H. Badgley, REDUCTION OF NOISE AND ACOUSTIC-FREQUENCY VIBRATIONS IN AIRCRAFT TRANSMISSIONS, AHS Paper Number 661, Presented at the 28th Annual National Forum of the American Helicopter Society, Washington, D. C., May 1972.

TABLE 3. CH-47 FORWARD ROTOR DRIVE GEARBOX DIMENSIONS AND PROPERTIES USED IN TORSIONAL RESPONSE CALCULATIONS

Sys Sta No.	Conc. Polar Moment of Inertia (lb-in.^{2})	Shaft Sect Length to Next Sta. (in.)	Stiffness Outer Diameter (in.)	Mass Outer Diameter (in.)	Stiffness and Mass Inner Dia. (in.)	Concentrated Compliance (rad/in.-lb)	Identifying Notes
1	652.9	1.0	4.12	4.12	0	0	
2	0.0	1.56	3.54	5.512	0	0	
3	0.0	4.25	3.348	5.216	0	0	Sync Shaft
4	46.3	3.828	3.0	3.0	0	0	
5	101.7	25.86	4.346	4.337	4.25	0	
6	46.4	26.68	4.346	4.337	4.25	0	
7	89.4	1.15	2.1	2.1	1.4	0	Thomas Coupling
8	0	2.04	2.1	2.1	1.4	0	Torque Bridge
9	0	0.81	2.1	2.1	1.4	0	
10	0	2.20	4.3	5.4	3.75	0	
11	0	0.97	4.3	5.4	3.95	0	
12	0	1.50	4.3	5.4	3.95	0	
13	0	2.03	4.3	5.4	3.95	0	Torque Bridge
14	0	2.0	4.7	5.4	3.95	0	Himmelstein
15	0.365	2.2	3.16	3.16	2.9	0	Xfmr 3-08
16	72.3	0	0	0	0	0	Spiral Bevel Pinion
17	0.216	0.95	0.86	0.86	0.52	0	Himmelstein
18	0.129	1.00	2.50	2.50	2.14	0	Xfmr 2-16
19	0.129	9.00	0.64	0.64	0.50	0	Sun Gear
20	0.174	3.4	0.64	0.64	0.50	0	Shaft Ext
21	4.2	4.20	3.00	3.50	2.50	0	
22	26.2	0.93	3.60	3.60	3.00	0	Lower End
23	0	2.50	4.10	4.10	3.70	0	of Sun
24	0	0.47	4.30	4.30	3.90	0	Gear Shaft
25	568.0	1.0	6.0	6.0	5.5	0	Spiral Bevel Gear
26	0	2.3	6.0	6.0	5.5	0	
27	0	0	0	0	0	0	Lower Stage Planetary
28	0	0	0	0	0	0	Upper Stage Planetary
29	0	7.08	6.9	6.9	6.1	0	
30	0	11.9	5.86	6.0	4.7	0	
31	0	11.5	5.3	5.3	3.4	0	
32	2148.7	7.955	5.625	11.22	3.25	0	
33	2656.5	1.235	11.251	13.109	0	0	
34	0	2.0	10.919	10.919	0	0	
35	0	10.88	8.178	9.0	0	0	
36	51673.3	21.406	18.25	18.25	16.624	0	
37	51673.3	15.75	8.178	9.00	0	0	
38	0	3.0	8.25	8.25	0	0	
39	0	2.75	9.333	9.333	0	0	Remainder of
40	0	4.62	9.752	12.7967	0	0	Torque Loop
41	0	1.53	6.985	6.985	0	0	in Test
42	0	2.03	7.483	10.433	0	0	Stand
43	0	0.69	8.25	8.25	0	0	
44	0	1.0	11.5	11.5	0	0	
45	4.885E6	0	0	0	0	0	
46	0	1.4	5.834	5.834	0.625	0	
47	0	2.6	6.30	9.3425	0	0	
48	0	0.69	7.04	7.04	0	0	
49	0	0.87	9.0	9.0	0	0	
50	52347.3	11.75	8.02	20.0	0	0	
51	0	1.44	5.89	6.758	0	0	
52	0	6.62	7.0	9.218	0	0	
53	0.72786E6	0	0	0	0	0	

Since the excitations of interest occur inside the test gearbox, the first step was to simplify the torsional model by removing, in successive steps, those portions of the drive branch and torque loop which were furthest from the test gearbox. Such a procedure is fully justified at the frequencies of interest since mesh-frequency vibrations propagate only a short distance into relatively large inertial elements of the type found in this drive train. The process of system simplification may be carried out only to the point at which changes begin to appear in those elements of the system which are of concern. Naturally, the fewer the system elements, the lower the cost of the calculations.

As a result of the above procedure, it was possible to remove the drive motor and speed clutch, the bevel gearbox which closes the torque loop, the torque device, and the majority of the helical gearbox from the system. The resulting simplified torsional model thus begins at the bevel gear driving the transmission input sync shaft, and ends at the input to the helical gearbox. A summary of the torsional model is contained in Table 3.

Table 3 includes the addition to the nominal gearbox drive train components of a torsional system branch to account for the torsional characteristics of a Himmelstein Rotary Transformer, Type 3-08, used to obtain readings from sensors rotating with the input gear. Further, the torsional system branch representing the lower end of the first stage sun gear shaft has been extended to account for the drive shaft and Himmelstein Rotary Transformer Type-2-16 used to obtain readings from sensors rotating with the sun gear. The remainder of the gearbox components, including the two planetary reduction stages, are modeled exactly as in a nominal gearbox.

Calculated Results

Gear Mesh Excitation Calculations - Since severe noise components are known to exist at the first-stage planetary and bevel mesh frequencies, excitation calculations were performed for these two meshes. Maximum torque on the gearbox was taken to be 1.06×10^6 lb-in. At 243 rpm on the output shaft, this is equivalent to a power level of 4080 hp. Steady-state tooth forces are as shown in Table 4.

Calculations of peak tangential excitation were performed for the tooth force levels shown in Table 4 for the first-stage planetary sun-to-planet and planet-to-ring meshes, and for the spiral bevel gear mesh. Results of these calculations are shown in Figures 28,29,and 30, respectively.

Note the variations of the calculated excitation with changes in tooth force in the two first-stage planetary spur gear meshes under consideration (Figures 28 and 29). These variations may be contrasted with the straight-line nature of the curve obtained for the spiral bevel mesh as shown in Figure 30. The differences are due to the approximations made for the bevel gear in which it is converted to an equivalent helical gear and subsequently to an equivalent spur gear. These approximations make the bevel mesh excitations considerably less rigorous than those for the spur gear meshes, and consequently less detail is included in the prediction. The major difference is that the equivalent spur gear is assumed to have a nominal involute tooth profile.

TABLE 4. TANGENTIAL TOOTH FORCES AT VARIOUS TORQUE LEVELS FOR CH-47 GEARBOX MESHES

Percent of Torque	Torque (in.-lb)x10^6	Spiral Bevel Mesh Tooth Force (lb)	1st Stage Planet Tooth Force (lb)	2nd Stage Planet Tooth Force (lb)
100	1.06	10,780	5,424	12,113
90	0.96	9,700	4,881	10,901
80	0.85	8,550	4,290	9,590
70	0.75	7,600	3,820	8,520
60	0.64	6,468	3,254	7,268
40	0.42	4,312	2,170	4,845

Torsional Response Calculations - Torsional response of the drive train may be predicted in several different ways. As a minimum, tooth dynamic forces should be calculated at each mesh frequency of interest with the proper excitation amplitude applied at the proper mesh location. Alternatively, response may be predicted using unit excitation over a frequency range in order to identify resonances.

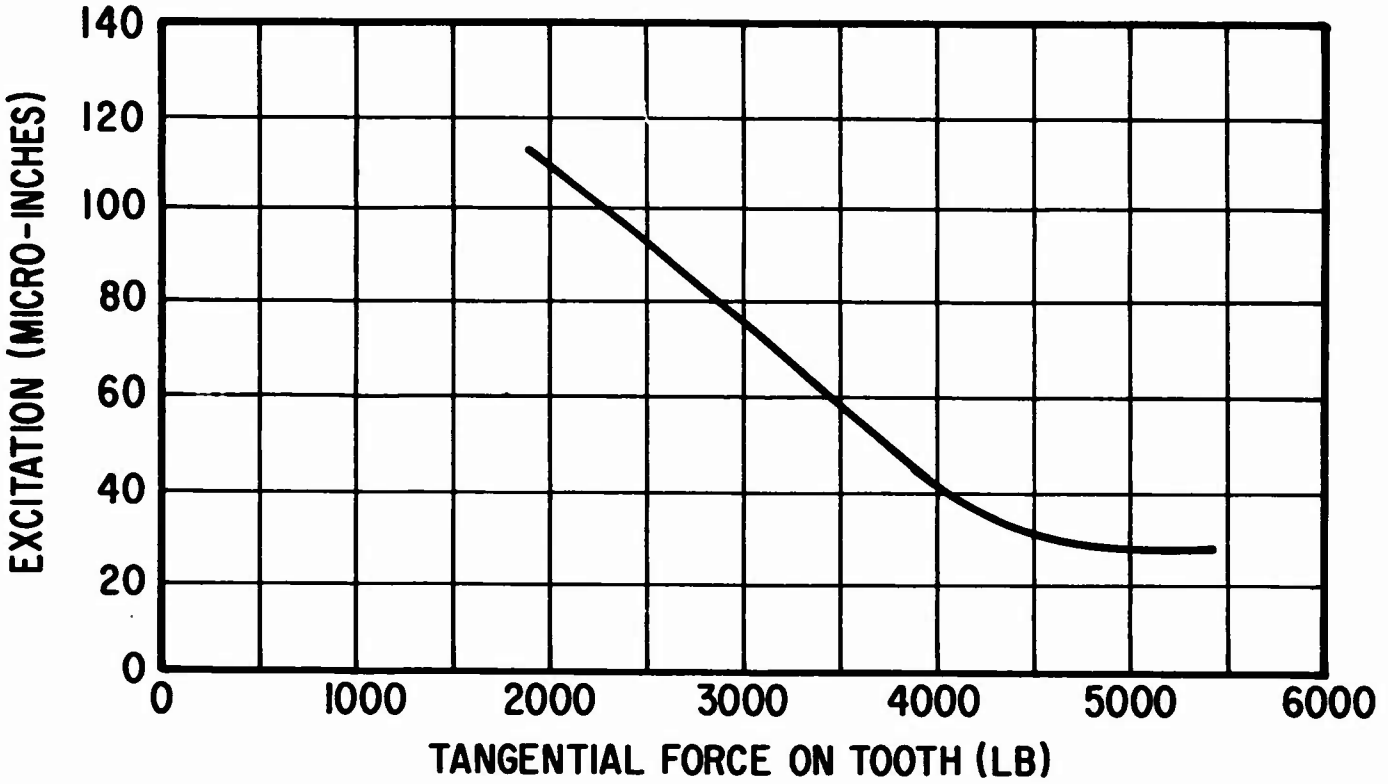

Figure 28. Peak Tangential Excitation Versus Tangential Tooth Force in Sun-Planet Mesh in CH-47C Forward Rotor-Drive Transmission Lower Planetary Reduction - Fundamental Component.

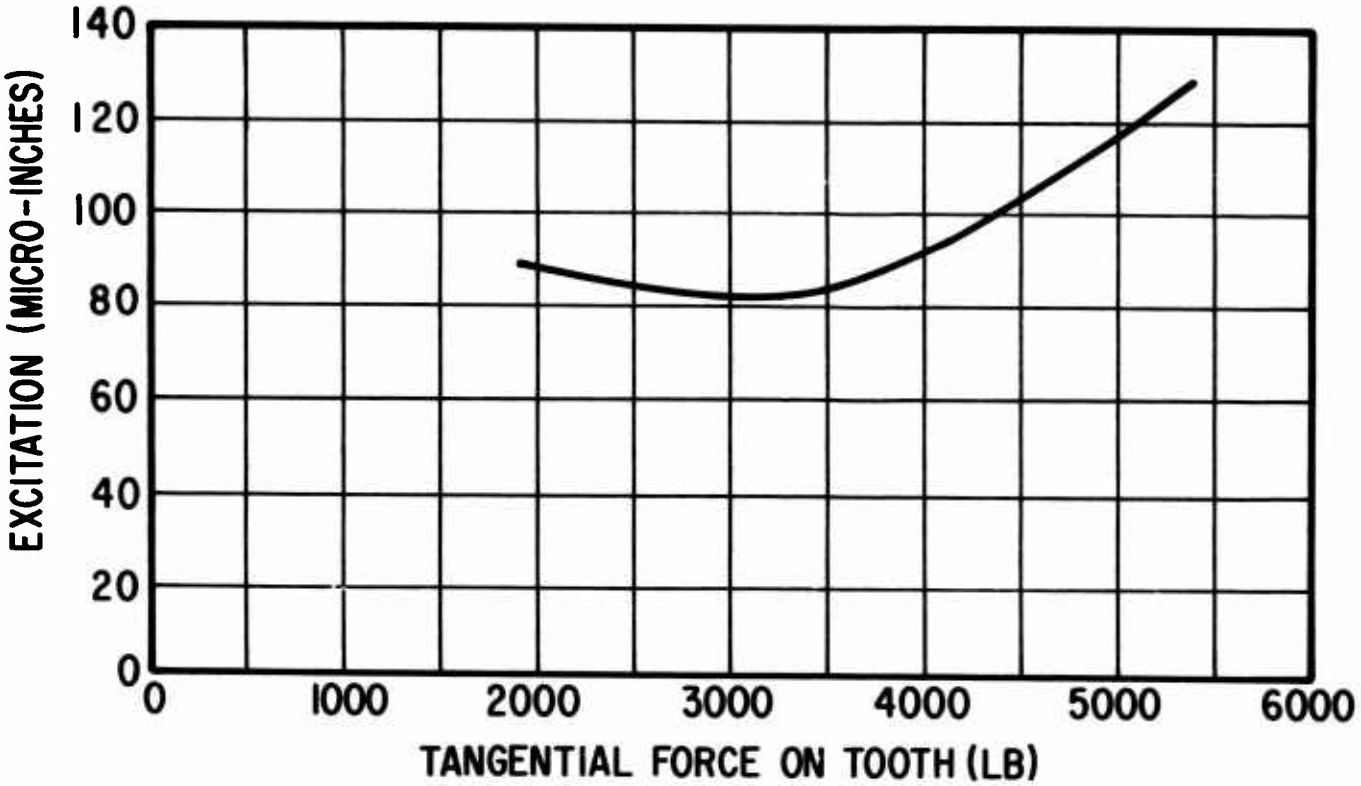

Figure 29. Peak Tangential Excitation Versus Tangential Tooth Force in Planet-Ring Mesh in CH-47C Forward Rotor Drive Transmission Lower Planetary Reduction - Fundamental Component.

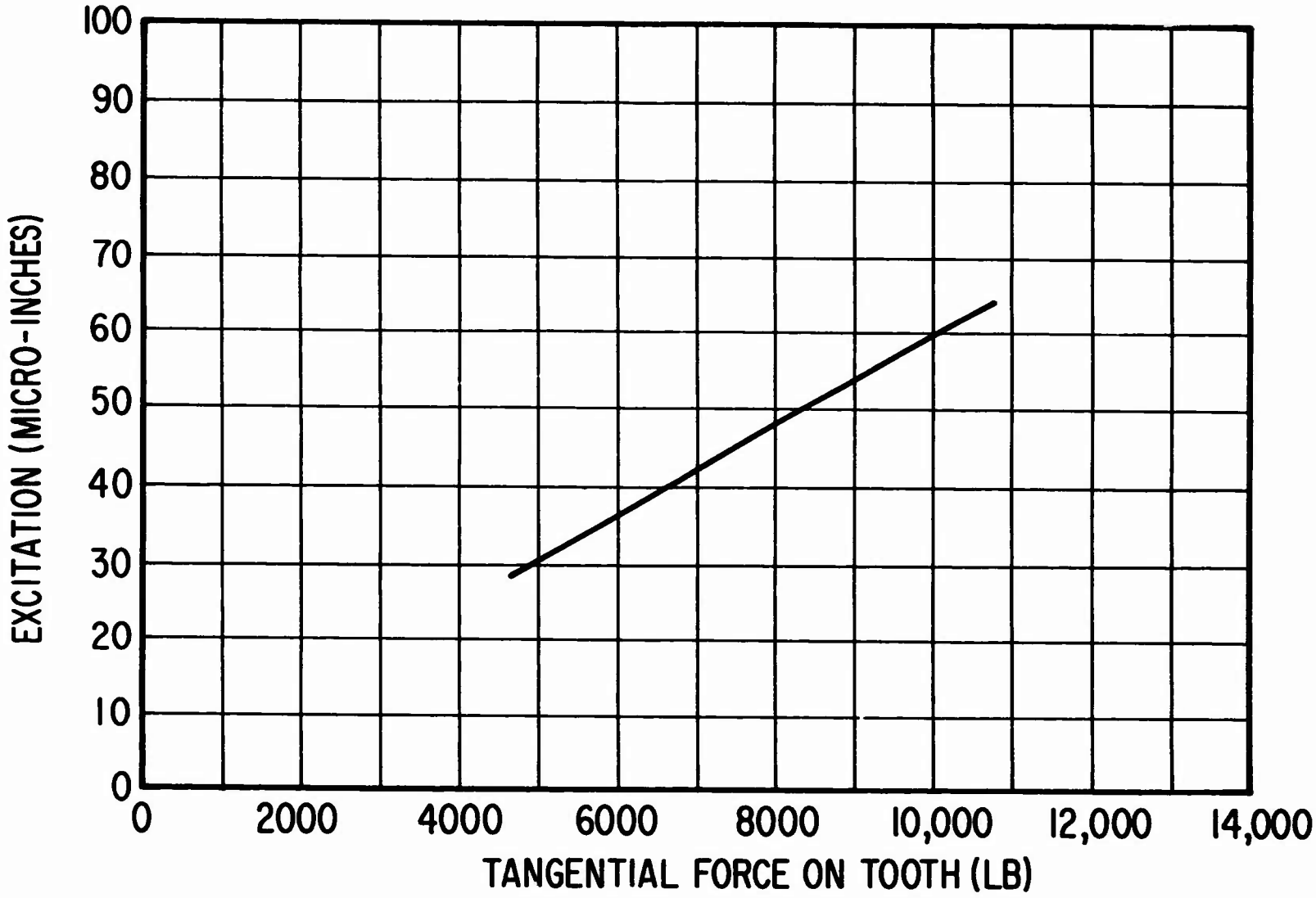

Figure 30. Peak Tangential Excitation Versus Tangential Tooth Force in CH-47C Forward Rotor Transmission Bevel Mesh - Fundamental Component.

A combination of the foregoing options has been selected for the test gearbox. First, excitation levels predicted to act at each of the several mesh frequencies have been utilized as inputs. Second, a large frequency range has been swept using these excitations in order to determine force and amplitude peaks--the system torsional natural frequencies. The resulting tooth dynamic forces are thus realistically close to those which would be anticipated for frequencies reasonably near the mesh frequency.

Figure 31 presents the results of the torsional response calculations in terms of the bevel gear peak dynamic tooth force for bevel gear excitations which are predicted to act at 80 percent of maximum torque (0.848×10^6 lb-in.). It should be noted that six torsional natural frequencies are thus identified, with the bevel mesh frequency predicted to lie between the fifth and sixth frequency so noted. At a frequency of 3412 Hz, a peak dynamic tooth force of about 1000 lb is predicted to act; this force decreases to about 850 lb at 3390 Hz.

The foregoing procedure was repeated for torque levels of 40 percent, 60 percent, 90 percent, and 100 percent with essentially no differences noted in the location of the critical speeds. This is because the effects of changes in tooth mesh compliance (variable with load) are not severe over the range of loads considered. The force levels do change proportionally to the excitation levels at the other torques. Note that the torsional response is independent of bearing stiffness, which also varies with load.

It is also of considerable interest to examine the predicted torsional mode shapes which occur under the action of the gear tooth excitations. This information, particularly when obtained at frequencies near a torsional natural frequency, will disclose which portions of the gear train are resonant and contributing to high dynamic tooth loads.

In the case of the test gearbox, torsional mode shapes are of greatest interest at the gear mesh frequencies, particularly at that of the bevel gear, since it is at these frequencies that the most severe noise components are produced. Figure 32 shows the system torsional mode shape obtained for excitation at the 80 percent torque level at the bevel gear mesh frequency when input shaft speed is 7060 rpm. As is apparent from Figure 32, peak torsional amplitudes are predicted to occur at opposite ends of the input bevel pinion shaft (stations 10 and 16) and between the bevel gear and sun gear locations (stations 24 and 27) on the first-stage sun gear shaft. Moreover, a node is predicted to occur at the bevel gear mesh location (between stations 16 and 24).

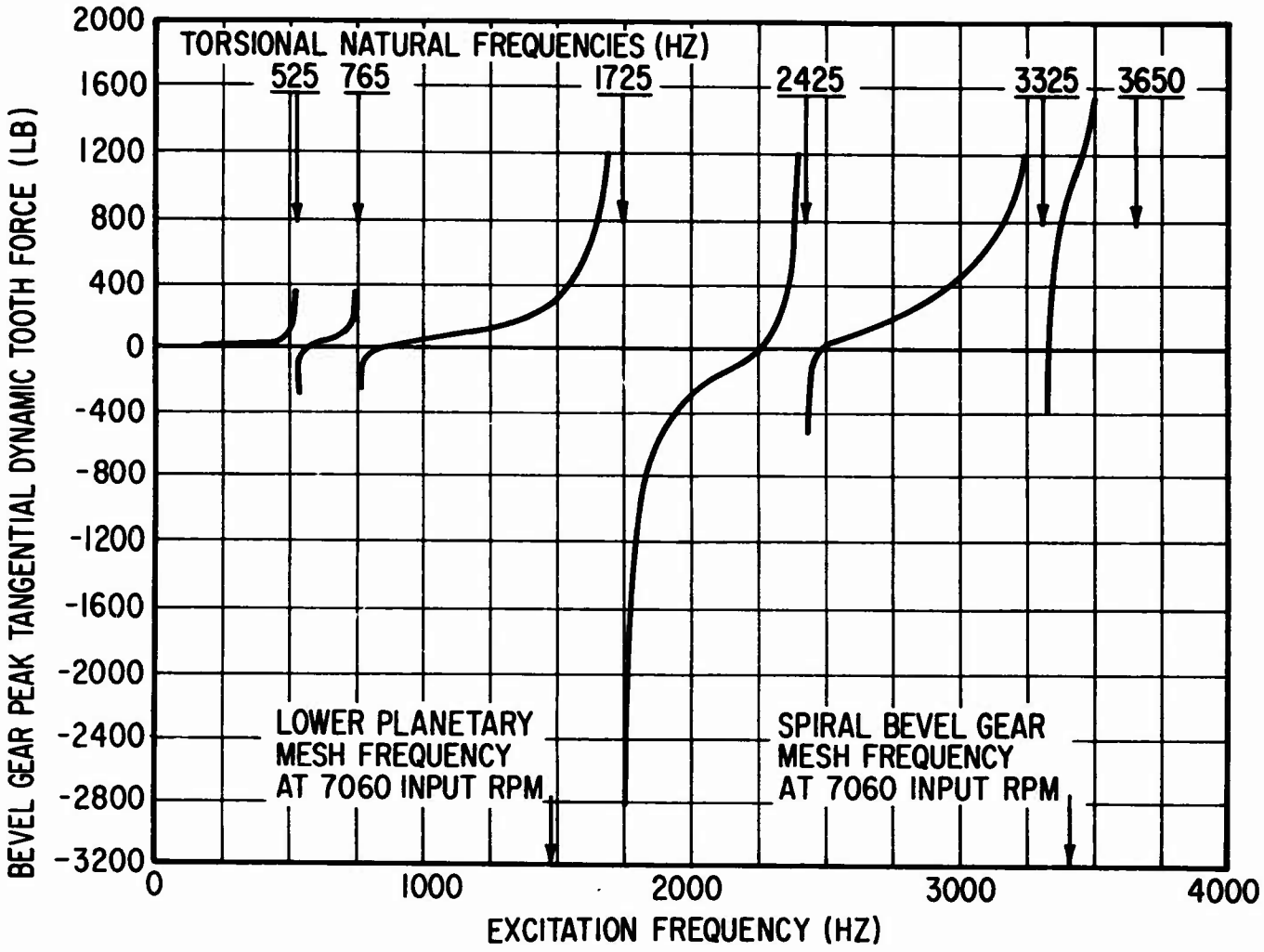

Figure 31. Peak Bevel Gear Tooth Tangential Dynamic Force Versus Excitation Frequency With Excitation in Spiral Bevel Mesh. CH-47 Forward Rotor Drive Gearbox in Boeing Vertol Test Stand. Excitation Calculated for 80 Percent Maximum Torque (848,000 Lb-In. Output).

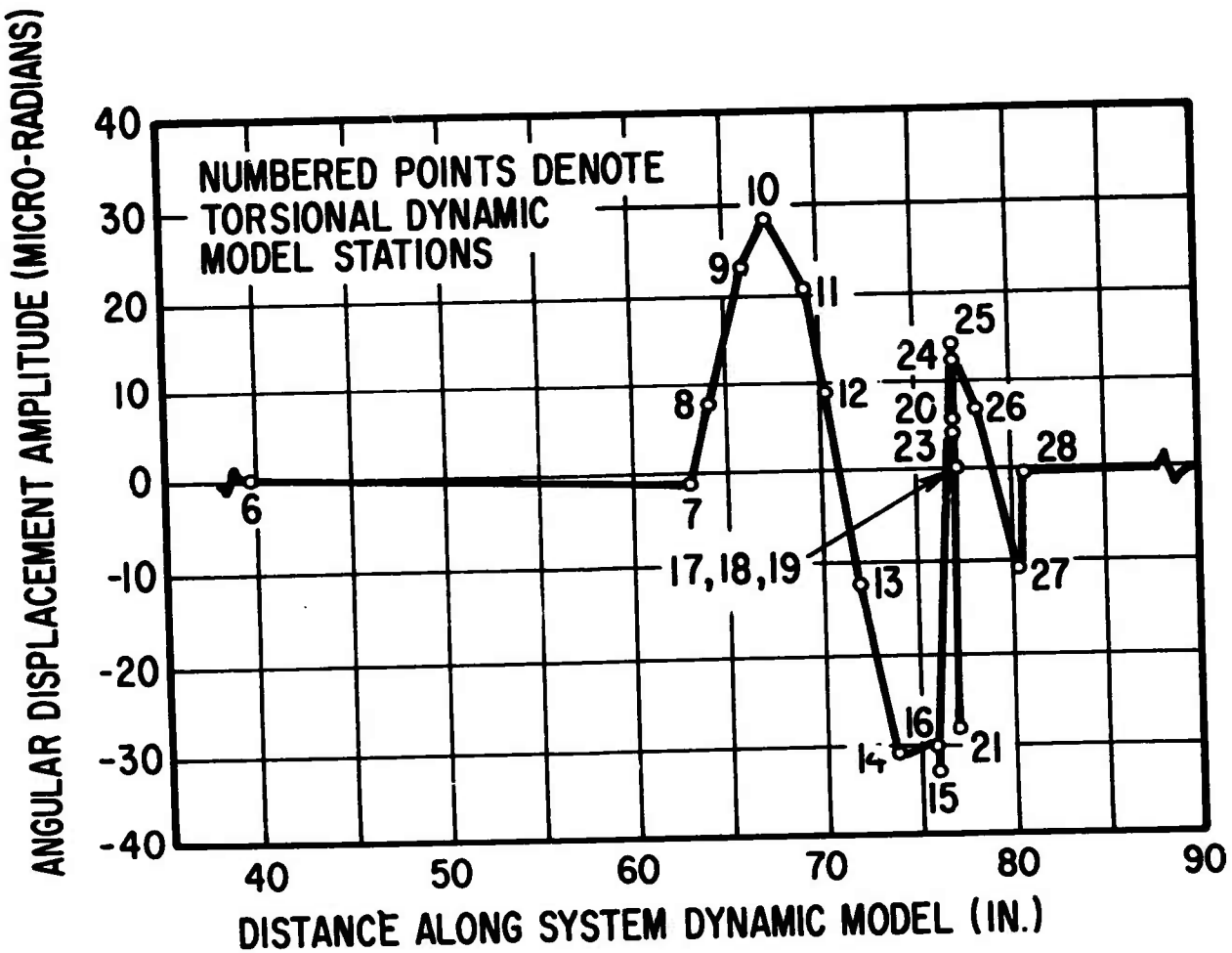

Figure 32. Angular Displacement Versus Position Along Drive Train for Excitation at Bevel Mesh Location at 3412 Hz (Input Speed = 7059 rpm) for 80 Percent Torque Condition.

Similar calculations have been carried out for other torque levels, resulting in curves very similar to Figures 31 and 32. The dynamic tangential bevel gear tooth force produced at 3412 Hz over the range of torques is summarized in Figure 33.

Similar response calculations have been performed with excitation in the first-stage planetary meshes. The dynamic tangential planet-to-ring gear tooth force produced over the torque range at 1482 Hz (the first-stage planetary mesh frequency when input shaft speed is 7060 rpm) is summarized in Figure 34. Note that there is a pronounced minimum value in these predicted dynamic forces, a phenomenon which is probably due for the most part to the shape of the corresponding excitation curve. Reference to Figure 31 does not disclose rapid force level changes in the region of the first-stage planetary mesh frequency. Such changes, which would be caused by close proximity of a torsional natural frequency to the mesh frequency, would be important because of the slight differences between Figure 31 type plots.

In addition to the dynamic force and torsional amplitude quantities described above, the torsional response computer program (TORRP) also yields peak dynamic torque predictions at each element of the dynamic model. These quantities have been extracted from the calculations for the locations at which the torque strain gage bridges are located, and are plotted in Figures 35 and 36 versus torque level for the input bevel gear shaft and first-stage planetary sun gear shaft, respectively.

In addition to these quantities, the acceleration levels corresponding to the peak dynamic angular amplitude predictions for the location of the rotating accelerometers inside the first-stage planetary sun gear have been calculated. These results are shown in Figure 37 versus torque level.

The information shown in Figures 35, 36, and 37 has been obtained with excitations at the corresponding mesh locations and frequencies and at the levels predicted by earlier analysis. Thus, for instance, at any strain gage location, the dynamic torque component at 1482 Hz would result from response calculations performed with tooth mesh excitations applied at the proper levels at the first-stage planetary reduction meshes. Similarly, the component at 3412 Hz would result from tooth mesh excitations applied at the bevel gear mesh. It should be noted that these forces and frequencies are not representative of the CH-47C transmission at normal operational speed (7460 rpm rather than 7060 rpm used above).

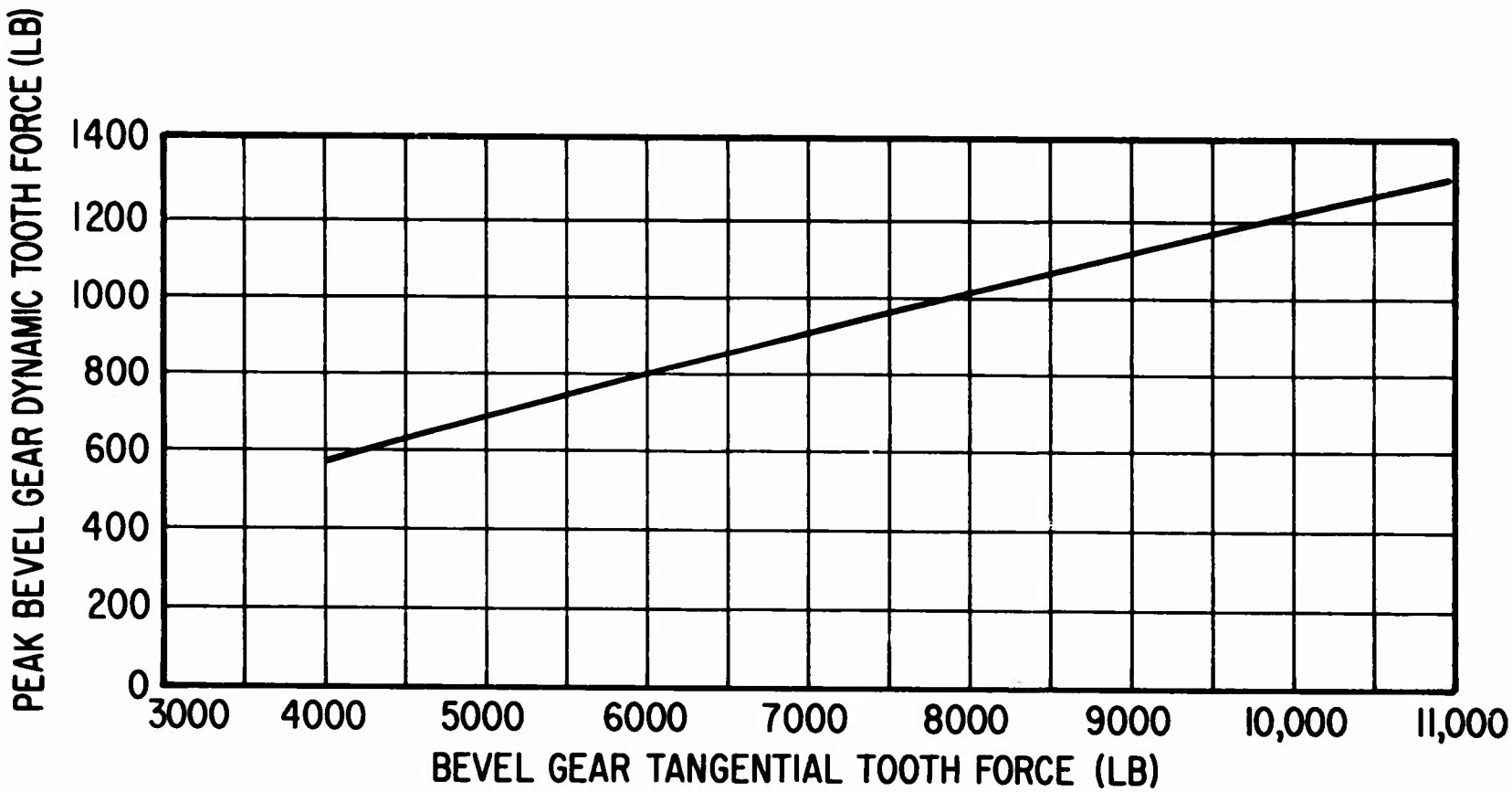

Figure 33. Peak Dynamic Tooth Force (Tangential Component) at Spiral Bevel Mesh. Excitation at Spiral Bevel Mesh at 3412 Hz.

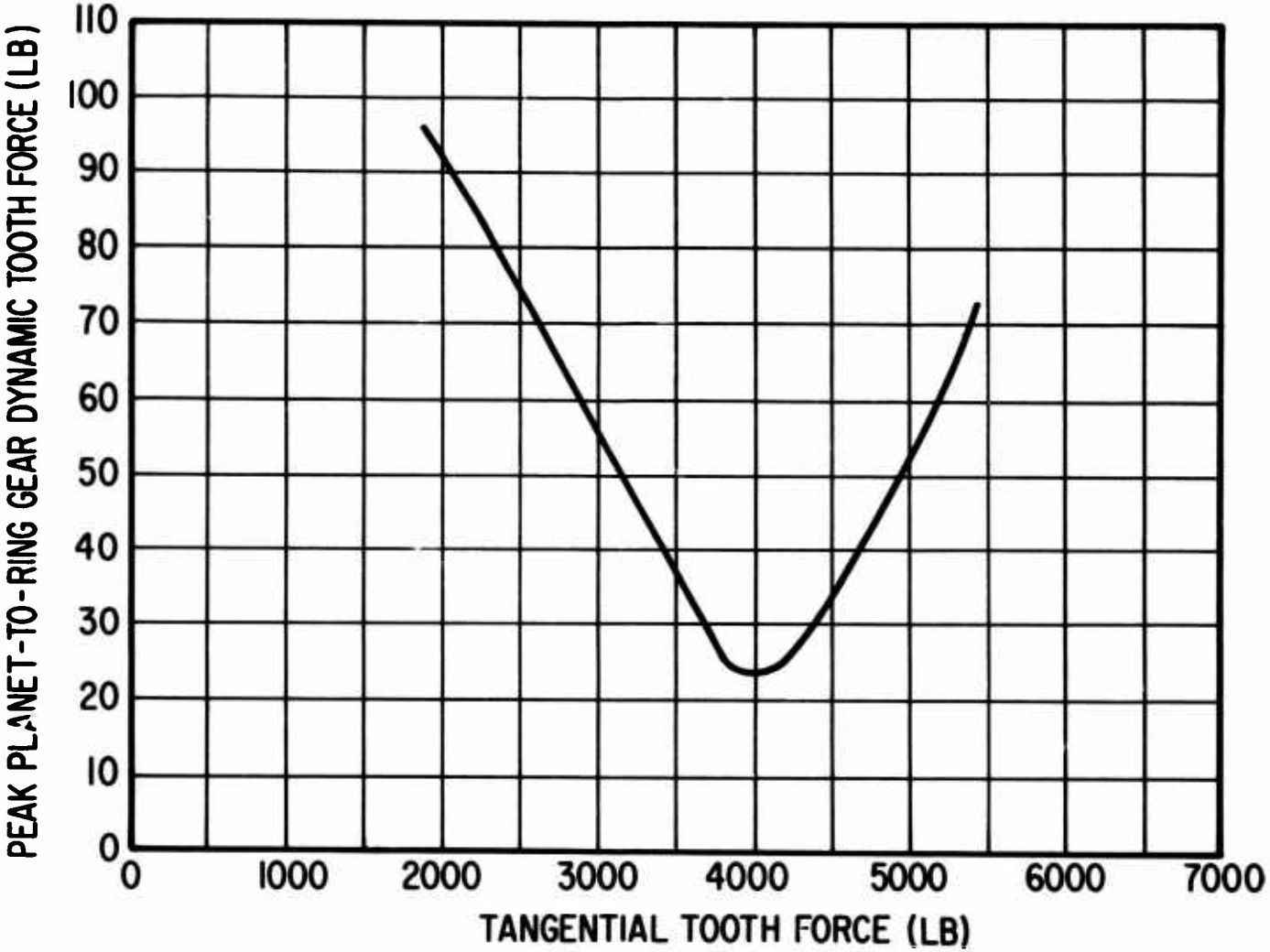

Figure 34. Peak Dynamic Tooth Force (Tangential Component) at Each Lower Planet-to-Ring Mesh Point. Excitation at Lower Planetary Meshes at 1482 Hz.

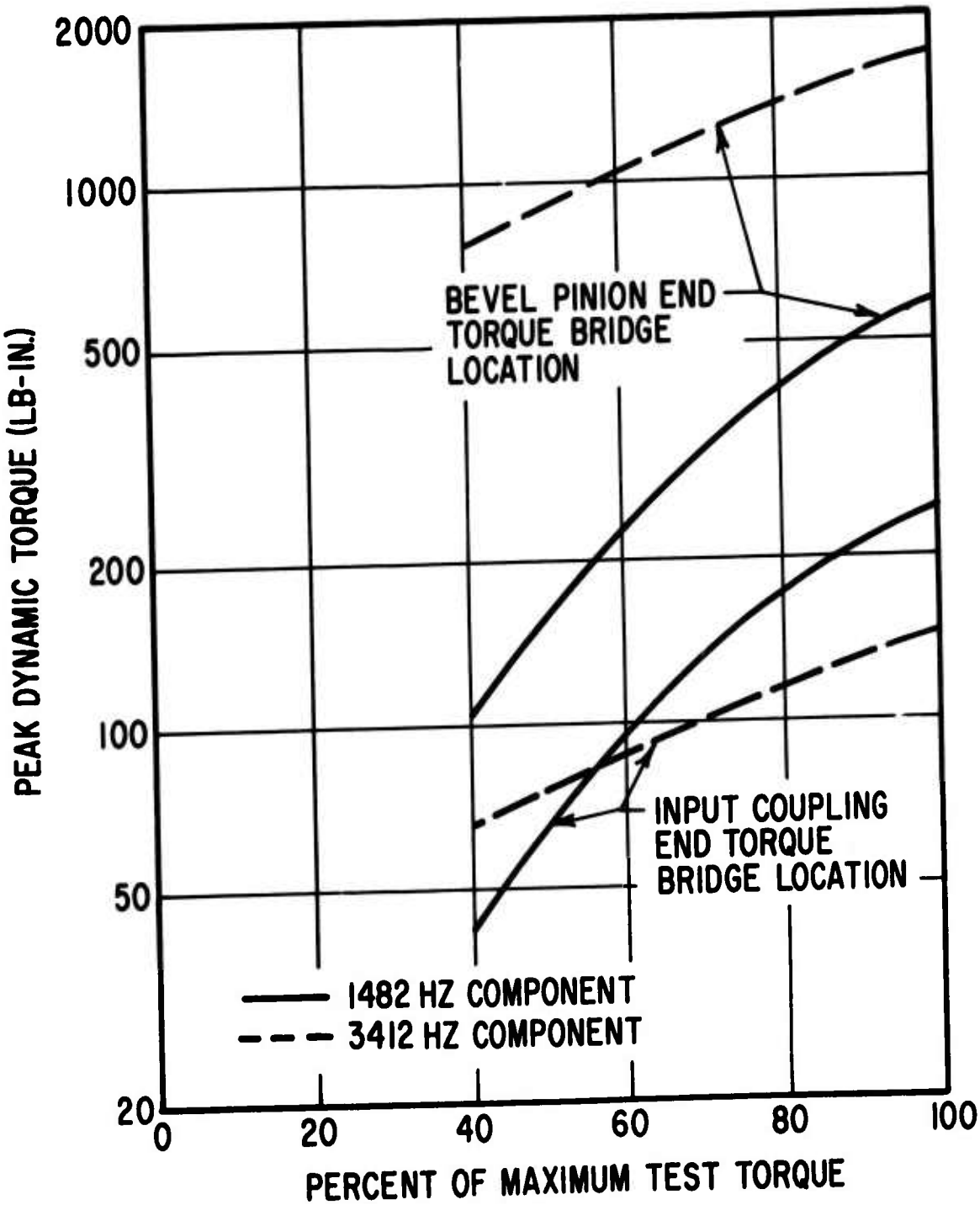

Figure 35. Predicted Peak Dynamic Torque Versus Percent of Maximum Steady-State Torque on Input Spiral Bevel Shaft. Input Shaft Speed = 7059 rpm.

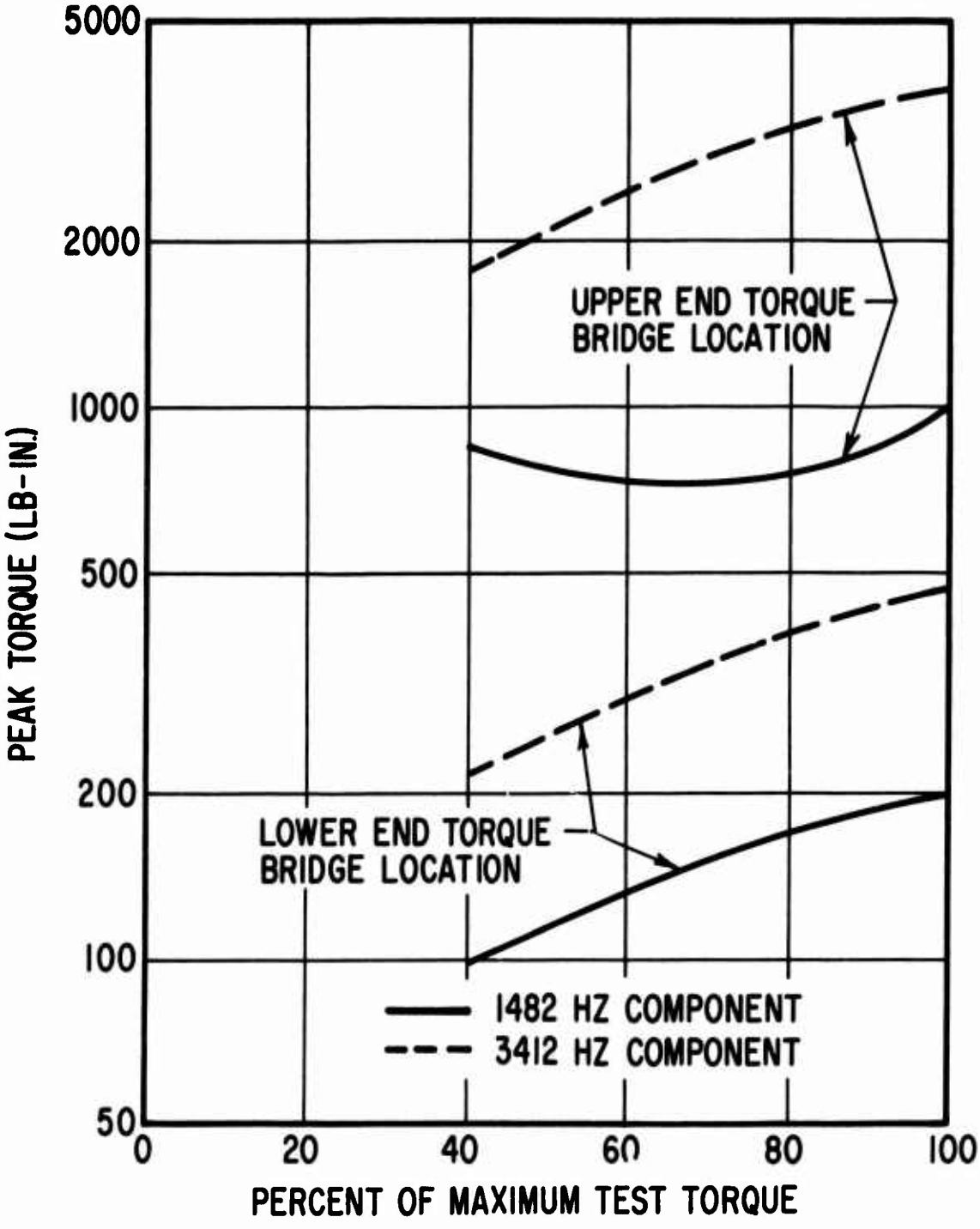

Figure 36. Predicted Peak Dynamic Torque Versus Percent of Maximum Steady-State Torque on Lower Planetary Sun Gear Shaft. Input Shaft Speed = 7059 rpm.

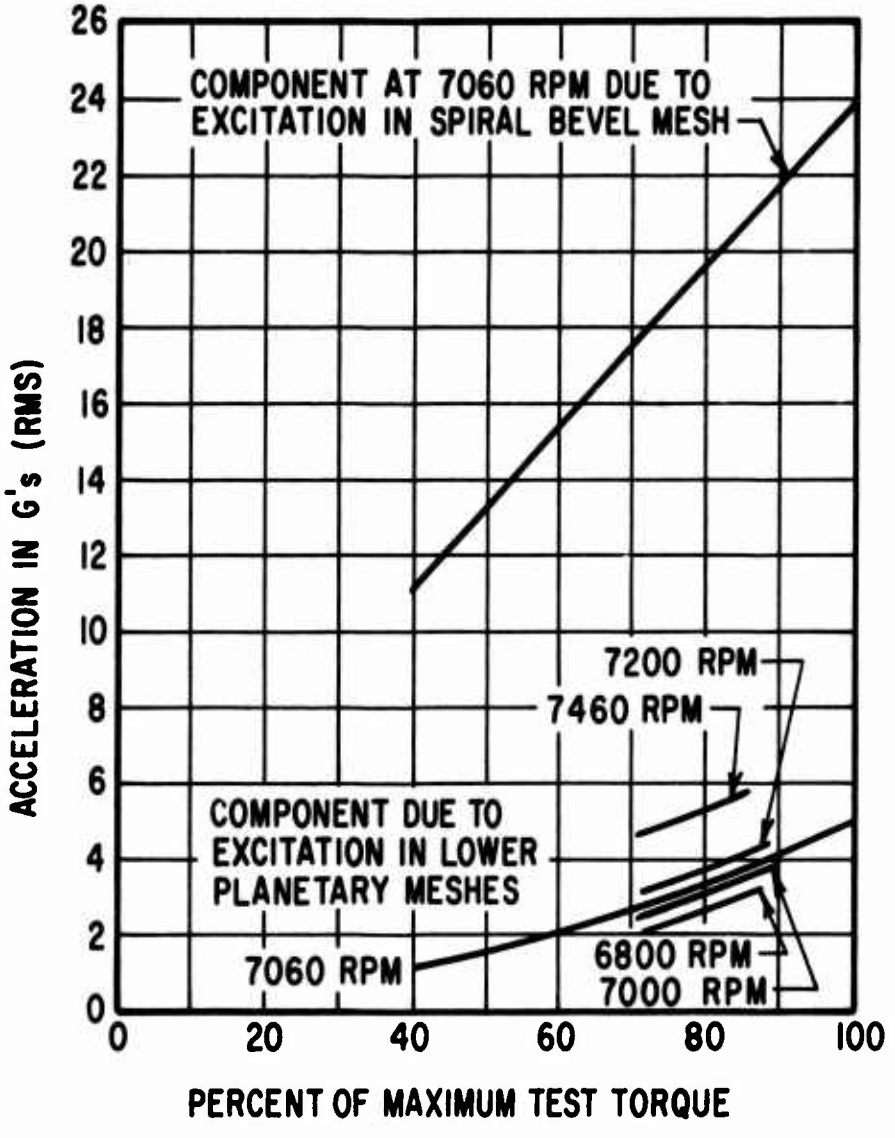

Figure 37. Calculated Tangential Acceleration at Lower Planetary Sun Gear Rotating Accelerometer Locations for Indicated rpm on Input Shaft.

Noise Level Predictions - Finally, as described in the section entitled "Empirical Noise Level Predictions", noise level predictions were made. In these calculations, which were made for a range of values of the empirical "Energy Conversion Factor (α)", the gear tooth excitations and dynamic forces at the bevel and the first-stage planetary reduction mesh frequencies were taken as inputs for the 80 percent torque condition. Owing to the fact that considerable test data had been reduced at 7000 rpm on the input shaft (3390 Hz bevel mesh frequency and 1470 Hz first-stage planetary mesh frequency), the dynamic force predictions described earlier were repeated for the slightly lower frequencies and the resulting dynamic force levels used. In the calculations, it was assumed that the microphone was located approximately 1 foot from the noise source (the assumptions accompanying the noise level calculations as discussed in References 4 and 9 should be briefly reviewed here). The "Environment Factor (β)" was taken to be 1.0. The results of the calculations are presented in Figure 38.

Comparisons of Calculated and Test Results - The gearbox test instrumentation system has been designed to provide information which may be compared with calculated data at a number of points in the analysis sequence. For instance, during the variable speed sweep runs, distinct peaks were observed in all recorded signals. The speeds at which these peaks occur, and particularly the values of the gear mesh frequencies at these speeds, may be compared directly to the frequencies at which peaks occur in the calculated response data. Alternatively, the measured speed peaks could be compared directly with calculated torsional natural frequency values if these are obtained separately. The former comparison was made in the present case.

During both sweep and steady-state gearbox operation, drive train torsional vibration test data was taken by means of accelerometers and torsion strain gages which rotated with the sun gear shaft, and by means of torsion strain gages which rotated with the bevel gear shaft. The rotating accelerometer data is particularly well suited to comparison with calculated results on a component-by-component basis. The calculated torque levels must, on the other hand, be converted to strain readings at the torsion strain gage locations for direct comparisons of these quantities. Therefore, the rotating accelerometer data was used for purposes of comparison with calculated torsional data.

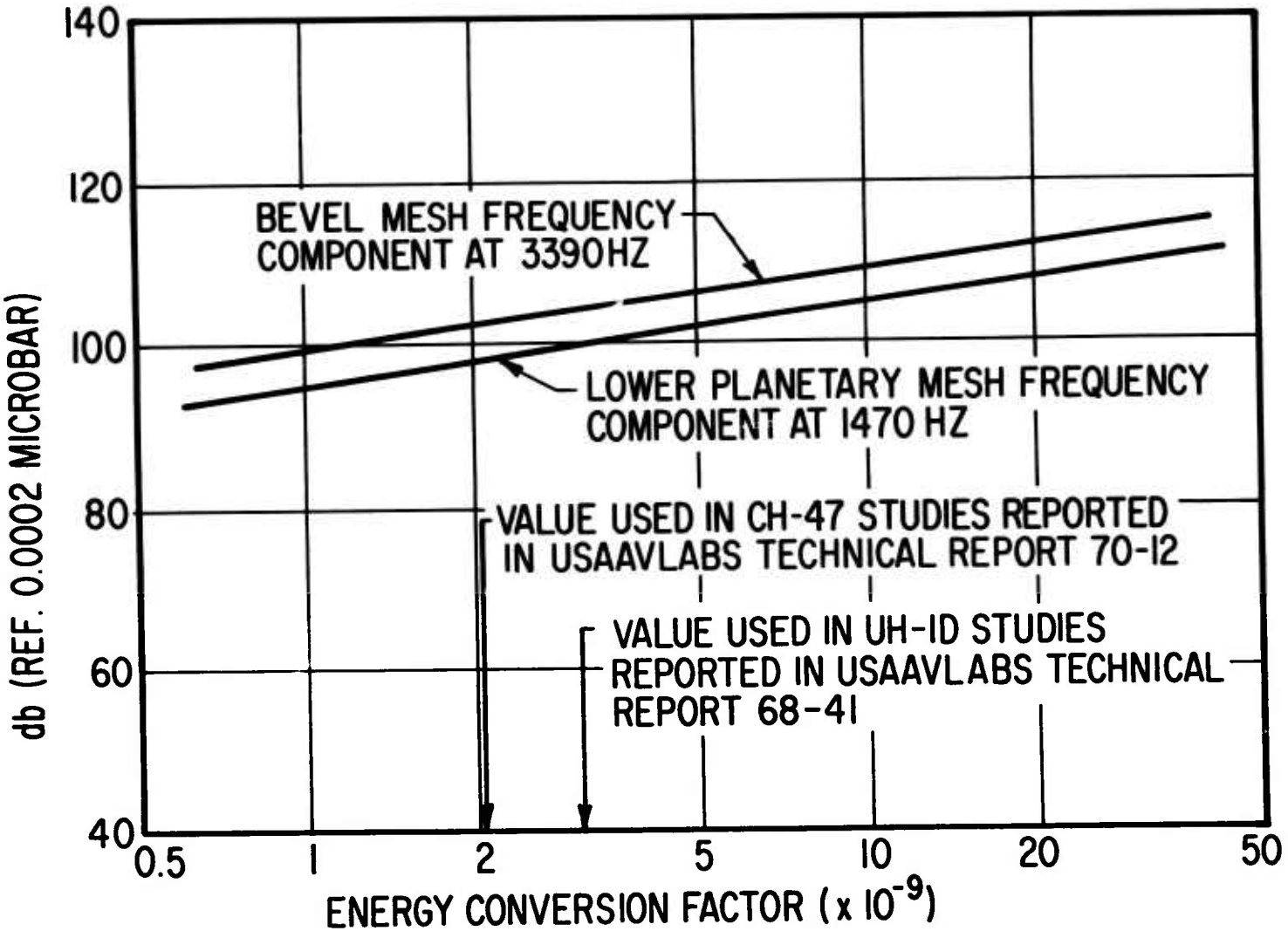

Figure 38. Calculated Noise Levels for Indicated Mesh Frequency Components at 80 Percent Torque Conditions and 7000 rpm Input Speed.

Noise levels external to the gearbox (but within the acoustic enclosure) were also measured over the complete range of test conditions. This data is also suitable for comparison with emiprically-calculated noise data.

Torsional Natural Frequencies - Reference to the rather voluminous sweep data obtained during the test program, and in particular that data reduced for the 80 percent torque condition, indicates rather pronounced signal peaks in three speed regions. At about 4700 rpm on the input shaft, groups of sensors exhibit peaks for the bevel mesh frequency component (at about 2300 Hz). This condition is thought to result from excitation of either the fourth system torsional critical speed (see Figure 31) or one of the predominantly bevel gear shaft related lateral critical speeds. (Recall that lateral critical speeds are calculated subsequent to the torsional criticals in the present analysis sequence. They are discussed in the section entitled "Analytical Approach to Predicting Response".

At about 6400 rpm on the input shaft, other groups of sensors exhibit peaks for the lower stage planetary mesh frequency component (at about 1350 Hz). This condition is thought to result from excitation of a predominantly sun gear shaft axial critical speed since no torsional critical speed is predicted to occur in this frequency range.

Finally, at about 7000 rpm on the input shaft, other groups of sensors exhibit a major peak for the bevel mesh frequency component (at about 3400 Hz). This is thought to result from excitation of the fifth system torsional critical speed (see Figure 31) by the bevel mesh disturbances. This in turn excites large lateral displacement of both the sun gear and the bevel gear (see Figures 45 and 46).

Demonstration of close correspondence between two major measured system resonance frequencies and the two calculated system torsional critical speeds in that speed range is considered to be a major step in the validation of the analytical mesh-frequency vibration prediction procedure. It is anticipated that later comparisons of mode shapes, vibration amplitudes, and the like will further add to this validation.

Acceleration Amplitudes at Sun Gear - Steady-state test data at the 80 percent torque condition was acquired at a number of gearbox operating speeds. Detailed data was recorded at 6800, 7000, 7200, and 7460 rpm, among other speeds. Accelerometer data at 7000 rpm from rotating

accelerometer number 2 (SGRA2) was selected for comparison with the predicted accelerations at this location (see Figure 37).

With input shaft speeds between 6800 and 7460 rpm, the bevel mesh frequency lies between 3290 Hz and 3610 Hz, respectively, and the lower stage planetary mesh frequency between 1430 Hz and 1565 Hz, respectively. Reference to Figure 31 discloses that the system operation is such that the bevel mesh frequency lies between the fifth and sixth torsional critical speeds and the lower stage planetary mesh frequency between the second and third torsional critical speeds. The system response may thus be expected, in general, to exhibit higher amplitudes and forces at higher frequencies and vice versa; and this is, in fact, the case. This effect is displayed in Figure 37 for the lower stage planetary component acceleration levels at the 80 percent torque condition.

Measured data obtained from rotating accelerometer number two yielded predictions of 2.94g (rms) for the lower stage planetary mesh component at 7000 rpm on the input shaft. Reference to Figure 37 will disclose that this result compares very well with the calculated data. In evaluating this result it should be remembered that:

1. The response predictions depend directly upon the excitation level (a calculated quantity which is produced by computer program GEARO). This program treats spur gears (such as those in the lower stage planetary) rigorously. On the other hand, spiral bevel meshes are treated only very approximately through equivalent spur gear models. Partial evaluation of the effectiveness of this spiral bevel modeling procedure has been done implicitly in part through the noise and response prediction to be described below. A complete evaluation must remain the subject of a separate investigation.

2. The foregoing comparison has been obtained through the use of data from only one rotating accelerometer. Additional correlation of the shaft vibration amplitudes of the sun gear and bevel gear shafts, discussed in the section entitled "Damped Forced Response (D-82)", also revealed very good comparison of predicted and measured results.

In light of the positive nature of the foregoing comparisons, it is concluded that the gear excitation and torsional response calculation procedures are performing satisfactorily their intended function, which is the prediction of torsional response due to spur gear mesh excitations. While important trends relative to spiral bevel mesh induced behavior may be and have been inferred by the use of the analysis, it is felt that a detailed study of existing bevel mesh frequency test results, and eventually a more rigorous treatment of spiral bevel mesh properties, is warranted.

Similarly, it is clear that an important portion of the gear mesh excitation dynamic problem may be treated by the computer program TORRP: in particular, the system response due to dynamic excitations introduced by planetary meshes. The response of a system containing unbalanced gear meshes (single meshes or nonphased planetary meshes) may, on the other hand, consist of coupled torsional-lateral (and even axial) vibrations. Rigorous treatment of this class of problem requires an extension of the existing response program. While the Damped Forced Response Program(D-82) has demonstrated considerable merit with regard to the coupled vibration problem (to be discussed in the section entitled "Analytical Approach to Predicting Response"), it is dependent on the computer program TORRP for several of its inputs. Also, the D-82 Computer Program does not address itself to rotational effects. It is instead anticipated that considerable benefits will be derived through incorporation of computer program TORRP with existing one or two dynamic level rotor response programs of the type used for nonsynchronous forced vibration response studies in rotating systems. The ease of preparing input for such a program together with its computational speed (Myklestad-Prohl-Lund matrix method) could yield a powerful design tool.

Noise Levels - As described above, steady-state test data at the 80 percent torque condition included a substantial amount of noise data. For comparison purposes, the data recorded at microphone location 5 was used. Narrow-band reduction of this data at 7000 rpm yielded readings of 98 dB for the lower stage planetary mesh frequency component and 101 dB for the bevel mesh frequency component.

Calculations for comparison with these values were conducted by means of the analysis reported in References 4 and 9, in which gear mesh excitations and dynamic tooth force levels appear as input quantities.

The excitations are obtained from computer program GEARO, and the dynamic tooth forces are obtained from computer program TORRP.

In order to provide an added dimension to the comparison, the predictions were repeated for a range of energy conversion factors as described earlier. Examination of results shown in Figure 38 shows relatively low variability of results with changes in the energy conversion factor, and comparison of measured results with predictions shows quite good correlation for the value of the energy conversion factor used in CH-47 studies.

In spite of the fact that the noise level procedure required the use of factors (α and β) which are not well understood, it appears to have significant utility.

DAMPED FORCED RESPONSE (D-82)

Forced Response - Helicopter vibration from excitation by rotor loads has been of primary concern in the design of the air frame. Much effort has been expended on the development of computer techniques to assist in the design of a structure with acceptable vibration levels. As a result of this program, the techniques developed for structure have been transferred to the transmission system. The Damped Forced Response (or Unified Structural Analysis) computer program (D-82), developed by J. Sciarra for the dynamic analysis of a helicopter fuselage, has been extended for this purpose.

The D-82 computer program[13,14] is capable of calculating the dynamic characteristics for a large, complex structure. A typical helicopter transmission math model usually contains over 250 structural elements. (A math model of the CH-47 forward transmission is illustrated in Figure 39.)

The major steps involved in the analysis are:

---

[13]J. Sciarra and R. Ricks, USE OF THE FINITE ELEMENT DAMPED FORCED RESPONSE STRAIN ENERGY DISTRIBUTION FOR VIBRATION REDUCTION, Presented at the ARO-D Military Theme Review, The Helicopter and V/STOL Aircraft Research Conference, Moffett Field, California, September 1972.

[14]J. Sciarra, A COMPUTER METHOD FOR DYNAMIC STRUCTURAL ANALYSIS USING STIFFNESS MATRICES, Journal of America, Vol. 6, No. 1, January-February 1969, pp. 3-8.

(1) Generation of a finite element structural idealization and discrete mass model (as described in the section entitled "Shafts-Modeling").

(2) Formulation of the complete transmission system stiffness matrix.

(3) Reduction in the stiffness matrix of the unloaded nodal degrees of freedom to the loaded nodal degrees of freedom (mass points).

(4) Dynamic matrix generalization combining mass and stiffness properties.

(5) Determination of eigen solutions.

(6) Calculation of dynamic tooth loads from system torsional response analysis (i.e., TORRP R-32).

(7) Formulation of dynamic equations considering a nodal representation of the transmission.

(8) Solution for the dynamic damped response resulting from the excitation of the vibratory tooth loads.

Regarding structural damping, a 3% damping ratio, which is an empirical number, has provided the best correlatable results to date. Some of these correlations have been for helicopters in flight, for nondestructive rotor blade resonance tests, and as part of this test program.

The damped forced response is the normal mode solution to the matrix equation

$$[M]\{\ddot{X}\} + [C]\{\dot{X}\} + [K]\{X\} = \{F_S\} \sin \Omega t + \{F_C\} \cos \Omega t$$

where $[M]$ = Mass matrix
$[C]$ = Damping matrix
$[K]$ = Stiffness matrix
F_S, f_C = Sine or cosine component of the exciting loads - lb, in.-lb
X = Displacement (in.) or rotation (radius)
Ω = Exciting frequency - rad/sec
t = Time - sec

The solution to this is

$$\{X\} = \{X_s\} \sin \Omega t + \{X_c\} \cos \Omega t.$$

where X_X, X_C = Sine or cosine components of the displacement (or rotation) of the modes of one structural element, in., radius

The resultant vibratory amplitude is

$$r = \sqrt{X_s^2 + X_c^2}$$

and the g-loading (acceleration) is

$$G = \Omega^2 r/386$$

Shafts

Modeling - The modeling of the dynamic components is an involved and lengthy procedure. It should be kept in mind in modeling that growth and change should be provided for in the development of the model. The procedure for modeling the shafts for the Damped Forced Response program (D-82), which is a finite element analysis, is outlined below:

1. The shafts are divided into several small, cylindrical sections. The lengths of these sections are usually determined by changes in the inside or outside diameter of the shaft. Conical sections are also divided into several small cylinders in a step-like manner.

2. Physical properties (such as mass, inertia, and cross-sectional area) are then calculated for these individual cylinders.

3. Masses and polar moments of inertia are averaged between adjacent stations if computer capacity allows. Otherwise, an equivalent mass and inertia are lumped at selected stations along the shaft length.

4. Gear meshes are represented by four masses located at the appropriate pitch diameter. These masses are connected to the main shaft by beams which have similar elastic properties of the actual gears. Additional beams are provided to keep the four masses at equal distance from each other. The amount of mass concentrated at the gear nodes should represent actual mass distribution.

5. Radial stiffness of bearings is represented by pairs of linear and torsional springs. To allow for non-uniform stiffness of bearings, two mutually perpendicular springs of different stiffness are required at each bearing location. Thrust stiffness is represented by an axial linear spring. These stiffnesses are a function of torque and are calculated by a

Boeing-Vertol computer program (S-04 or S-33) which is based on a scheme developed by A. Jones.[15]

6. Meshing gears are represented by a spring having a stiffness similar to the tooth stiffness as calculated by computer program GEARO (R-33).

7. The sync shaft is modeled as a torsional spring as determined by hardware geometry.

8. The presence of the planetary stages is modeled by a torsional spring whose stiffness is extracted from the computer program TORRP (R-32) output.

9. The four planets of the lower stage planetary system are represented by four equally spaced linear springs. The stiffness for these springs has been determined to be approximately one-half of the calculated carrier post stiffness.

The model developed for the CH-47C is shown in Figure 39. The necessity to couple the shafts resulted from on-line analysis of the test results.

Correlation of Damped Forced Response (D-82) - Prior to the utilization of the D-82 analysis for the HLH gearbox, the analysis was validated by correlating predicted responses to experimental measurements. Since this noise reduction program was an integral part of the on-going HLH/ATC transmission design project, the available time for correlation studies was severely limited, in order to utilize the analysis for design recommendations on the HLH/ATC program. Because of this, only selected operating conditions were used for the correlation studies. The logic used in selecting which mode shapes should be evaluated was as follows:

1. Only noise-making modes were analyzed. This limited the correlation to 6600 RPM for the sun mesh frequency and 7000 RPM for the bevel mesh frequency.

2. Only 80% torque was considered. This is a typical flight operational torque.

3. Predicted natural frequencies were compared to those determined from sweep data.

---

[15]A. B. Jones, A GENERAL THEORY FOR ELASTICALLY CONSTRAINED BALL AND RADIAL ROLLER BEARINGS UNDER ARBITRARY LOAD AND SPEED CONDITIONS, ASME Publication 59-LUB-10, New York, New York, October 1959.

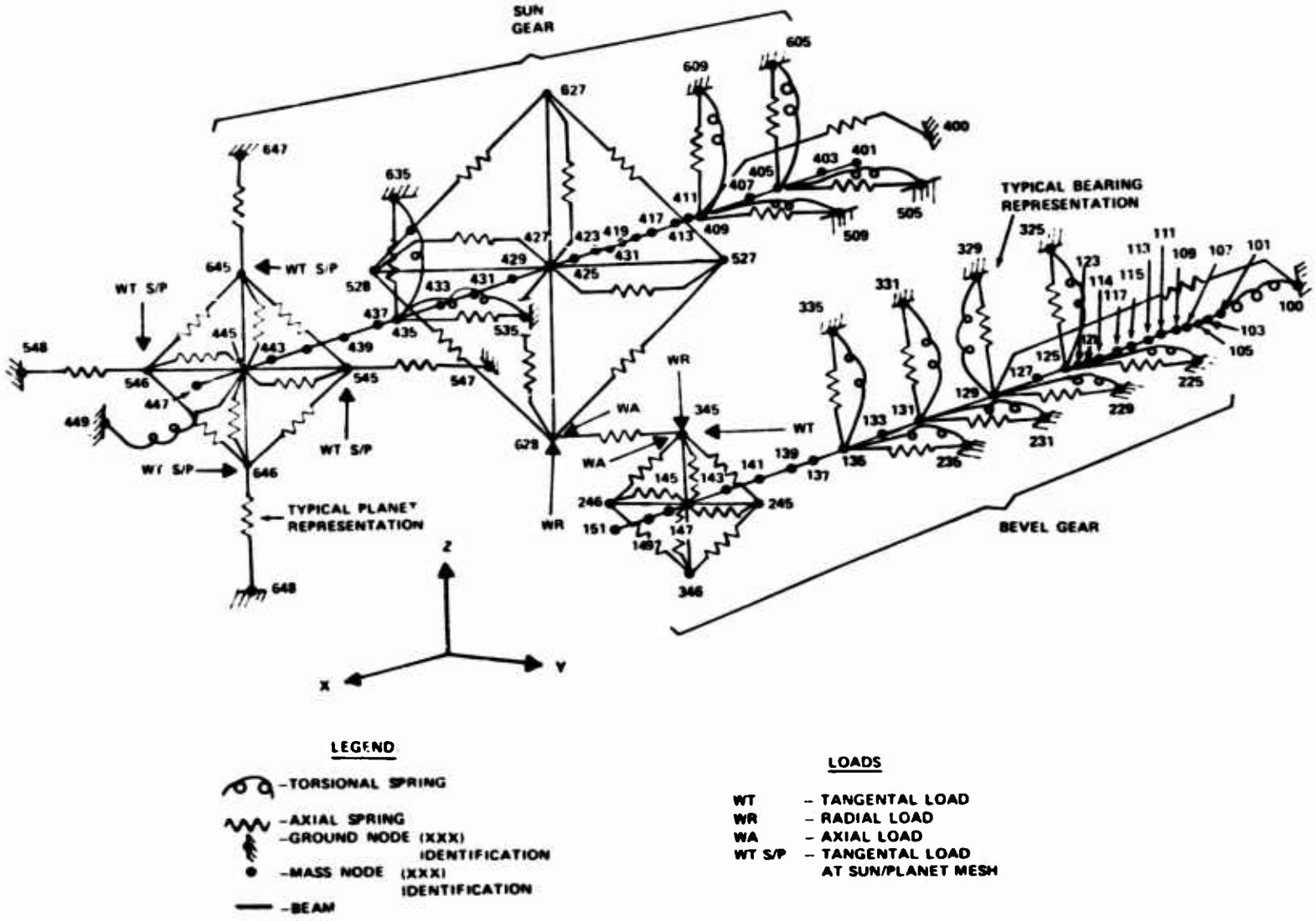

Figure 39. Math Model of CH-47 Transmission.

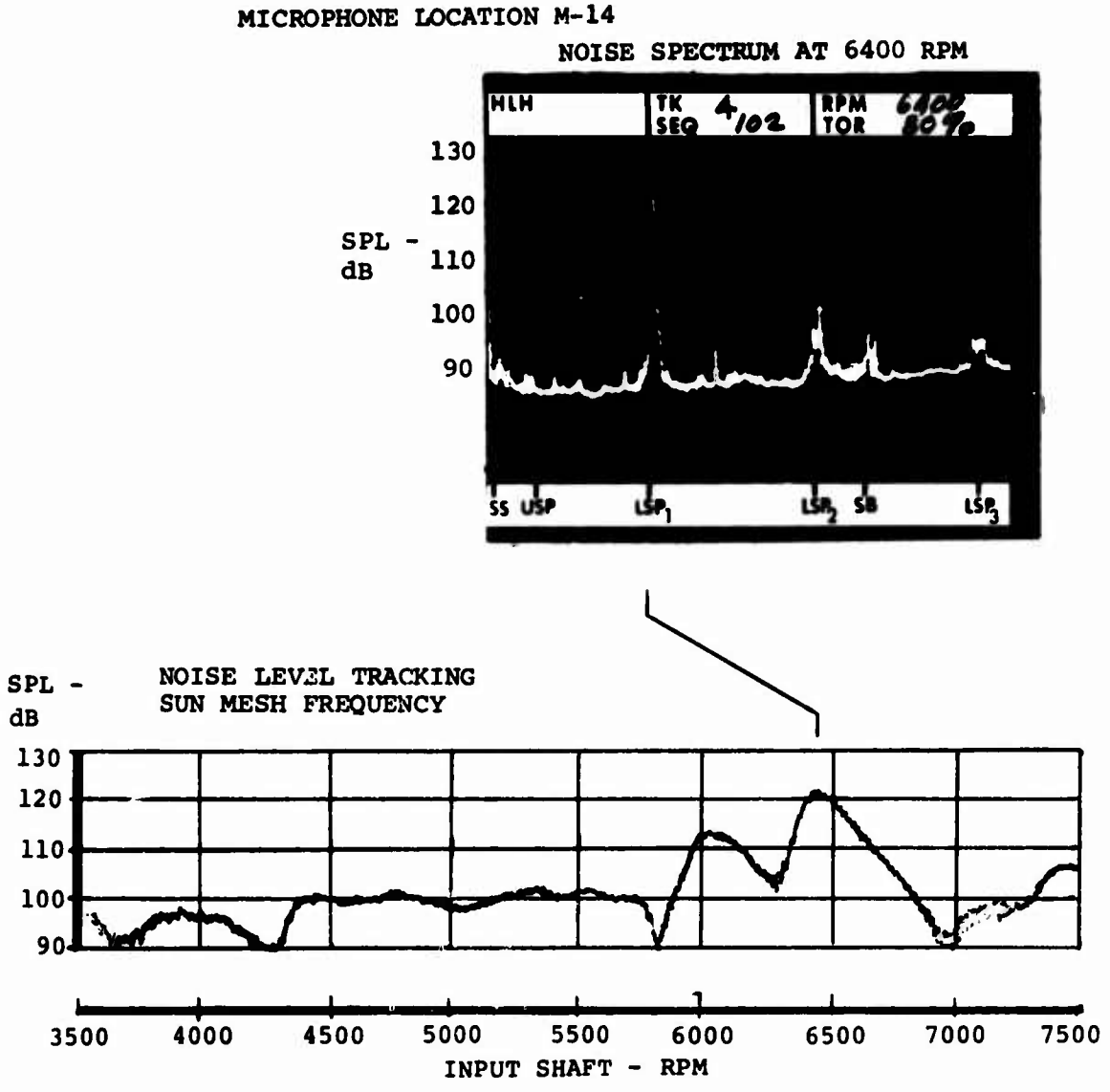

Figure 40. Selection of Correlation RPM for Lower Stage Sun Mesh Frequency.

MICROPHONE LOCATION M-17

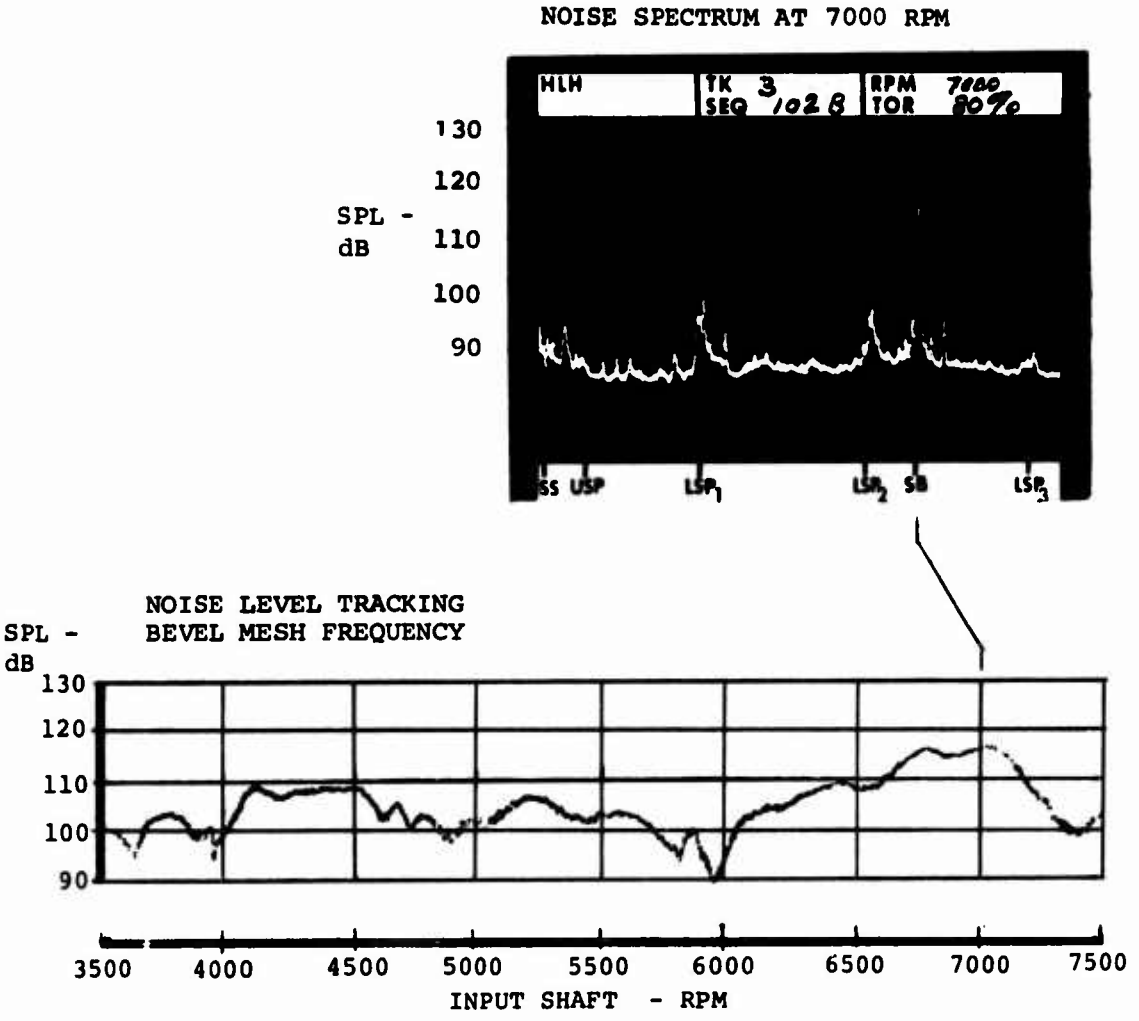

Figure 41. Selection of Correlation RPM for Spiral Bevel Mesh Frequency.

4. Amplitudes of the predicted displacements at bearing location were compared to measured displacements as determined by probe and probe acceleration data.

5. Mode shapes of forced responses were correlated by consideration of relative phasing of proximity probes.

Determination of the noise-making modes is demonstrated in Figure 40 for the sun mesh frequency and in Figure 41 for the bevel mesh frequency. In these figures, the analyzer is tracking the gear mesh frequency. The high noise level noted at 6600 RPM for the sun frequency and 7000 RPM for the bevel frequency justified the selection of 6600 and 7000 RPM for correlation. Superimposed in these figures are the sound spectra which indicate the predominance of the sun mesh frequency at 6600 RPM and the bevel mesh frequency at 7000 RPM.

In Figure 42 the excitation frequencies are shown as functions of input shaft RPM. Superimposed on this figure are the predicted critical frequencies. The figure indicates that at 6600 RPM, the sixth and seventh critical frequencies are being excited by the upper side band of the sun mesh frequency; and at 7000 RPM, the thirteenth and fourteenth critical frequencies are being excited by the upper and lower sidebands of the bevel mesh frequency.

The damped forced response (DFR) is determined by applying the calculated dynamic forces to the D-82 model.

The DFR of these shafts at these frequencies is shown in Figures 43 through 46. Note that for the sun gear responding to the sun frequency (Figure 44), an axial mode of the sun gear is being excited. No instrumentation was installed to measure such an excitation; however, it is easy to imagine how such a mode would excite the case. The critical mode being excited by the bevel frequency is an elastic bending mode and was selected for detail correlation.

The DFR of the gears responding to the bevel frequency is shown in Figures 45 and 46. In these figures, the displacements at right angles to each other (identified as y and z) and the torsional displacements (identified as θ) are seen. Since these displacements are not in the direction of the proximity probes, a section cut through the plane of the probes must be examined.

If the probes are located in the plane of a model mode station, then a "Lissajous" figure can be constructed from the computer output listing of the amplitude and phase angle of the two (i.e., y and z) simple harmonic motions. If the probes do not fall in the plane of a mode (as in this case)

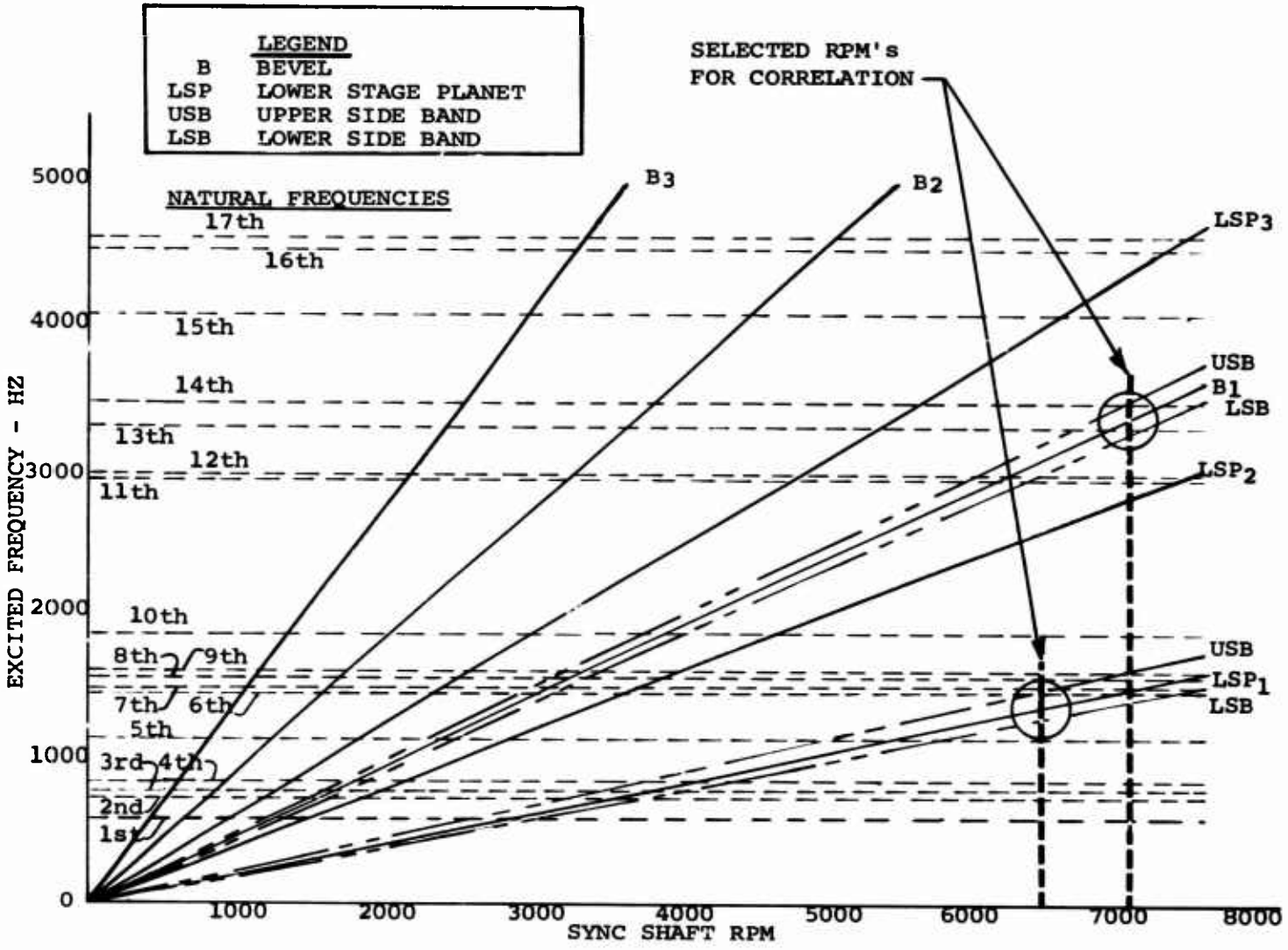

Figure 42. Natural Frequency Spectrum.

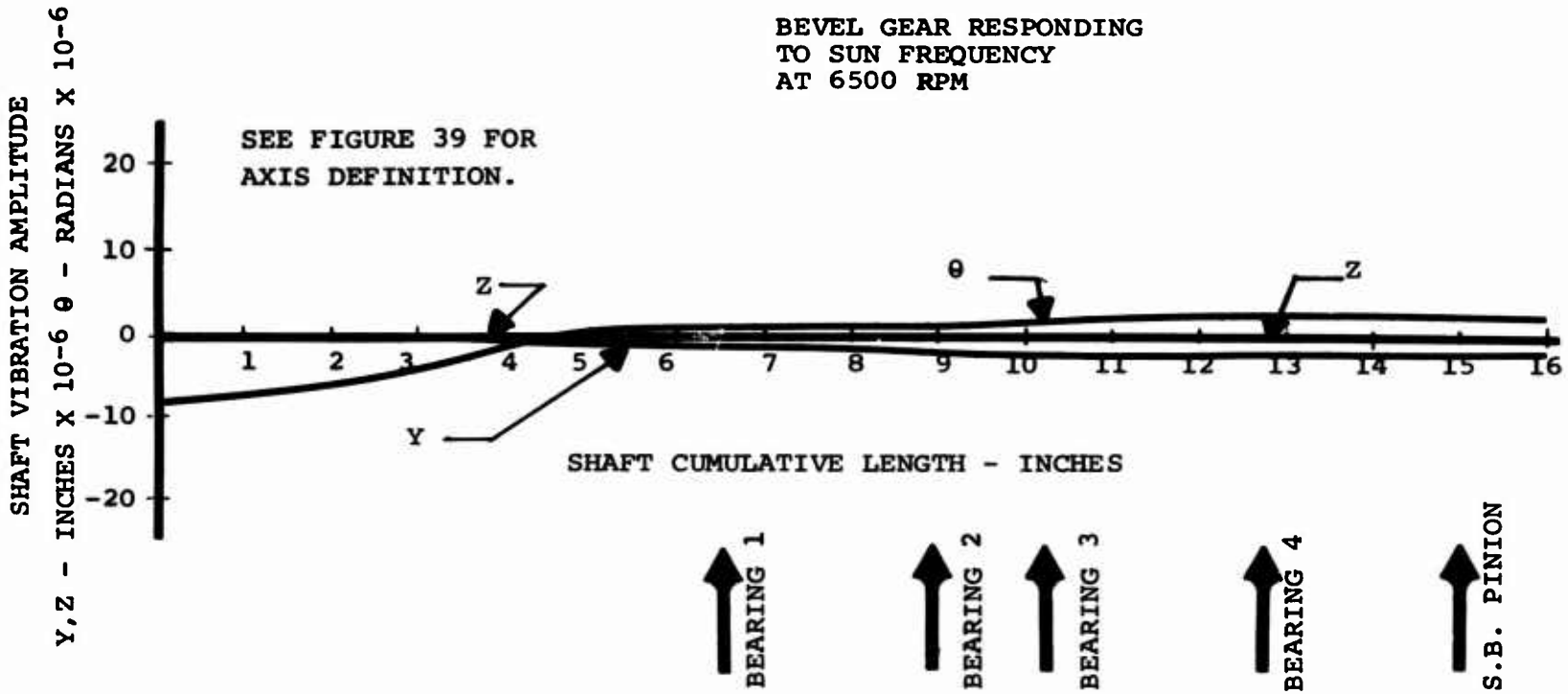

Figure 43. Bevel Gear Shaft Responding to Sun Frequency.

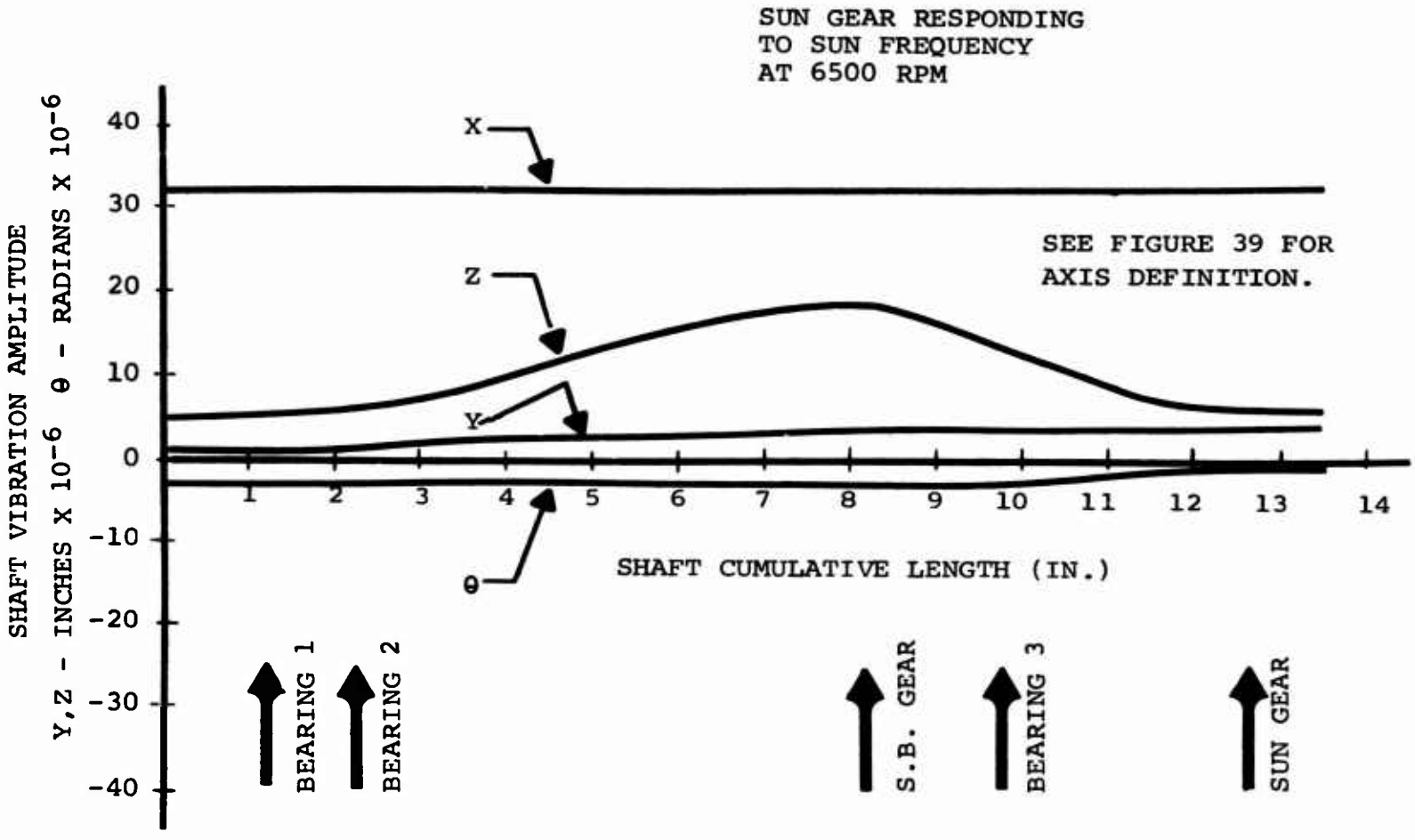

Figure 44. Sun Gear Shaft Responding to Sun Frequency.

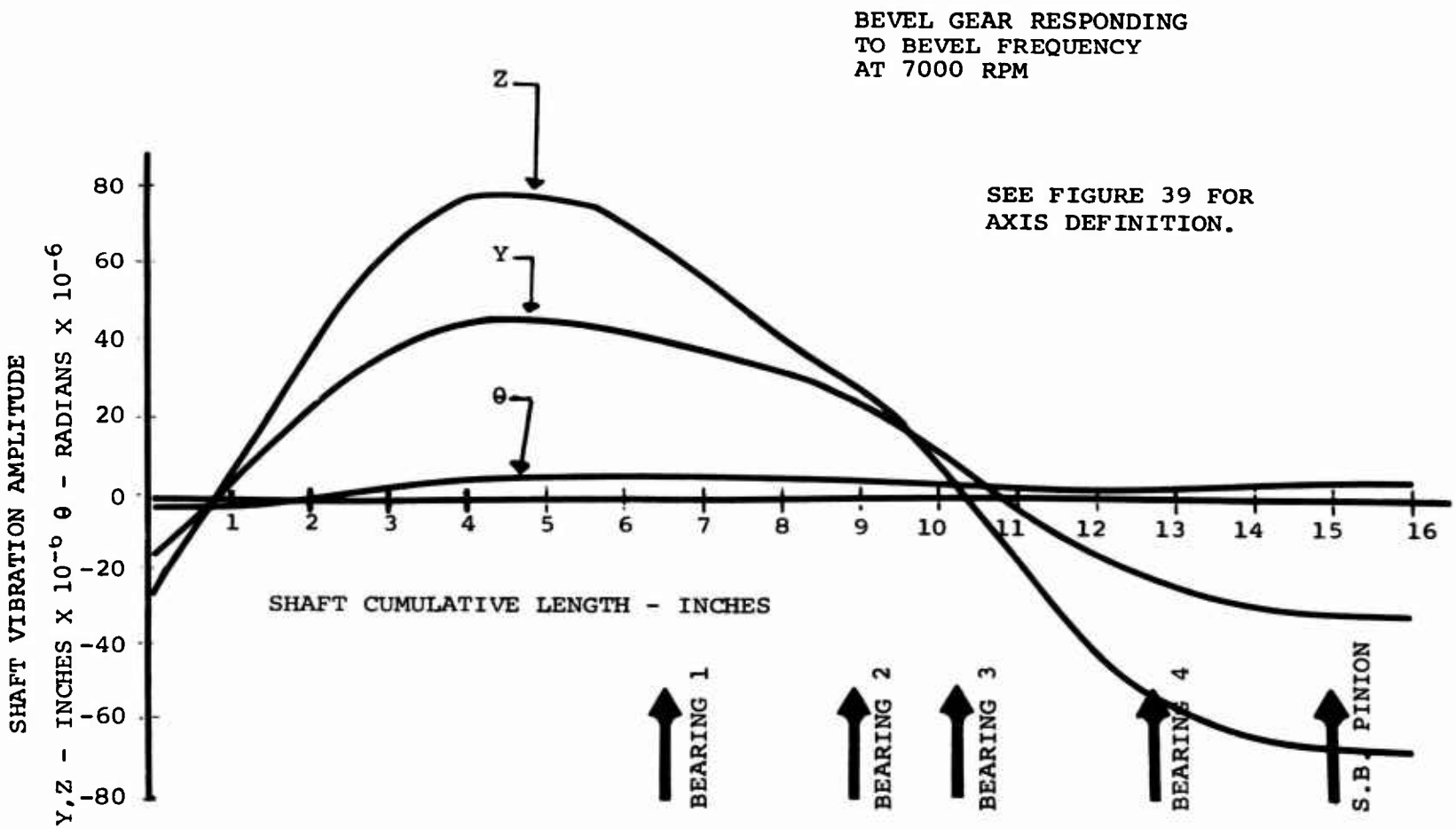

Figure 45. Bevel Gear Shaft Responding to Bevel Frequency.

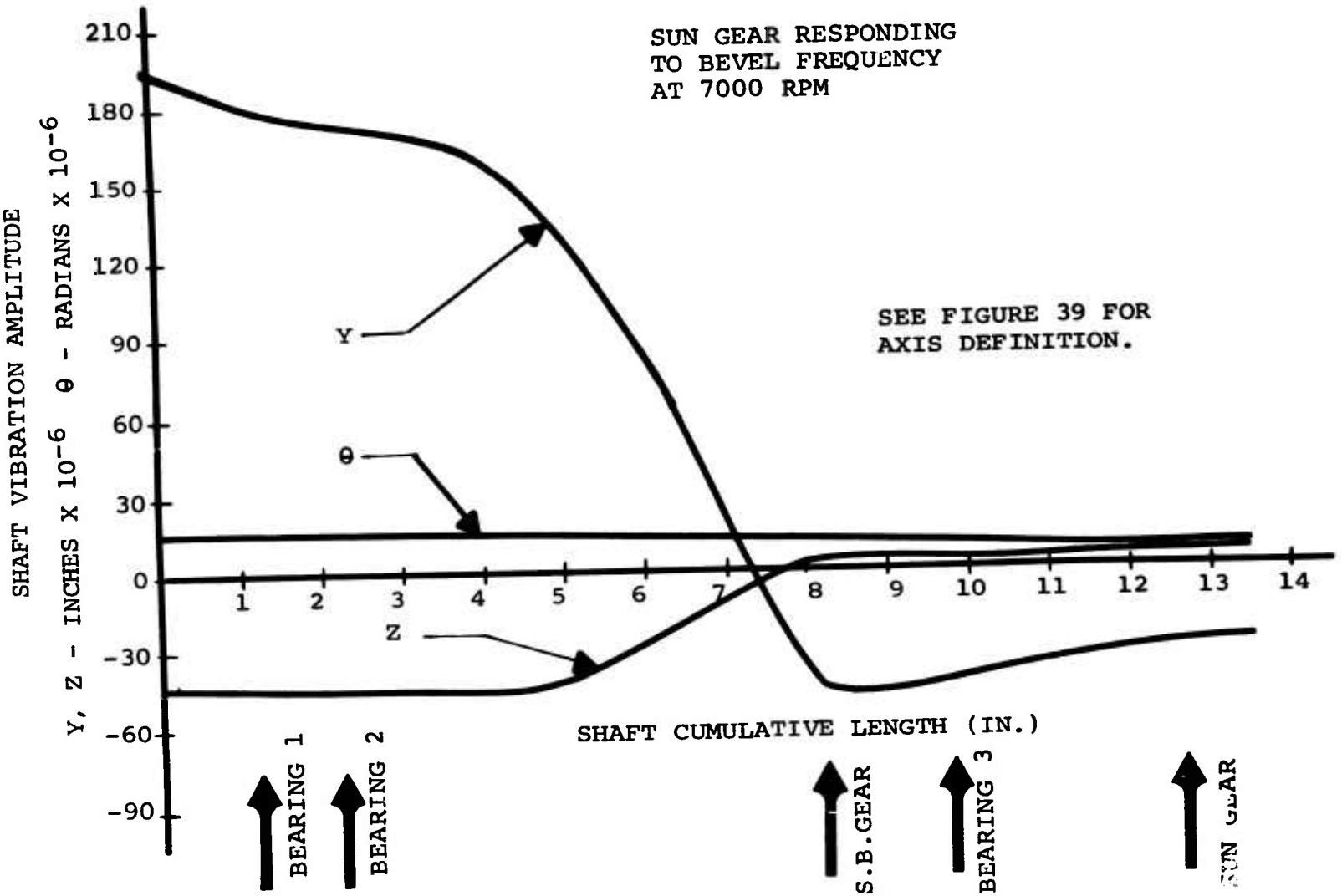

Figure 46. Sun Gear Shaft Responding to Bevel Frequency.

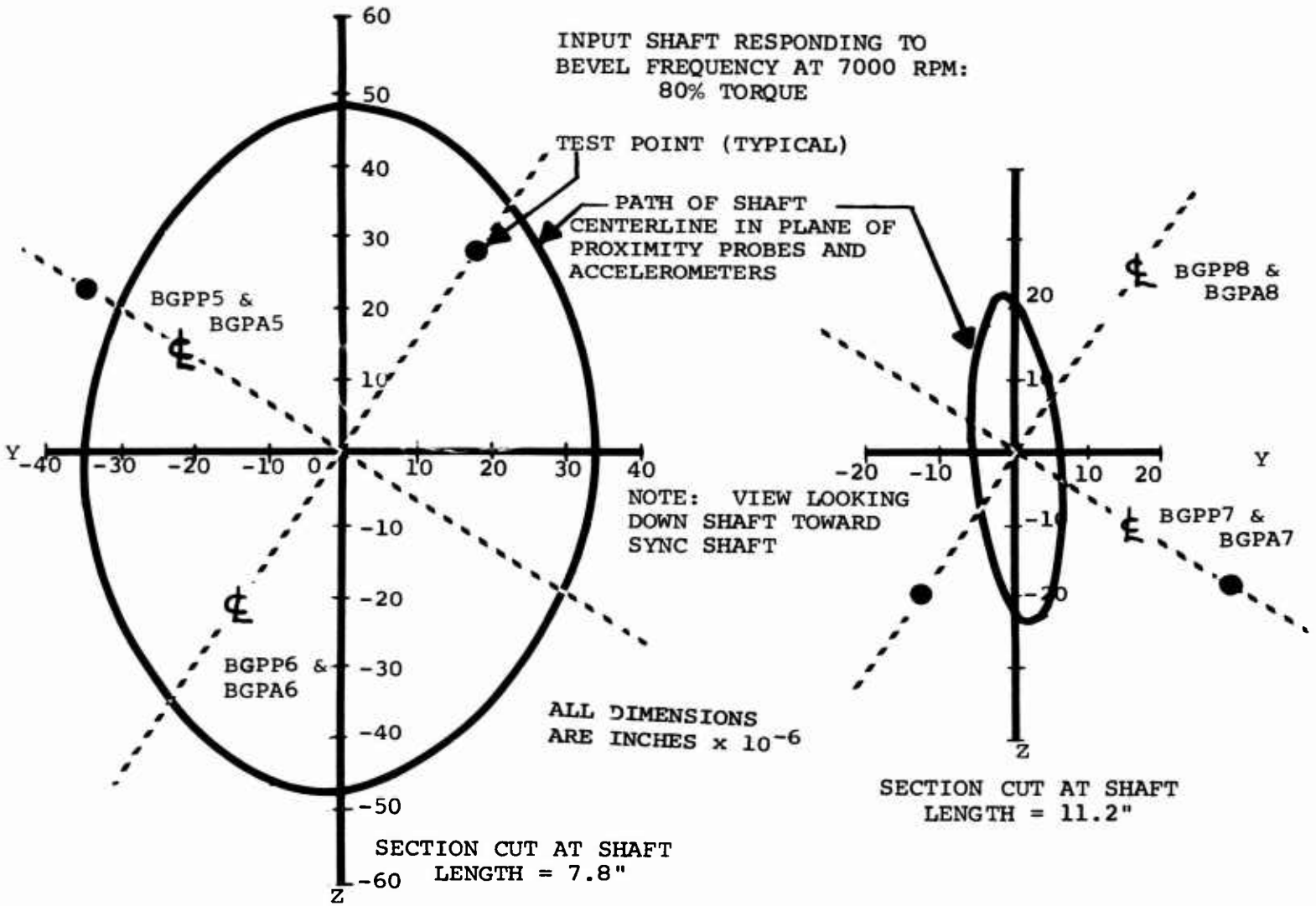

Figure 47. "Lissajous" Figures of Bevel Gear Shaft Responding to Bevel Frequency.

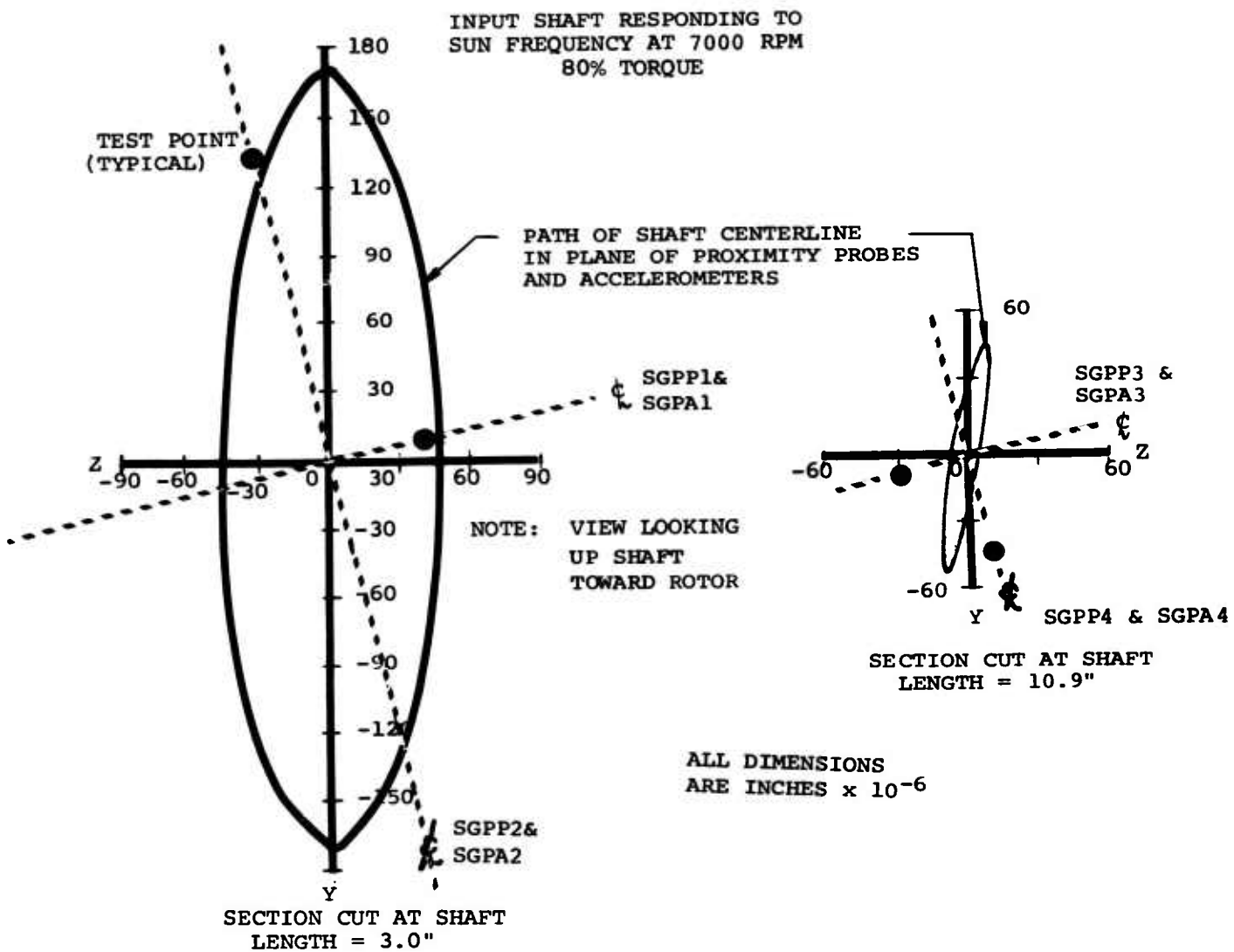

Figure 48. "Lissajous" Figures of Sun Gear Shaft Responding to Bevel Frequency.

then "Lissajous" figures must be constructed for the neighboring mode stations and interpolated in the probe plane. This has been done for the two shafts in the planes of the probes; see Figures 47 and 48. These "Lissajous" figures can be considered to be the coplanar path in which the shaft centerline will travel for this frequency at this torque.

Superimposed on these figures are the test results, as determined by phase corrected proximity probe data. In terms of amplitude, the agreement of the predicted and measured displacement is excellent for the larger displacement. The correlation with the smaller displacement is not quite so good as for the larger displacements. However, several things must be considered in evaluating these very small displacements: one, the smaller displacements (i.e., less than 30 μ inches) are usually associated with nodes, and a small error in predicting the node crossing could result in a sizable error in displacement (at least in terms of percentage); two, instrumentation error became a factor for the very small displacements; and three, small displacements are a measure of "goodness" and therefore are not as interesting as the large displacements.

In general, an agreement with a factor of 2 may be considered satisfactory for displacements less than 30 μ inches. For the larger displacement (i.e., displacement greater than 100 μ inches) agreement within a factor of 1.25 is considered good. The important thing is to be predicting large displacements when the displacements are large and small displacements when the displacements are small.

It should be noted that the correct prediction of these displacements provides an additional check on the TORRP (R-32) and GEARO (R-33) predictions. Since the dynamic forces are predicted by TORRP, which in turn gets inputs from GEARO, this correlation infers correctness of those programs.

Even more important than predicting displacements is the prediction of mode shapes. The DFR under consideration is particularly convenient for determining mode shape since a node had been predicted between the two proximity probe locations. On analysis of the phase relation between the two probes, it was determined that the two signals were 180^{o} out of phase. This confirmed the presence of a node between these two stations. A photograph of the two signals is superimposed on the DFR in Figure 49. As the pitching modes of this shaft have been confirmed to be at a much lower frequency, there is little doubt but that this is the correct mode. Examination of strain gage data further confirms this finding.

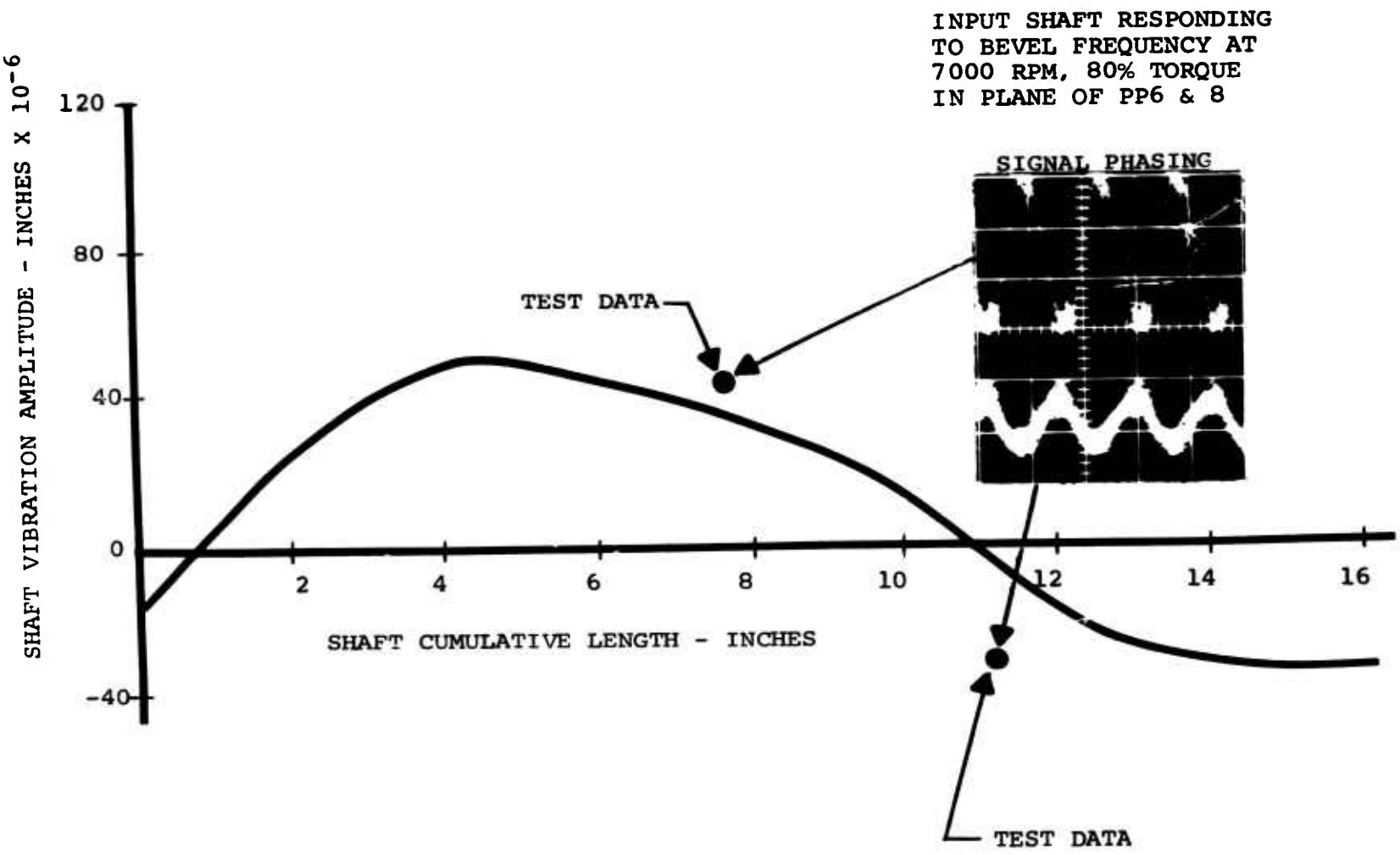

Figure 49. Mode Shape Correlation of Bevel Gear Shaft Responding to Bevel Mesh Frequency.

Model Improvements - One final aspect of the data correlation phase was to evaluate the mathematical model and modify it as indicated by test data. Generally, no major defect was found in the modeling technique. Two changes to the model, however, were incorporated. One was that the data indicated strong coupling between the bevel and the sun shafts. This necessitates the coupling of the shafts in the model, as previously discussed in "Modeling". The second change to the original model was to approximate the planet support to the sun gear by linear springs having stiffnesses equal to 50% of the calculated carrier post stiffness. This value presented the best correlation with test results. The effect of planet support on the DFR of the sun gear is seen in Figure 50. It would appear that the two opposite carrier posts are acting as springs in series to maintain the sun gear in position. Therefore, a 50% post stiffness was used in all the preceding predictions and will be used in the mathematical model of the HLH transmission.

Noise Reduction - The relation of the resultant noise reduction to the change in shaft displacement is very complex. If a single shaft were supported by a single bearing, the resultant noise reduction would behave approximately as below:

$$\Delta \text{SPL} = 20 \log \frac{(k\chi)\ \text{New}}{(k\chi)\ \text{Baseline}}$$

where $F = k\chi$ is the dynamic force at the bearing station. However, real transmissions have two primary shafts (excluding the rotor shaft) and several supporting bearings. This results in considerable difficulty in estimating the noise reduction.

Several ways of considering this problem are available. One is to consider all bearings as separate noise sources. Another is to consider all the bevel shaft bearings as one noise source and all the sun shaft bearings as a second source. A third is simply to consider the case as a big noise source being driven by the resulting sum of the dynamic forces. However, without knowledge of how the case will respond, none of the above models have much meaning.

In the absence of better information, the following method of estimating this relation is as follows:

1. Establish a dB level for each bearing dynamic force, using the largest force as the reference force. These are the referred noise levels.

2. Logarithmically sum the referred noise levels. This sum can be considered as the referred baseline SPL.

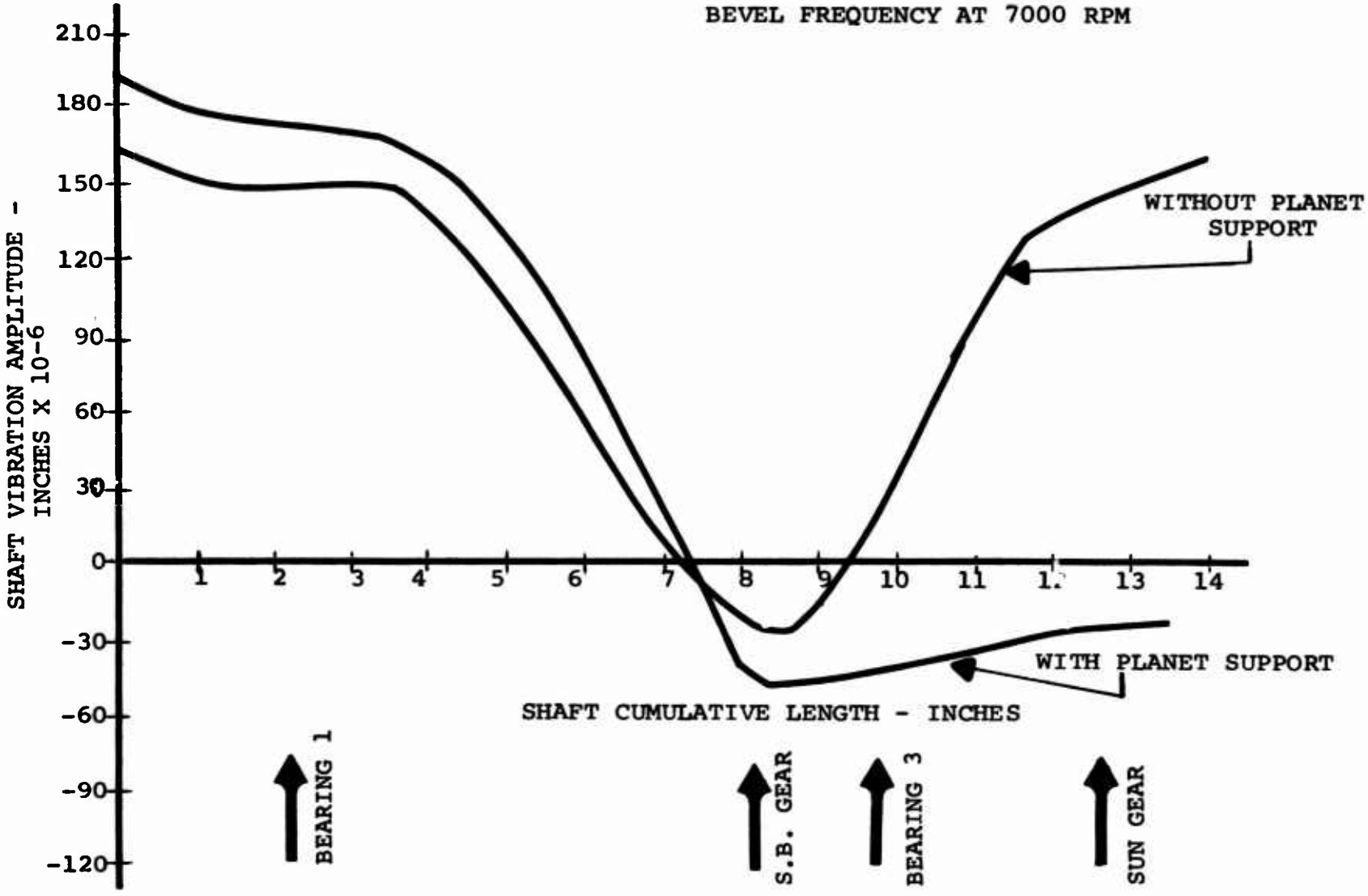

Figure 50. Effects of Planet Support Stiffness.

3. Using equation above, calculate the Δ SPL for each bearing and add to the referred noise levels. These are the referred modification noise levels.

4. Logarithmically sum the referred modification noise levels. This sum can be considered as the referred modification SPL.

5. The difference between the referred baseline SPL and the referred modification SPL is the most probable SPL reduction.

6. Repeat 1 through 5 above for each mesh frequency.

An arbitrary example of this procedure is shown in Table 5 for a transmission with two shafts supported by two bearings each.

TABLE 5. EXAMPLE OF NOISE REDUCTION CALCULATION

	(kX) Baseline	(kX) Modif.	$20 \log \frac{(kX)BL.}{(kX)MAX.BL.}$	$20 \log \frac{(kX)MOD.}{(kX)BL.}$	SUM
Brg. 1	1000	800	-6	-1.9	-7.9
Brg. 2	2000	1000	0	-6.0	-6.0
Brg. 3	500	400	-12	-1.9	-13.9
Brg. 4	100	20	-26	-14.0	-40.0
LOG SUM			1.2		-3.4

Then $\Delta SPL_{XMSN} = 1.2 - (-3.4) = 4.6$ dB at mesh frequency

The message in the above example is clear. If the dynamic forces of all the bearings setting the noise level are not substantially reduced, the resulting Δ SPL can be quite disappointing. Another interesting point in the above example is that the apparent 14 dB reduction, at bearing number 4, contributes very little to the total noise reduction. This, of course, seems very unfair. In consolation, it can be pointed out that the increase in bearing life and transmission reliability makes the improvement very worthwhile, even if it did not change the noise level. One word of caution is in order here. This type of analysis does not consider phasing nor case response and therefore should be used only as an approximate order of magnitude. Actual test results indicated that there is potential for over 10 dB reduction, to the overall SPL spectrum of the transmission, through control of bearing displacements.

Considerably more research will be required to relate the changes in shaft displacement to changes in SPL more rigorously. The experimental data available,as a result of this program should provide the information to establish this relation.

Ring Gear

Modeling - The CH-47 ring gear was analyzed using the D-82 computer program in much the same way as were the shafts. The ring gear and station planes are seen in Figure 51, and the mathematical model is shown in Figure 52. This model consists of five planes of eight nodes apiece (around the circumference of the ring gear) with adjacent nodes in each plane and in adjoining planes connected with a network of beams and axials. Masses are lumped at the nodes and are capable of motion in all six degrees of freedom. The ring gear is supported from above and below by a series of beams and axials which simulate the transmission case stiffness. This is one aspect of modeling in which a finite element approach is believed superior to a shell analysis approach. This is because end fixity can be modeled rather than assuming either a free-free, simply supported, or built-in end conditions, none of which properly simulates the actual conditions. It should be pointed out that in future studies, a complete model of the transmission casing stiffness and mass distribution will be attempted. This could eventually lead to optimization of transmission case geometry for minimum noise generation.

Correlation - The trace of a ring gear accelerometer tracking the sun mesh frequency is seen in Figure 53. The predicted natural frequencies are superimposed on these traces. The response of the ring gear to the sun frequency is interesting in that the first natural frequency is predicted at 5400 RPM and no response is noted prior to that. The nearness of the first five criticals probably accounts for the retained height of the peak. Why the peak does not drop off is not clearly understood. What is speculated is that assumptions used in modeling the end fixity of the ring gear were not quite representative of the actual end fixity. By changing the fixity to provide for a stiffer constraint, the lower predicted frequencies can be shifted to the right (i.e., to higher RPMs). This can be done without substantially shifting the higher critical frequencies.

The response of the ring gear to the bevel mesh frequency is much more pronounced than that of the sun frequency response. The peaks occurring at RPMs where natural modes are not predicted are believed to be forced by the internal shafting. To show this, the trace of a torsional strain gage, tracking the bevel mesh frequency, is given for the sun gear and the bevel gear in Figure 54. Repeated in this figure is the

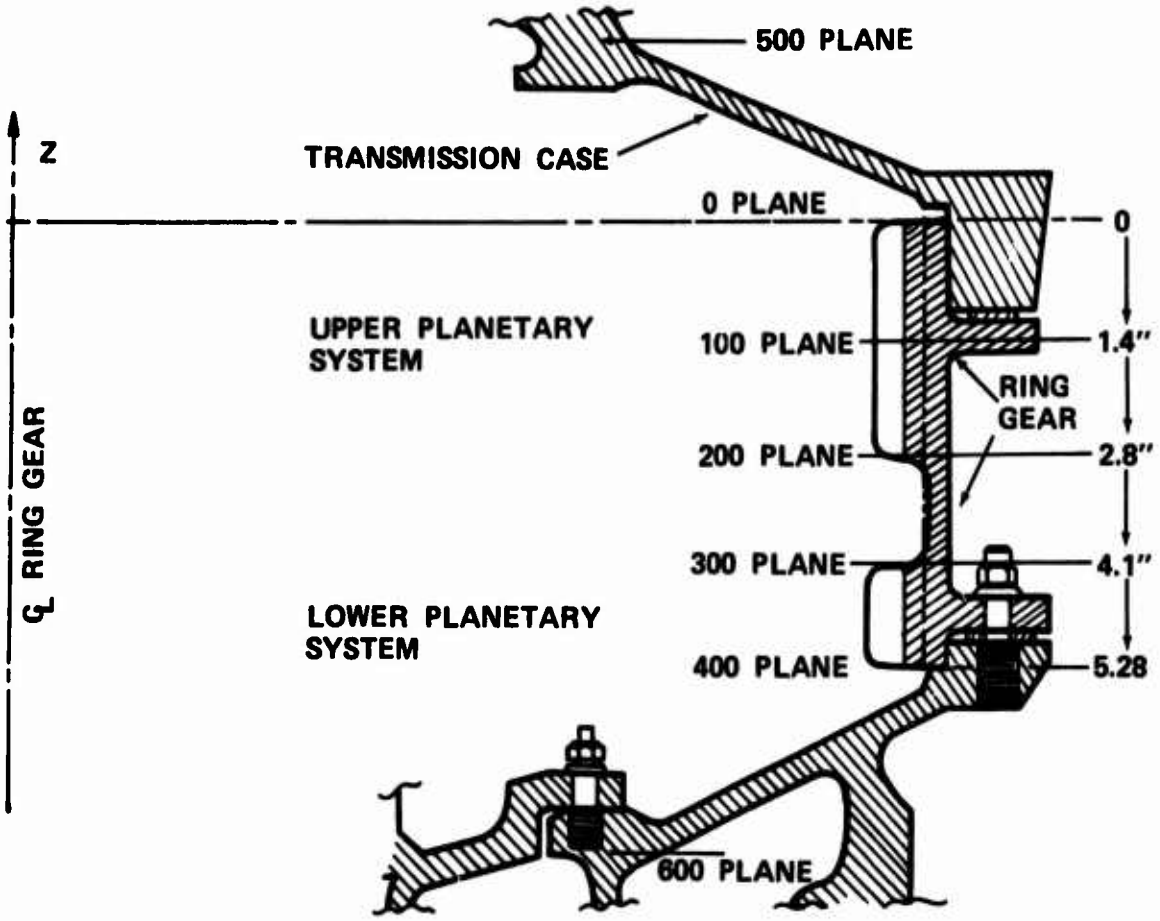

- RING GEAR MODEL IS SUPPORTED FROM ABOVE AND BELOW BY A SERIES OF BEAMS AND AXIALS WHICH SIMULATE TRANSMISSION CASE STIFFNESS.

Figure 51. CH-47 Ring Gear.

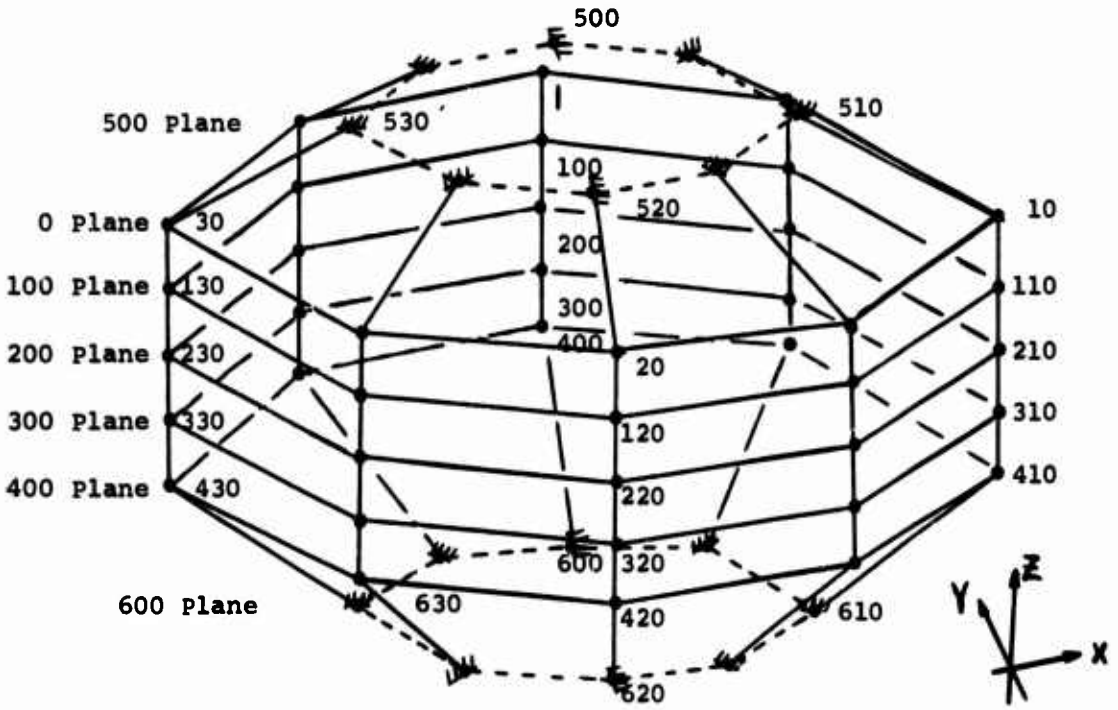

Planes 0 thru 400 have (Ring Gear Planes)

- 8 Beams Bending Radially
- 8 Beams Bending Axially (Along Z Axis)
- 8 Axials Relative Motion Between Nodes Horizontally

Between Each Plane:

- 8 Beams Bending Radially
- 8 Beams Circumferential Twist
- 8 Axials Relative Motion Between Planes Vertically

Planes 500 & 600 (case planes) are grounded

Figure 52. Math Model of Ring Gear.

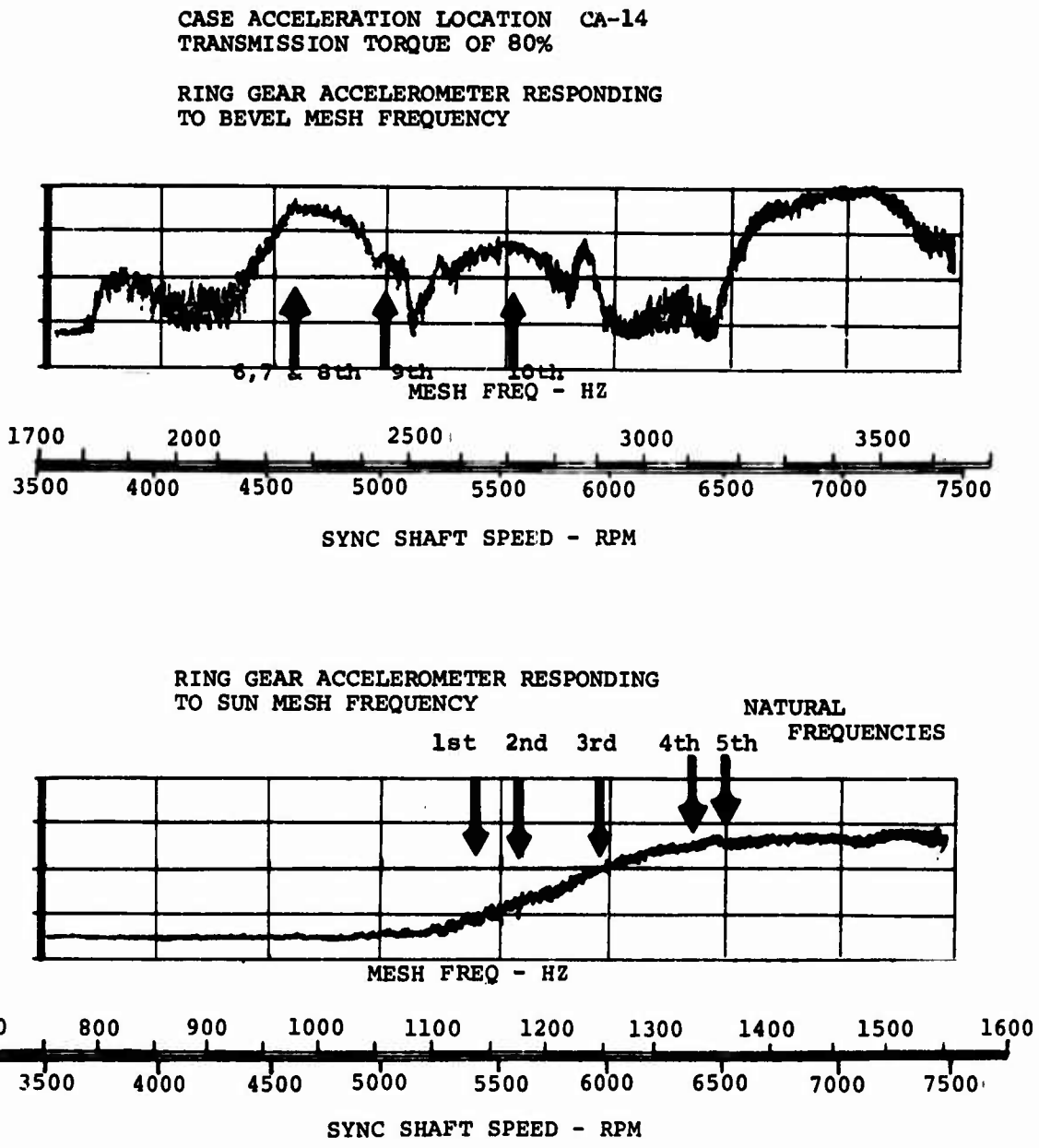

Figure 53. Ring Gear Response to Gear Mesh Frequencies.

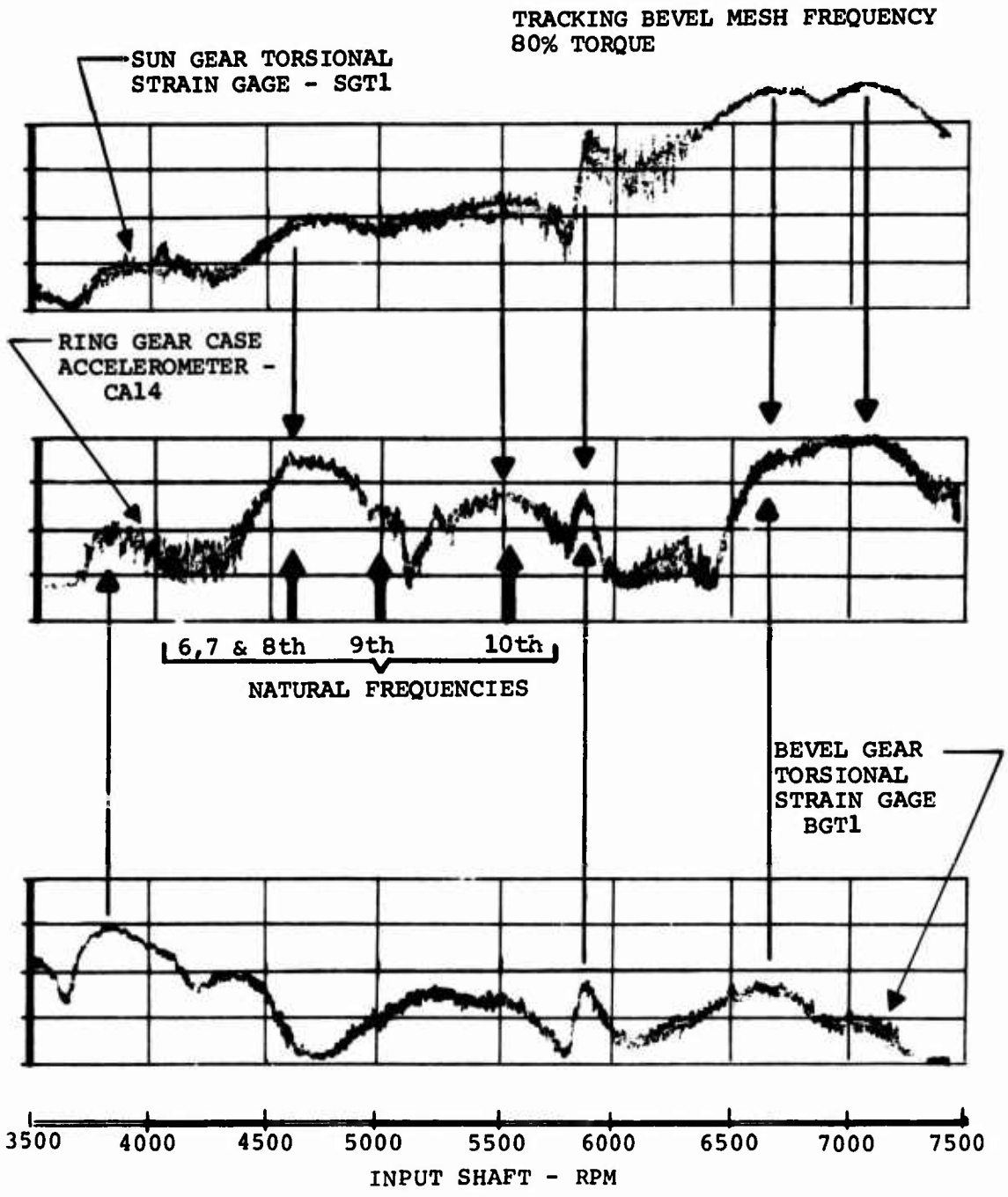

Figure 54. Correlation of Ring Gear Response With Torsional Response of Shafts.

trace of the ring gear accelerometer responding to the bevel mesh. The sixth through tenth critical frequencies are indicated on the ring gear response. This figure can be interpreted as follows: the sixth through eighth critical modes appear to be triggered by a sun gear torsional excitation; likewise, the tenth critical mode. The ninth critical is not being excited and does not have a pronounced peak. The ring gear response at 3800 RPM appears to be a forced response triggered by a bevel gear torsional excitation. The ring gear response at 5800 RPM appears to be a system torsional resonance. Finally, the large peak between 6500 RPM and 7300 RPM seems to be forced, first by a system torsional excitation and then by a sun gear torsional excitation.

Model Improvements - As a result of this program, two modifications were made to the D-82 mathematical model. First, the end fixity was stiffened to provide for better simulation of actual conditions. Second, experimental data indicated that the ring gear fixity was nonsymmetrical. Therefore, the mathematical model used for the HLH design studies was modified accordingly.

Noise Reduction - To predict the noise reduction, a method described in References 4 and 9 has been used. This scheme predicts the radiated noise based on a volume displacement analysis. The normal displacement of the model nodes is used to calculate the average normal displacement amplitude $\bar{W}(\theta, Z)$ used in the expression

$$P = 1.62 \times 10^{-4} \quad \omega^2 \bar{W}^2 A \quad \text{(watts)}$$

where

$$\bar{W} = \frac{1}{A} \iint_A W \, dA$$

ω = Frequency - Hz

A = Surface Area - sq cm

for the acoustic power generated by the vibrating ring gear casing. To relate acoustic power P to a change in sound pressure level (Δ SPL), the following expression is used:

$$\Delta \text{ SPL} = 10 \log \frac{P_{\text{baseline}}}{P_{\text{modified}}} \quad \text{(dB)}$$

DATA BASE

As a result of this test program, a large quantity of data has been collected. It is estimated that over 25,000 channel data

points were recorded. Only a small portion of this data has been reduced and an even smaller portion analyzed. A complete set of raw data is being stored at the Vertol Acoustic Laboratory. This data fills 80 rolls of 14-channel magnetic tape. A complete tape log is included in Appendix C. Also stored at Vertol is the complete set of data which was reduced for preparation of this report.

In reducing sweep data, it was found convenient to present the signal output in terms of dB, with 1 volt established as full scale, and each block representing 10 dB. To convert dB to engineering units, refer to the sensitivity tables in Appendix B. By utilizing this calibration technique, considerable savings in data reduction time are achieved. Since the primary purpose of sweep data is to identify high response frequencies, no particular penalty is associated with using a vertical dB scale (spectra is used for magnitude).

DESIGN METHODOLOGY

Now that the mechanism of noise production has been defined, and methods of analyzing the dynamic response developed and verified, the next logical step is to incorporate this knowledge into a design procedure. Such a procedure has been developed[16,17] and is shown in Figure 55. There are nine main steps in this procedure:

1. From the design drawings, determine the detail gear, shaft and bearing data. Several computer programs are available for this purpose.

2. Determine tooth compliances and pulsation curves (GEARO) for the various meshes.

3. Determine dynamic tooth forces (TORRP).

4. Calculate transmission SPL spectrum.

---

[16]R. Hartman, MODEL 301 HLH/ATC TRANSMISSION NOISE REDUCTION PROGRAM, Boeing-Vertol IOM 8-7446-1-923, 23 May 1972.

[17]R. Hartman, MODEL 301 HLH/ATC TRANSMISSION NOISE REDUCTION PROGRAM - PHASE II MODEL, Boeing-Vertol IOM 8-7446-1-931, 19 June 1972.

5. Model the ring gear and shafts and determine the forced damped response (D-82).

6. Modify the ring gear and shafts until an improved DFR is obtained.

7. Determine change in SPL as a result of modification.

8. Determine weight penalty of modification (if any).

9. Consider weight, cost, reliability, and maintainability compared to alternative acoustical treatments to determine the optimum configuration.

APPLICATION OF ANALYSIS TO HLH TRANSMISSION

Design Study

The HLH transmission is shown in Figure 56, and its mathematical model used for this analysis is seen in Figure 57. The procedure for modeling was described in "Shafts-Modeling". Several modifications to internal dimensions were considered. External modifications were not considered due to the excessive redesign required with such changes. Finally, a limited number of bearing stiffness modifications were analyzed. Details of the shaft modifications and their forced response are documented in the appendix of Reference 18.[18] The shaft modifications which provided the largest noise reduction, at both frequencies, are seen in Figures 58 thru 61. Also seen in these figures is the DFR of the modified shaft and the baseline shaft. It is estimated that these modifications will result in an overall noise reduction of 12 dB at the sun mesh frequency and 10 dB at the bevel mesh frequency. The weight penalty associated with these shafts is 9 pounds for the bevel gear and 26 pounds for the sun gear. Of significance is the large reduction in the displacement of both shafts, responding to the excitation at the sun frequency. This reduction should substantially increase the bearing lives and transmission reliability.

---

[18] R. Hartman, MODEL 301 HLH/ATC TRANSMISSION NOISE REDUCTION PROGRAM - DESIGN RECOMMENDATIONS, Boeing-Vertol IOM 8-7446-1-949, 31 August 1972.

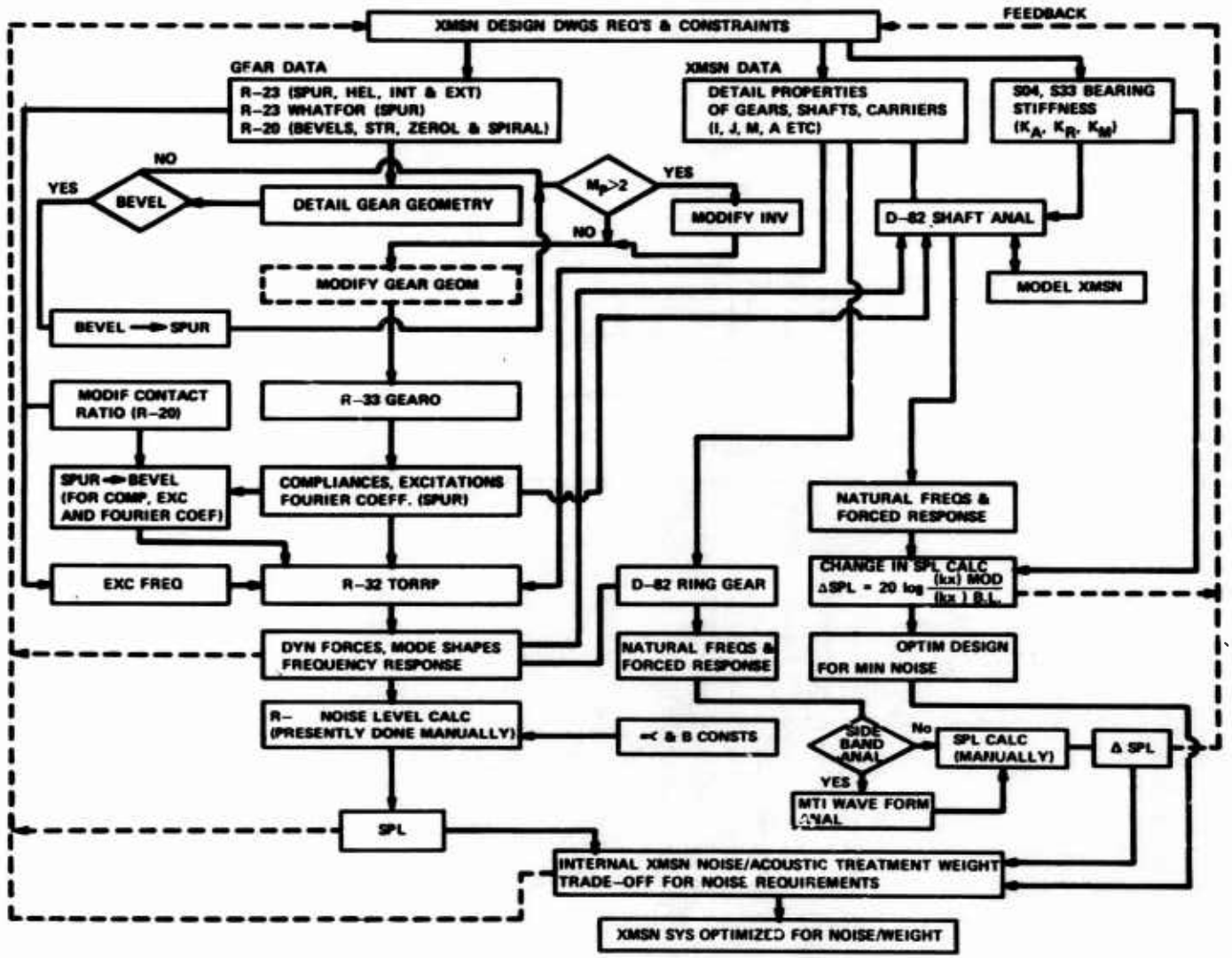

Figure 55. Flow Chart of Design Process.

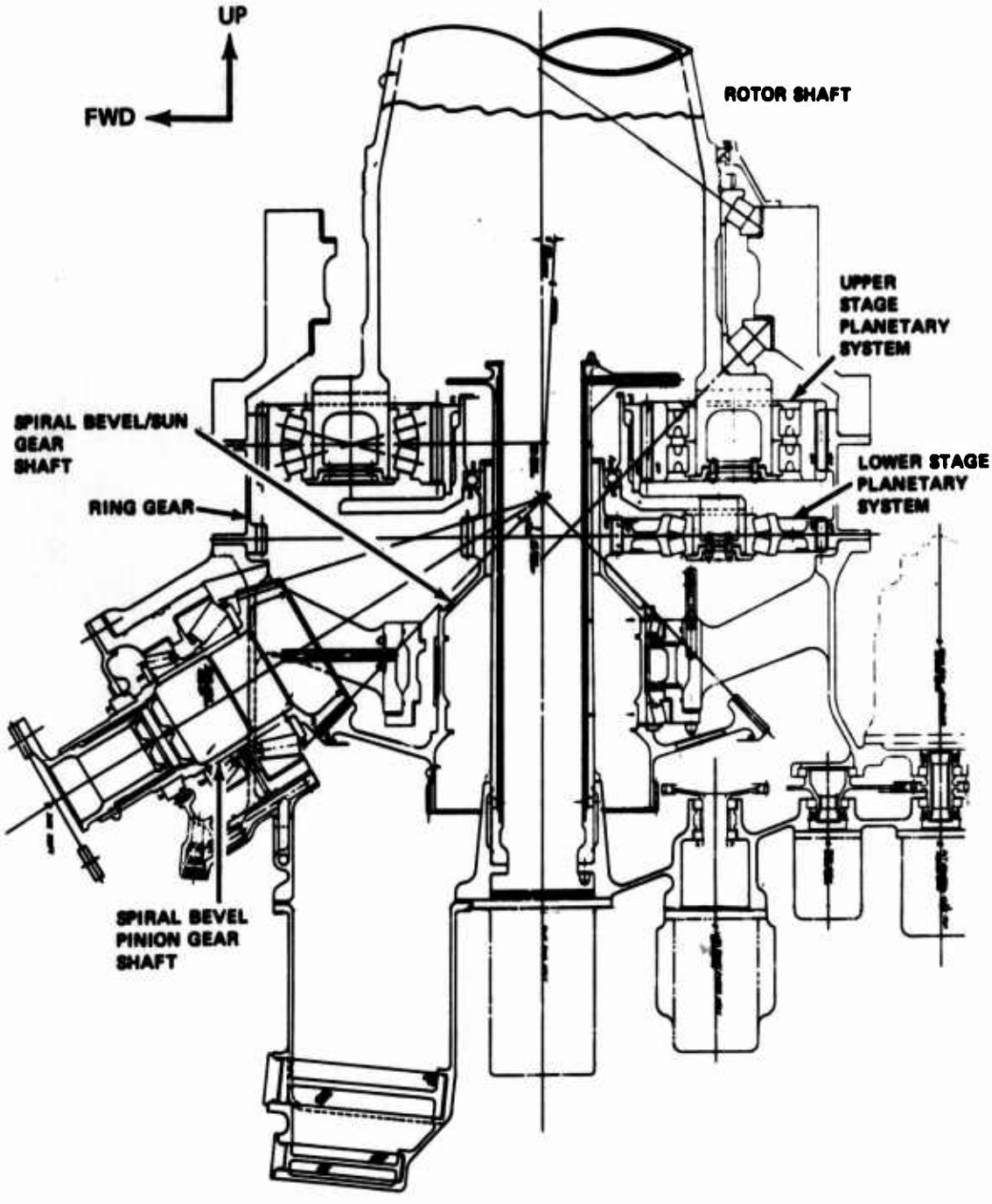

Figure 56. HLH Aft Transmission.

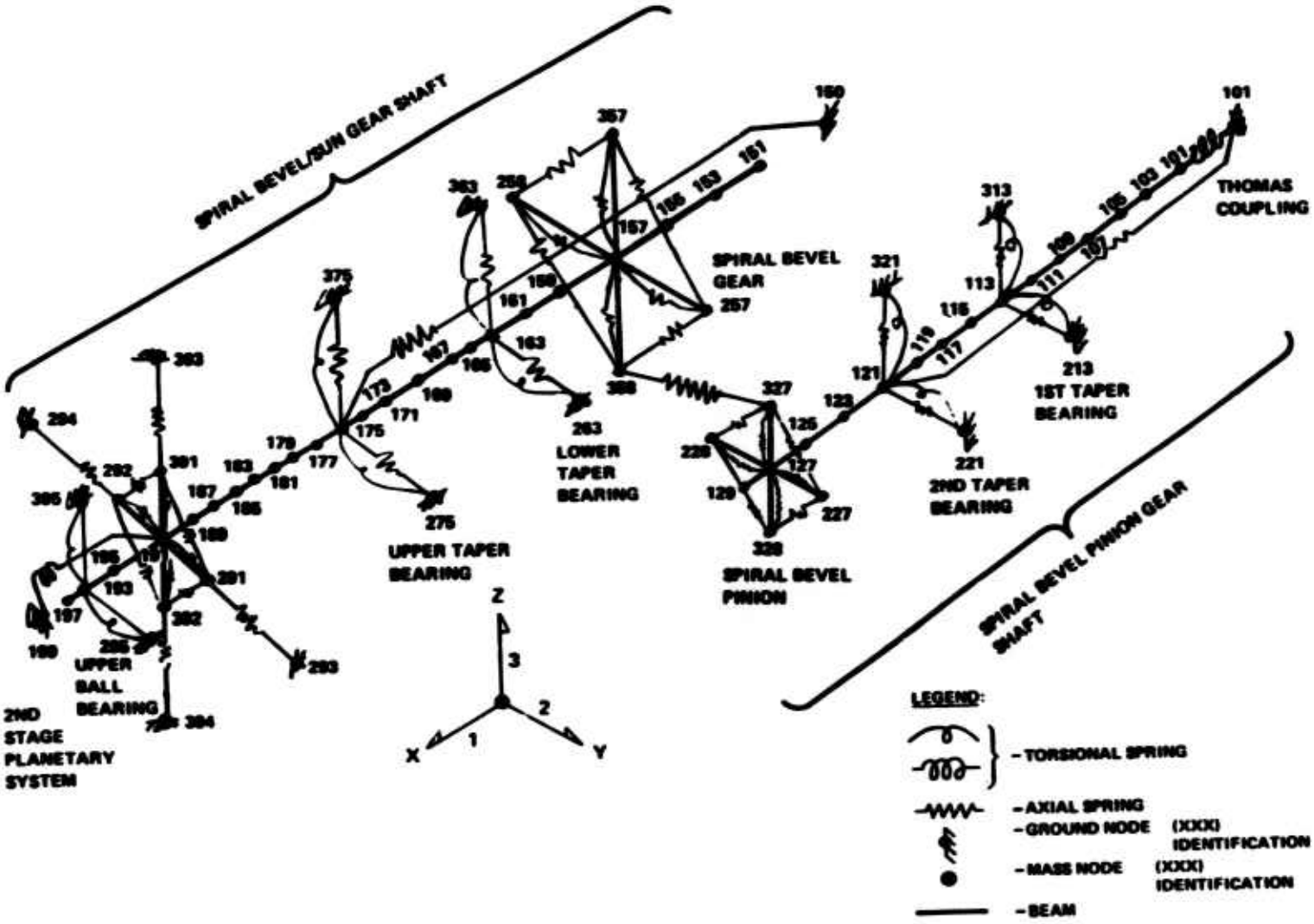

Figure 57. Coupled Bevel Gear and Sun Gear HLH/ATC Transmission Model.

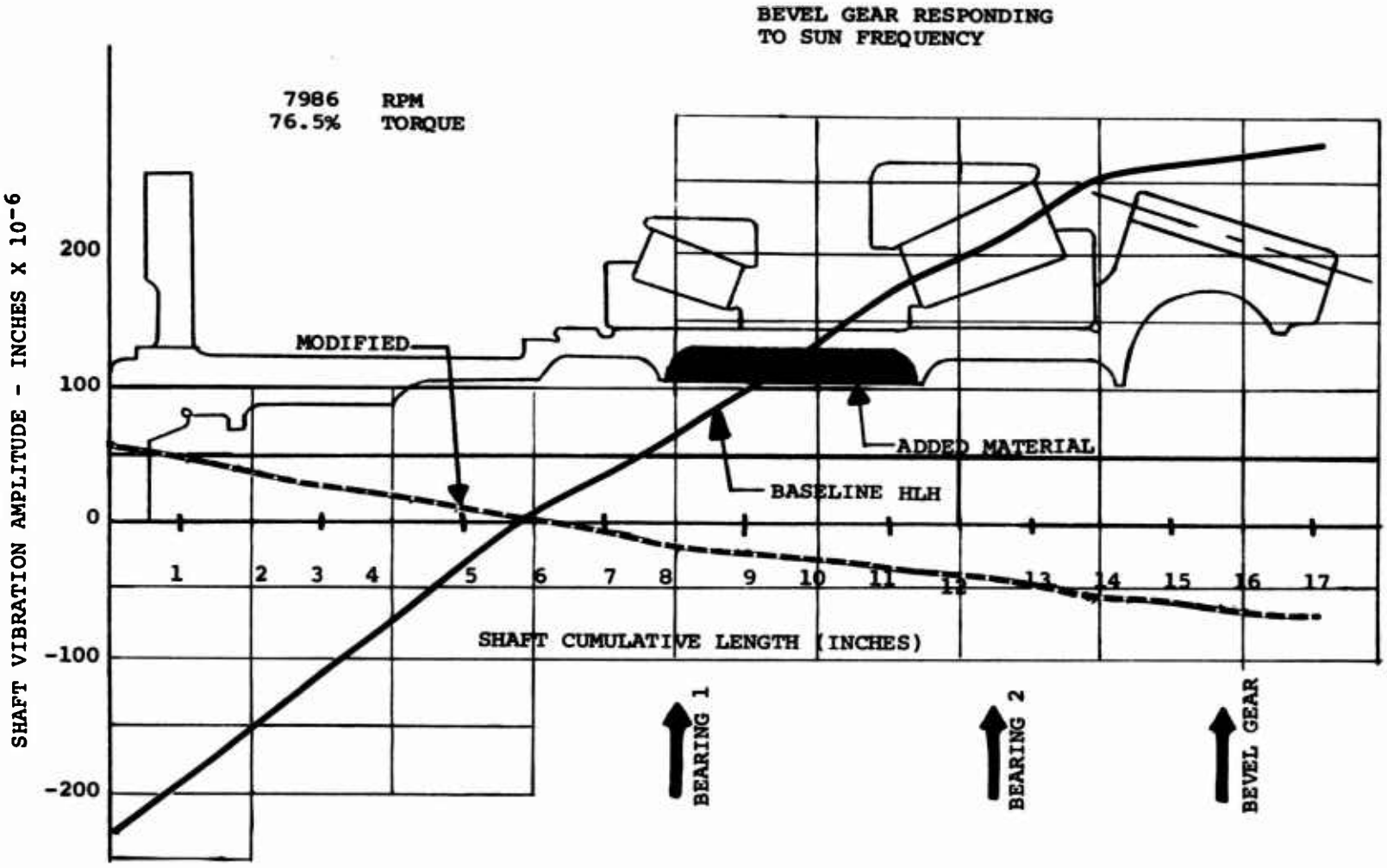

Figure 58. Effects of Bevel Gear Modification on Forced Damped Response (Sun Frequency) - HLH.

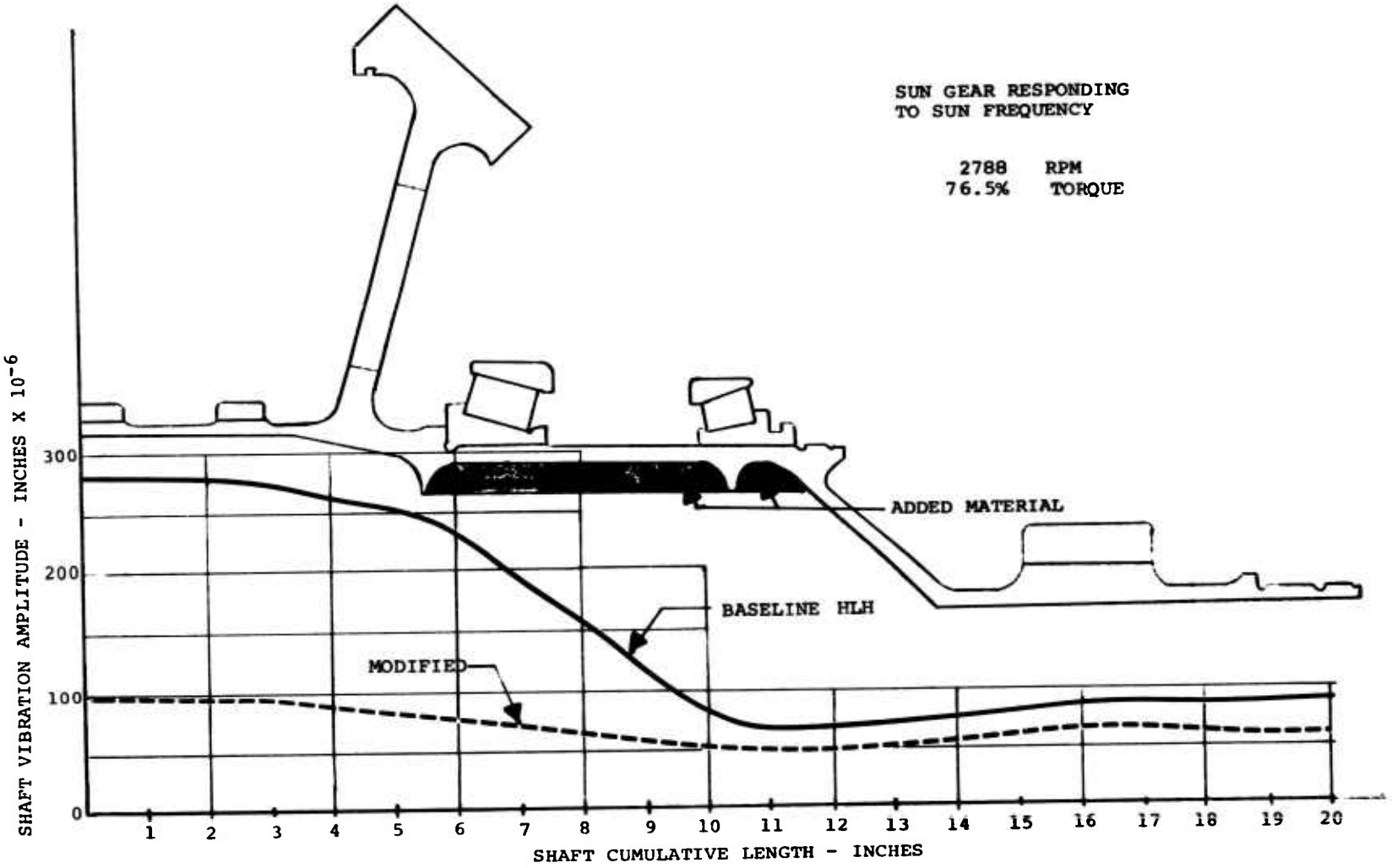

Figure 59. Effects of Sun Gear Modification on Forced Damped Response (Sun Frequency) - HLH.

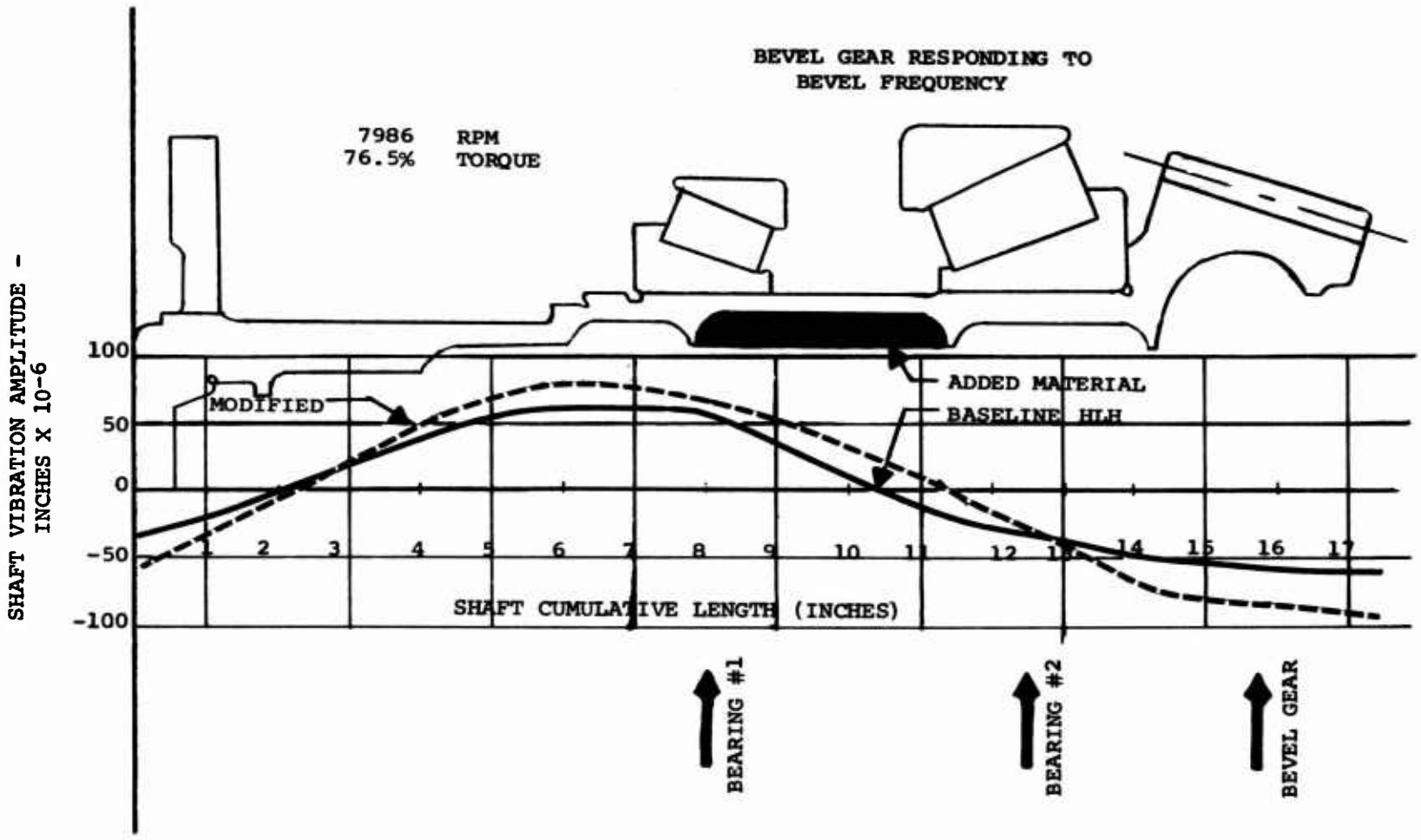

Figure 60. Effects of Bevel Gear Modification on Forced Damped Response (Bevel Frequency) - HLH.

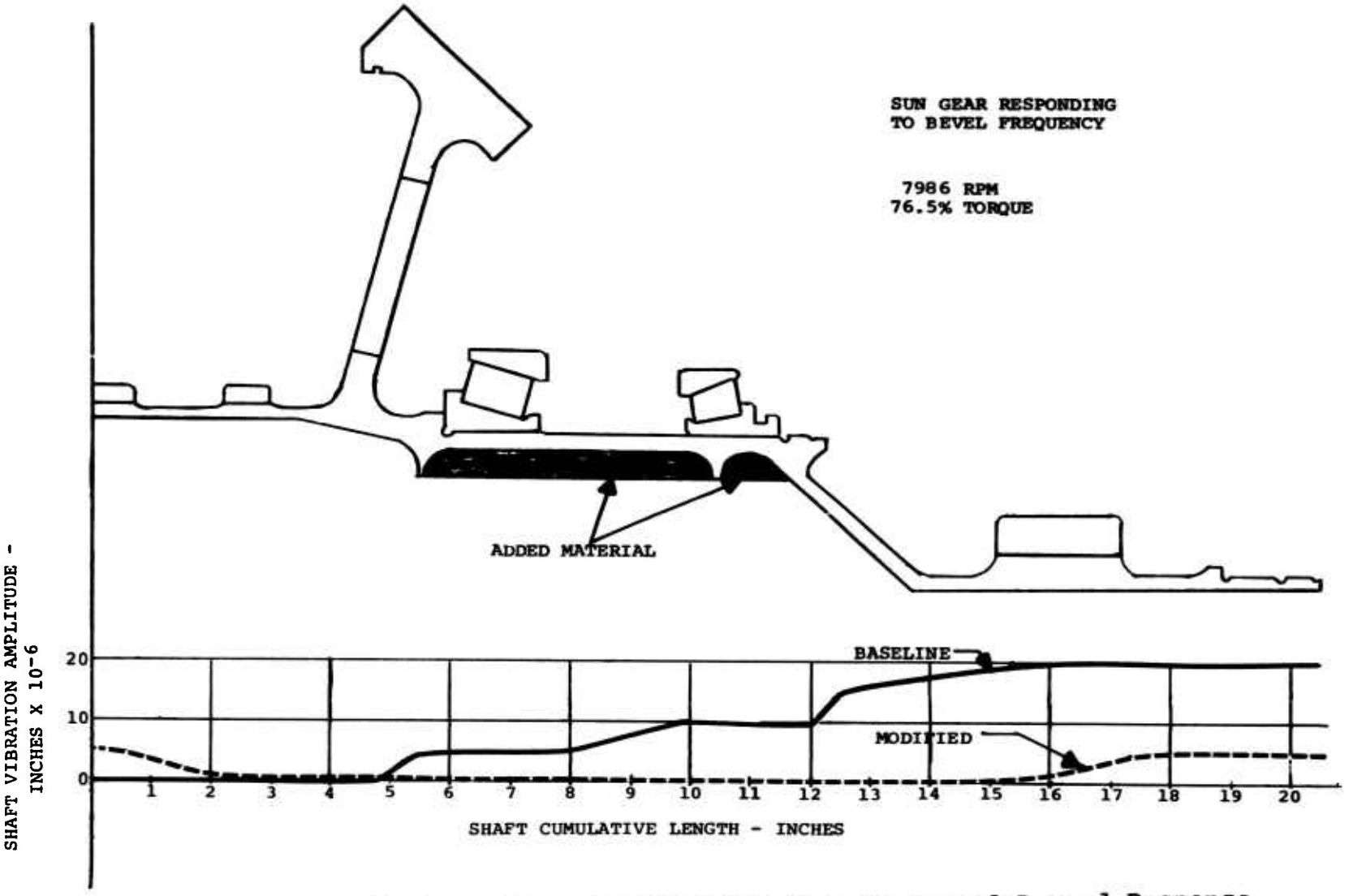

Figure 61. Effects of Sun Gear Modification on Forced Damped Response (Bevel Frequency) - HLH.

The DFR of the baseline ring gear was also determined and two modifications were analyzed.[19,20] These gears are shown in Figure 62. The displacements of the baseline and the modification which resulted in a better response are tabulated in Tables 6 and 7. From these tables, an overall noise reduction of 7.5 dB was calculated using the method discussed in "Ring Gear - Noise Reduction". The weight of this modification is 38 pounds.

Using the method for predicting transmission noise described in "Empirical Noise Level Predictions", it was estimated that the sound pressure level of the HLH baseline transmission without the above modifications would have been approximately 54 dB above MIL-A-8806 specification level at the bevel mesh frequency. This is at the most critical crew area location, which is the flight engineer's station located immediately below the forward transmission. Based on the above analysis, 17 dB of the required reduction is achievable through modification of the shafts and ring gear discussed.

A case attenuation material coating test, performed concurrently with this program, and reported in Reference 3, indicated that another 10 dB reduction could be obtained by coating the transmission case with an Energy Absorbing Rubber (E.A.R.) coating. An interesting result of the case attenuation material test was that a 10 dB attenuation was also possible at higher weight with a self-sealing coating material which would provide a measure of survivability (with an associated weight penalty). This still leaves 27 dB to be attenuated by some form of acoustical enclosure.

---

[19]C. Fredrickson, MODEL 301 ATC TRANSMISSION NOISE REDUCTION PROGRAM - RING GEAR RESONANCE ANALYSIS, Boeing-Vertol IOM 8-7453-1-2768, 8 August 1972.

[20]R. Hartman and G. Howland, MODEL 301 HLH/ATC TRANSMISSION NOISE REDUCTION PROGRAM - FORCED RESPONSE OF RING GEAR, Boeing-Vertol IOM 8-7446-1-956, November 1972.

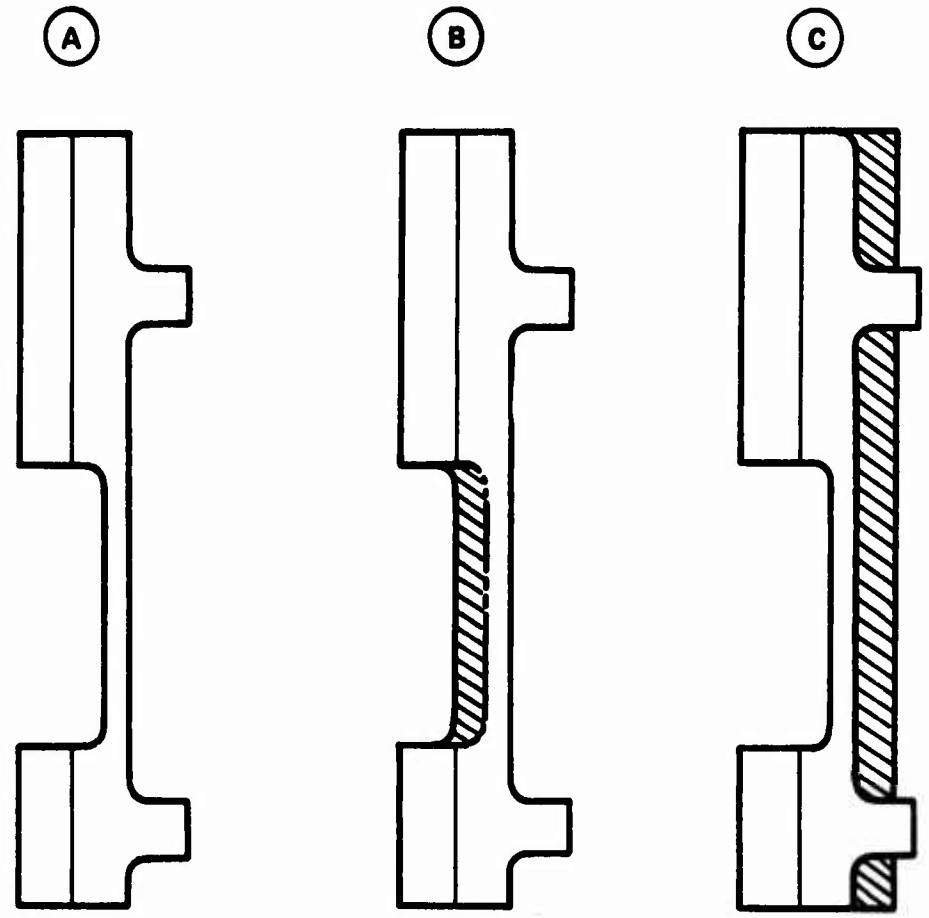

CONFIGURATION A – **PRESENT DESIGN**

CONFIGURATION B – **MATERIAL BETWEEN UPPER AND LOWER GEARS NOT REMOVED**

CONFIGURATION C – **EIGHT VERTICAL RIBS ADDED @ 45" INTERVALS**

Figure 62. HLH Ring Gear Configurations Analyzed.

TABLE 6. HLH BASELINE RING GEAR RESPONSE (MOD. A)

BASELINE HLH RING-GEAR
AMPLITUDE OF NORMAL DISPLACEMENT
AT BEVEL MESH FREQUENCY OF 4920 CPS

θ (deg) / Z x10^{-6} INCHES	0	45.0	90.0	135.0	180.0	225.0	270.0	315.0	360.0
0.0	3	2.24	0	2.24	- 3	2.24	0	2.24	3
1.750	15	12.21	0	12.21	-15	12.21	0	12.21	15
3.50	18	15.0	0	15.0	-18	15.0	0	15.0	18
6.250	28	17.03	0	17.03	28	17.03	0	17.03	28
7.8750	25	14.21	0	14.21	25	14.21	0	14.21	25

TABLE 7. MODIFIED RING GEAR RESPONSE (MOD. B)

MODIFIED HLH RING-GEAR
AMPLITUDE OF NORMAL DISPLACEMENT
AT BEVEL MESH FREQUENCY OF 4920 CPS

θ (deg) / Z x10^{-6} INCHES	0	45.0	90.0	135.0	180.0	225.0	270.0	315.0	360.0
0.0	0	2.828	0	2.828	0	2.828	0	2.828	0
0.750	1	5.385	0	5.385	- 1	5.385	0	5.385	1
3.50	1	5.385	0	5.385	- 1	5.385	0	5.385	1
6.250	-19	3.606	0	3.606	-19	3.606	0	3.606	-19
7.8750	-13	3.606	0	3.606	13	3.606	0	3.606	-13

The predicted sound spectrum for the unmodified transmission is shown in Figure 63. Also shown in this figure are the associated noise reductions due to the modifications. As mentioned in the "Introduction", noise attenuation of 20 to 25 dB can be realistically obtained with conventional acoustic enclosures with butt-type seals, and up to 35 dB with improved overlapping-type seals (.5 to .1% leakage). Attenuation of greater than 35 dB requires fume-tight seals (.1 to 0% leakage). Therefore, satisfaction of the Mil Spec using an enclosure only would necessitate a fume-tight enclosure; whereas, by incorporating the above modification, an enclosure with improved seals will suffice.

Trade-off Study

In order to compare the weight of the alternative approaches, the weight of acoustic enclosures as a function of noise attenuation was estimated for the HLH configuration. The weight of the enclosure hardware (fasteners, seals, hinges, etc.) was estimated to be approximately 50 pounds for a fume-tight enclosure (leakage less than .1%) and 20 pounds for a non-fume tight enclosure (leakage greater than .1%). To this enclosure hardware weight, the weight of the acoustical barrier must be added. This weight is a function of the attenuation required, the frequency, the surface area, and the enclosure leakage. Such a relation has been estimated for the HLH based on a review of current and advanced acoustical materials. This relation is shown in Figure 64 for 0.0, 0.1 and 0.5% leakages, for the spiral bevel mesh frequency (4925 Hz) and an estimated barrier area of 152 square feet. Of interest in this figure is that if the required attenuation is reduced to less than about 32 dB, a weight saving is associated with the reduced complexities of the non-fume tight enclosure. With the aid of this figure and the modified shaft and ring gear weights estimated above, comparative weight estimates were developed.

A comparison of the alternative concept weights and characteristics is summarized in Table 8. From this table, it is apparent that with a non-fume tight acoustic enclosure (Cases 3 & 4), an energy absorbing coating will be required in addition to modified shafts and ring gear. The shaft and ring gear modifications will provide an additional benefit in reliability, while the avoidance of a fume-tight enclosure provides for increased maintainability. Finally, the estimated weight savings for this approach could be

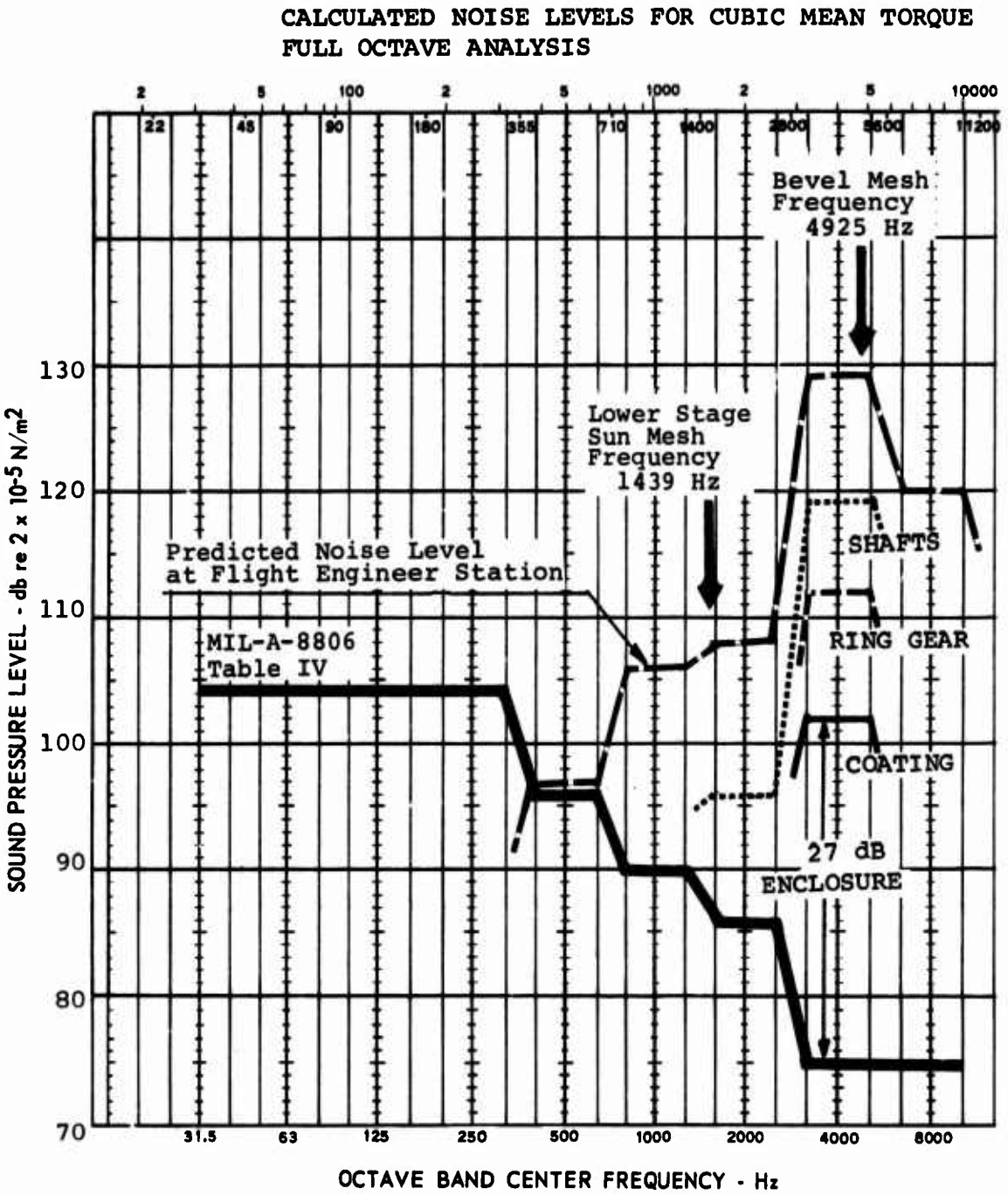

Figure 63. Comparison of Predicted Baseline Transmission Sound Spectrum to Mil Spec.

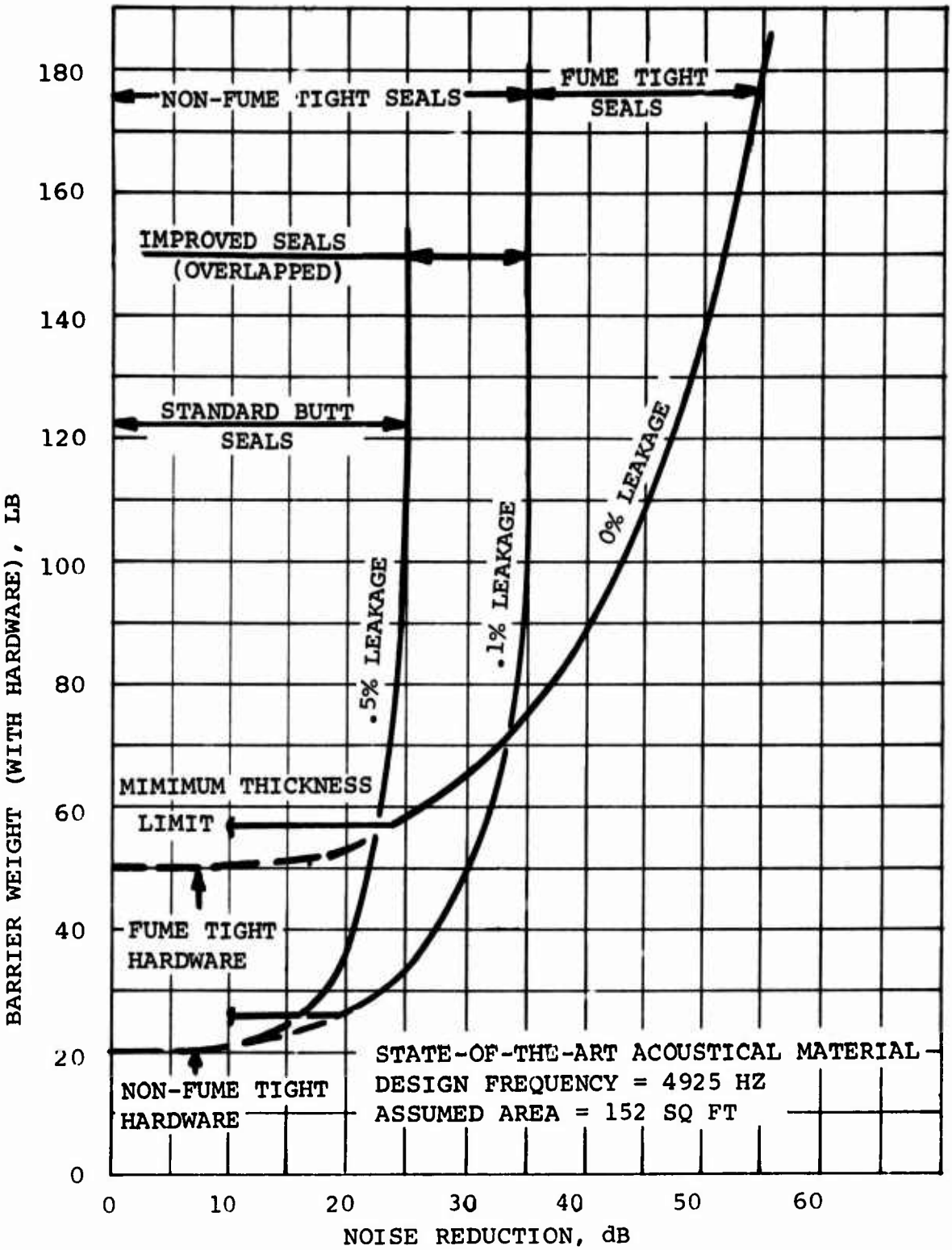

Figure 64. Estimated HLH Forward Transmission Barrier Weight (With Hardware).

TABLE 8. MODIFICATION/BENEFIT TRADE-OFF SUMMARY FOR SPECIFIED SOUND PRESSURE LEVEL

MODIFICATION	ΔSPL REQD ~ dB (NOTE 1)	TYPE ENCL REQD	ENCLOSURE WT ~ LB (NOTE 2)	Δ XMSN WT OF MODS ~ LB	TOTAL WT REQD FOR SPEC ~ LB	ADDITIONAL BENEFITS (NOTE 3)
1. None (Baseline Xmsn)	54	Fume Tight	170	0	170	None
2. Shafts	44	Fume Tight	110	35	145	Weight & Reliability
3. E.A.R.Coating + Shafts + Ring Gear	27	Non-Fume Tight	35	113	148	Weight, Reliability & Maintainability
4. Self-sealing Coating + Shafts + Ring Gear	27	Non-Fume Tight	35	143	178	Reliability, Maintainability & Survivability

NOTES:
1. Predicted Δ SPL required for spiral bevel mesh frequency of 4925 Hz at the flight engineer's station to meet MIL-A-8806.
2. Enclosure weight from Figure 64 using 0% leakage (fume tight) for Cases 1 & 2 and .1% leakage (non-fume tight) for Cases 3 & 4.
3. Increased reliability results from reduced displacements at bearings. Increased maintainability results from avoidance of fume-tight enclosures. Increased survivability results from 1/2-inch-thick self-sealing ballistic coating.

used for a self-seal coating to provide increases survivability as indicated. This could provide a transmission with increased reliability, better maintainability, and increased survivability for essentially the same total weight as a fume-tight enclosure used alone.

DYNAMIC ANALYSIS OF HLH COMBINER TRANSMISSION

Although noise is not of primary concern with regard to this box, the beneficial effects of reducing shaft displacements at the bearings were felt to be sufficient reason to perform a dynamic analysis. The Damped Forced Response (D-82) computer program was again used to determine the damped forced response of the box components.

The HLH combiner box is shown in Figure 65, and its mathematical model used for this analysis is seen in Figure 66. The coupled response of the six main components (center shaft, right-hand and left engine shafts, slant shaft, center engine shaft, and rotor brake) was analyzed for the three primary frequencies (idler mesh frequency, pump mesh frequency, and rotor brake mesh frequency).

Ten mass variations were evaluated. (Note: by varying mass (without changing stiffness), considerable computer time can be saved.) Once the apparent optimized mass distribution is determined, the stiffness is then changed accordingly. The complete results of this study are documented in Reference 21.[21]

With six shafts responding to three frequencies, and sixteen supporting bearings, the optimum configuration is at best a compromise. The modification which provided the best overall response is seen in Figure 67. For the 18 conditions analyzed, (six shafts at three frequencies), this modification was determined to be "better than" the baseline for eight cases, "equal to" for seven cases, and "worse than" for three cases.

This modification was designed as a removable slug inserted in the spur gear end of the center shaft. This will allow for a "with" and "without" comparison as a further verification of this type of dynamic analysis.

---

[21] R. Hartman, MODEL 301 HLH/ATC MIX BOX DYNAMIC ANALYSIS - FINAL DESIGN RECOMMENDATIONS, Boeing-Vertol IOM 8-7446-1-957.

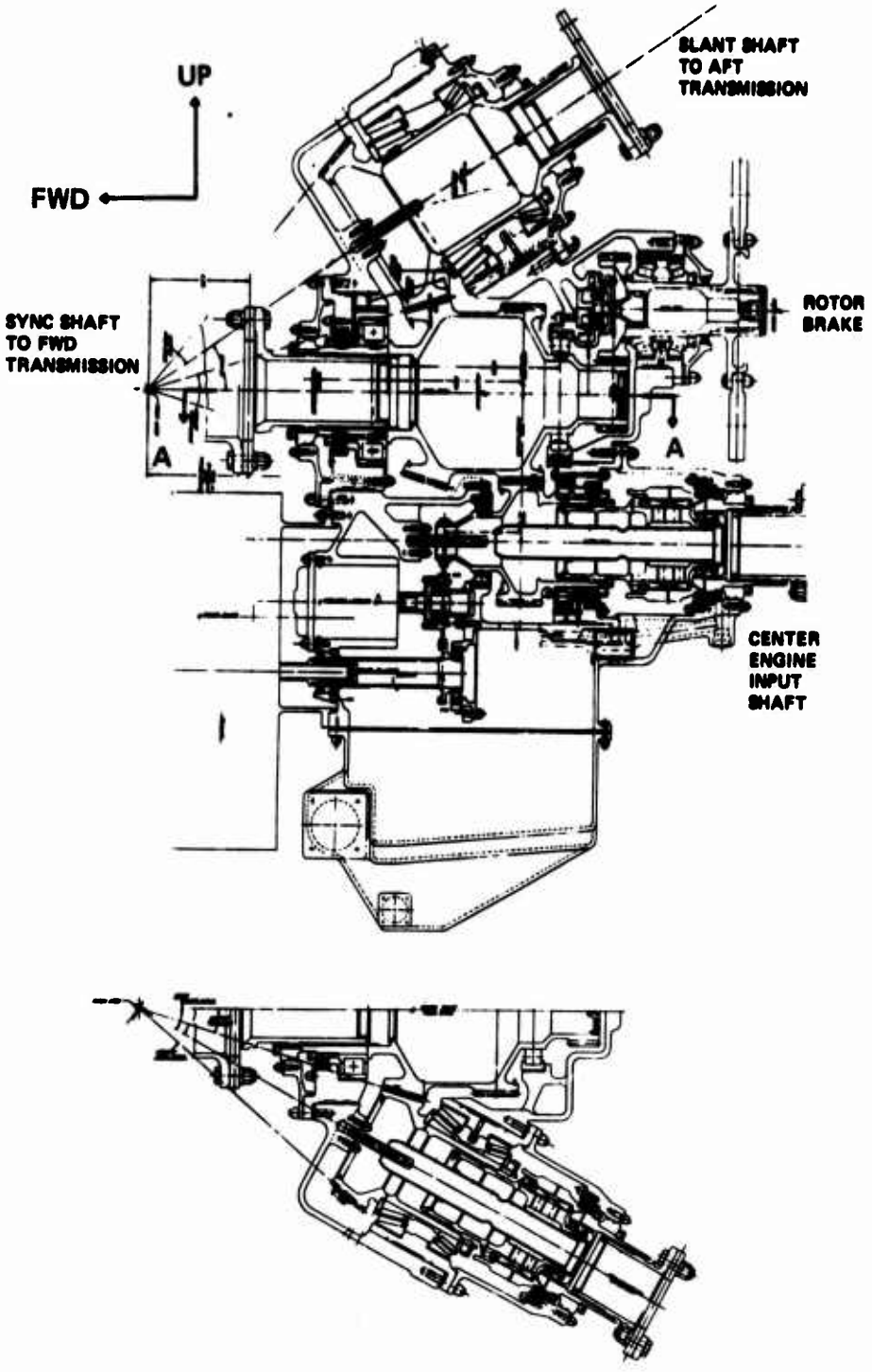

SECTION A–A

L.H. ENGINE INPUT SHAFT (SHOWN)
R.H. ENGINE INPUT SHAFT (OPP)

Figure 65. HLH Combiner Transmission.

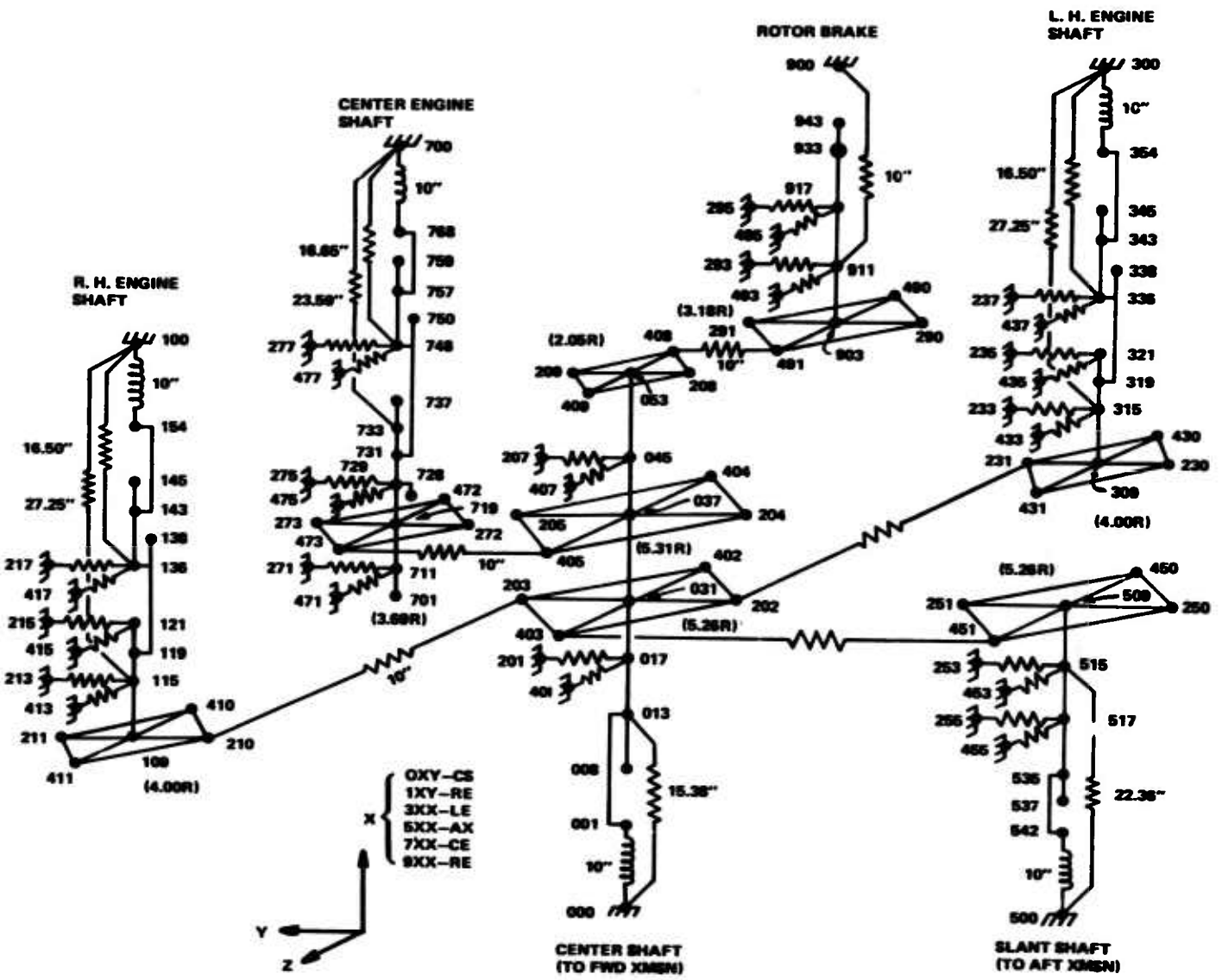

Figure 66. Combiner Transmission Computer Model.

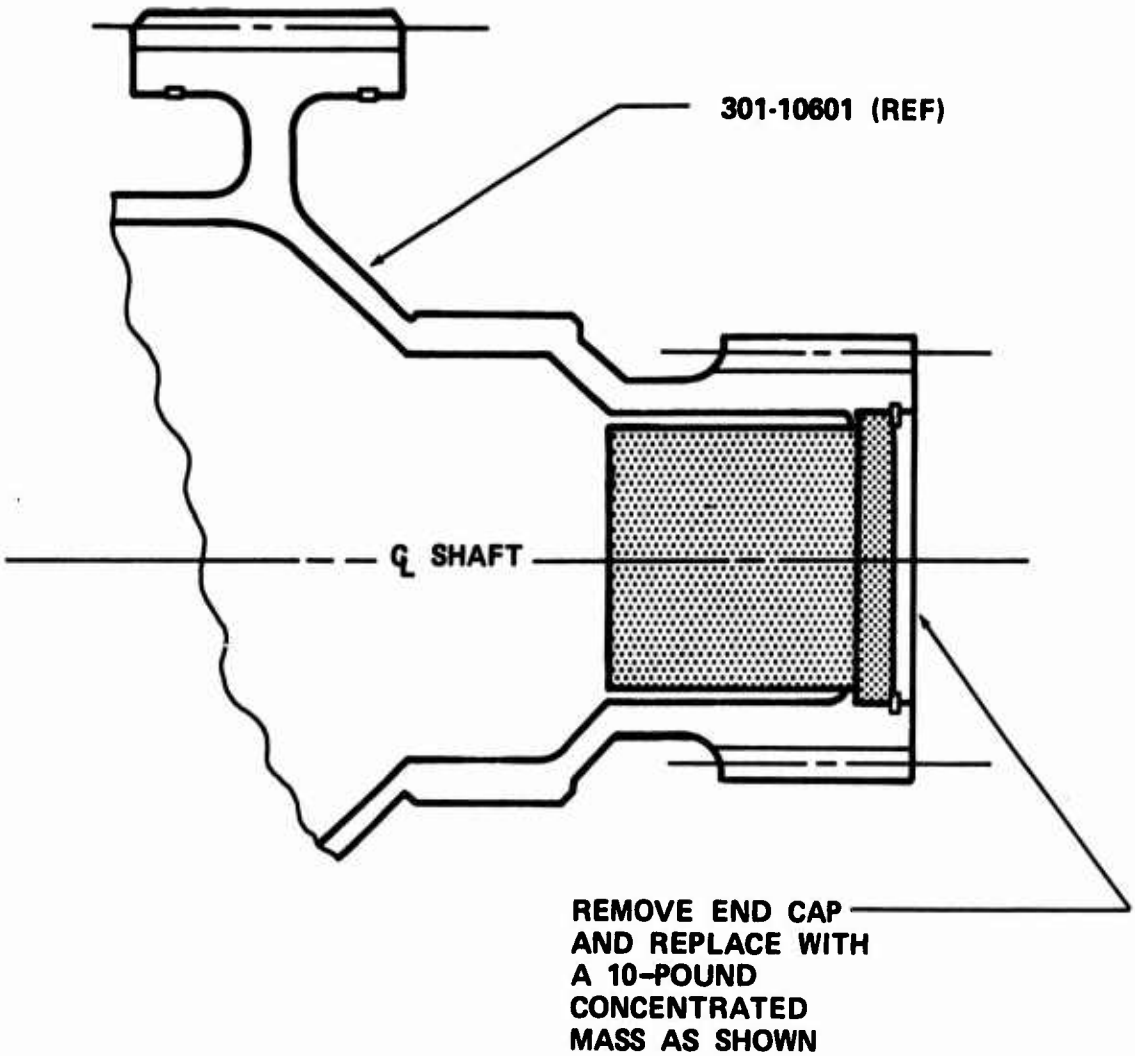

Figure 67. Modification to HLH Mix Box Center Shaft.

CONCLUSIONS

From the testing performed on the CH-47 forward transmission, the following conclusions were established:

1. The hypothesis that transmission noise is radiated from the transmission case, as a result of the non-uniform transfer of torque from pinion to gear due to elastic bending of gear teeth under load, has been validated. This nonuniform transfer of torque produces a dynamic force at the gear mesh frequency, resulting in a coupled torsion/bending response of the gear shaft. The bending produces a displacement at the bearings which in turn cause the case to vibrate, thereby producing noise.

2. The computer programs, TORRP and GEARO, have been validated.

3. The method of predicting transmission SPL spectrum has been validated.

4. The finite element approach (as utilized in the D-82 computer program) for predicting the damped forced response of the transmission components has been validated. The mathematical model should include the following:

    - Shaft to shaft coupling
    - Torsion/bending coupling
    - Six degrees of freedom
    - Proper end fixity

5. Additional weight associated with transmission component modifications to achieve reduced noise levels is competitive with alternative approaches.

6. The HLH noise specification at the flight engineer's station may be met with a non-fume tight enclosure, case coating, and tuning of the transmission components to minimize shaft deflections and case radiated noise.

In conjunction with the development of this noise reduction program, many areas of uncertainties have been uncovered. Some of these areas arrive from the inability of available computer programs to rigorously handle high-contact-ratio gearing and spiral bevel gears. These shortcomings have been circumvented by engineering approximations, based on limited test data.

A second area of uncertainty is the prediction of the change in overall SPL associated with changes in displacement at bearing locations. To properly address this problem, a knowledge of the case response is necessary. A method of predicting this noise reduction is presented in this report; however, considerably more development is required in this area. Also, the relation of reliability to bearing displacement is not well established.

Finally, a large volume of data has been accumulated as a result of this test program, of which only a small fraction was analyzed.

In light of the above comments, it is also concluded that the following programs are required to further develop the ability to predict and reduce transmission noise:

1. Extend GEARO to high contact and spiral bevel gearing.

2. Extend TORRP to incorporate bending.

3. Establish relation of change in bearing displacements to change in sound pressure level.

4. Develop case response analysis.

5. Continue reduction and analysis of test data.

In conclusion, sets of HLH shafts and ring gear as modified per this program and as originally designed are being manufactured. Energy-absorbing coatings will also be applied to the case. This will provide for experimental validation of the effects of the design modifications and external noise, and form the basis for definition of the acoustical treatment for the HLH.

REFERENCES

1. Sternfeld, H., Spencer, R. H., and Schaeffer, E. G., STUDY TO ESTABLISH REALISTIC ACOUSTIC DESIGN CRITERIA FOR FUTURE ARMY AIRCRAFT, Vertol Division, The Boeing Company, TREC TR 61-72, U. S. Army Transportation Research Command, Fort Eustis, Virginia, June 1961.

2. Sternfeld, H., Schairer, J., and Spencer, R., AN INVESTIGATION OF HELICOPTER TRANSMISSION NOISE REDUCTION BY VIBRATION ABSORBERS AND DAMPING, Vertol Division, The Boeing Company, USAAMRDL TR 72-34, U. S. Army Air Mobility Research and Development Laboratory, Fort Eustis, Virginia, August 1972.

3. Schaeffer, E. G., and Shadburn, E., TEST RESULTS REPORT - HLH/ATC EVALUATION OF TRANSMISSION NOISE ATTENUATION MATERIALS, The Boeing Company, Vertol Division, Report T301-10176-1, December 1972.

4. Badgley, R. H., and Laskin, I., PROGRAM FOR HELICOPTER GEARBOX NOISE PREDICTION AND REDUCTION, Mechanical Technology Incorporated, USAAVLABS TR 70-12, U. S. Army Aviation Materiel Laboratories, Fort Eustis, Virginia, March 1970, AD 869 822.

5. Badgley, R. H., and Chiang, T., INVESTIGATION OF GEARBOX DESIGN MODIFICATIONS FOR REDUCING HELICOPTER GEARBOX NOISE, Mechanical Technology Incorporated, USAAMRDL TR 72-6, U. S. Army Air Mobility Research and Development Laboratory, Fort Eustis, Virginia, March 1972.

6. Sternfeld, H., TEST PLAN - MODEL 301 HLH/ATC TRANSMISSION NOISE REDUCTION PROGRAM, The Boeing Company, Vertol Division Report D301-10091-1, January 1972.

7. Alberti, J., and Lemanski, A., INVESTIGATION OF INCREASED LOAD CAPACITY OF SPUR AND HELICAL GEARS WITH INCREASED CONTACT RATIO, The Boeing Company, Vertol Division, Report D210-10190-1, October 1970.

8. D'Agostini, A., DRIVE SYSTEM NOISE REDUCTION DATA ACQUISITION SYSTEM, Boeing-Vertol Test Memorandum Report TMR 1362, 30 August 1972.

9. Laskin, I., Orcutt, F. K., and Shipley, E. E., ANALYSIS OF NOISE GENERATED BY UH-1 HELICOPTER TRANSMISSION, Mechanical Technology Incorporated, USAAVLABS TR 68-41, U. S. Army Aviation Materiel Laboratories, Fort Eustis, Virginia, June 1967, AD 675 457.

10. Badgley, R.H., and Chiang, T., REDUCTION OF VIBRATION AND NOISE GENERATED BY PLANETARY RING GEARS IN HELICOPTER AIRCRAFT TRANSMISSIONS, ASME Paper Number 72-PTG-11, Presented at ASME Mechanisms Conference and International Symposium on Gearing and Transmissions, San Francisco, California, 8-12 October 1972.

11. Badgley, R.H., GEARBOX DYNAMICS - THE KEY TO UNDERSTANDING AND REDUCING ACOUSTIC-FREQUENCY ENERGY IN GEARED POWER TRAINS, Presented at the Meeting of the Aerospace Gearing Committee of the American Gear Manufacturers Association, Cleveland, Ohio, 17-18 January 1972.

12. Badgley, R.H., REDUCTION OF NOISE AND ACOUSTIC-FREQUENCY VIBRATIONS IN AIRCRAFT TRANSMISSIONS, AHS Paper Number 661, Presented at the 28th Annual National Forum of the American Helicopter Society, Washington, D.C., May 1972.

13. Sciarra, J., and Ricks, R., USE OF THE FINITE ELEMENT DAMPED FORCED RESPONSE STRAIN ENERGY DISTRIBUTION FOR VIBRATION REDUCTION, Presented at the ARO-D Military Theme Review, The Helicopter and V/STOL Aircraft Research Conference, Moffett Field, California, September 1972.

14. Sciarra, J., A COMPUTER METHOD FOR DYNAMIC STRUCTURAL ANALYSIS USING STIFFNESS MATRICES, Journal of America, Vol. 6, No. 1, January-February 1969, pp. 3-8.

15. Jones, A.B., A GENERAL THEORY FOR ELASTICALLY CONSTRAINED BALL AND RADIAL ROLLER BEARINGS UNDER ARBITRARY LOAD AND SPEED CONDITIONS, ASME Publication 59-LUB-10, New York, New York, October 1959.

16. Hartman, R., MODEL 301 HLH/ATC TRANSMISSION NOISE REDUCTION PROGRAM, Boeing-Vertol IOM 8-7446-1-923, 23 May 1972.

17. Hartman, R., MODEL 301 HLH/ATC TRANSMISSION NOISE REDUCTION PROGRAM - PHASE II MODEL, Boeing-Vertol IOM 8-7446-1-931, 19 June 1972.

18. Hartman, R., MODEL 301 HLH/ATC TRANSMISSION NOISE REDUCTION PROGRAM - DESIGN RECOMMENDATIONS, Boeing-Vertol IOM 8-7446-1-949, 31 August 1972.

19. Fredrickson, C., MODEL 301 ATC TRANSMISSION NOISE REDUCTION PROGRAM - RING GEAR RESONANCE ANALYSIS, Boeing-Vertol IOM 8-7453-1-2768, 8 August 1972.

20. Hartman, R., and Howland, G., MODEL 301 HLH/ATC TRANSMISSION NOISE REDUCTION PROGRAM - FORCED RESPONSE OF RING GEAR, Boeing-Vertol IOM 8-7446-1-956, November 1972.

21. Hartman, R., MODEL 301 HLH/ATC MIX BOX DYNAMIC ANALYSIS - FINAL DESIGN RECOMMENDATIONS, Boeing-Vertol IOM 8-7446-1-957.

APPENDIX A
SEQUENCING SCHEDULES

HLH TRANSMISSION NOISE REDUCTION TEST		
SEQUENCE NO. 1 TAPE SYSTEM A		
TRACK	PARAMETER	DESCRIPTION
1	STEP	
2	Spiral Bevel Probe PP7	BGPP7
3	Spiral Bevel Probe PP5	BGPP5
4	Spiral Bevel Probe Acceleration PA7	BGPA7
5	Spiral Bevel Probe Acceleration PA5	BGPA5
6	Case Acceleration #3	CA3
7	Case Acceleration #17	CA17
8	Spiral Bevel Bending B1	BGB1
9	Spiral Bevel Bending B2	BGB2
10	Spiral Bevel Bending BG3	BGB3
11	Spiral Bevel Bending B4	BGB4
12	Spiral Bevel 1/Rev	BG1/Rev
13	60 per Rev - Synch Shaft	
14	Voice Identification	
Function - Spiral Bevel Bending		

HLH TRANSMISSION NOISE REDUCTION TEST

SEQUENCE NO. 1 TAPE SYSTEM B

TRACK	PARAMETER	DESCRIPTION
1	Sun Probe Acceleration Upper PA4	SGPA4
2	Sun Probe Acceleration Lower PA2	SGPA2
3	Sun Gear Probe Upper PP4	SGPP4
4	Sun Gear Probe Lower PP2	SGPP2
5	Case Acceleration #1	CA1
6	STEP	
7	Case Acceleration #9	CA9
8	Sun Gear Bending B1	SGB1
9	Sun Gear Bending B2	SGB2
10	Sun Gear Bending B3	SGB3
11	Sun Gear Bending B4	SGB4
12	Sun Gear 1/Rev	SG1/Rev
13	60 per Rev - Synch Shaft	
14	Voice Identification	

Function - Sun Gear Bending

HLH TRANSMISSION NOISE REDUCTION TEST		
SEQUENCE NO. 2 TAPE SYSTEM A		
TRACK	PARAMETER	DESCRIPTION
1	Spiral Bevel Probe PP5	BGPP5
2	STEP	
3	Spiral Bevel Probe PP6	BGPP6
4	Spiral Bevel Probe PP7	BGPP7
5	Spiral Bevel Probe PP8	BGPP8
6	Spiral Bevel Acceleration PA5	BGPA5
7	Spiral Bevel Acceleration PA6	BGPA6
8	Spiral Bevel Acceleration PA7	BGPA7
9	Spiral Bevel Acceleration PA8	BGPA8
10	Case Acceleration #8	CA8
11	Case Acceleration #9	CA9
12	Spiral Bevel 1/Rev	BG1/Rev
13	60 per Rev - Synch Shaft	
14	Voice Identification	
Function - Spiral Bevel Gear Lateral		

HLH TRANSMISSION NOISE REDUCTION TEST		
SEQUENCE NO. 2 TAPE SYSTEM B		
TRACK	PARAMETER	DESCRIPTION
1	Sun Gear Acceleration RA1	SGRA1
2	Sun Gear Acceleration RA2	SGRA2
3	Sun Gear Probe Acceleration PA1	SGPA1
4	Sun Gear Probe Acceleration PA2	SGPA2
5	Sun Gear Probe Acceleration PA3	SGPA3
6	Sun Gear Probe Acceleration PA4	SGPA4
7	STEP	
8	Sun Gear Probe PP1	SGPP1
9	Sun Gear Probe PP2	SGPP2
10	Sun Gear Probe PP3	SGPP3
11	Sun Gear Probe PP4	SGPP4
12	Sun Gear 1/Rev	SG1/Rev
13	60 per Rev - Synch Shaft	
14	Voice Identification	
Function - Sun Gear Lateral		

HLH TRANSMISSION NOISE REDUCTION TEST		
SEQUENCE NO. 3 TAPE SYSTEM A		
TRACK	PARAMETER	DESCRIPTION
1	Sun Probe Upper DD4	SGPP4
2	Sun Probe Lower PP2	SGPP2
3	STEP	
4	Spiral Bevel Probe Upper PP7	BGPP7
5	Spiral Bevel Probe Lower PP5	BGPP5
6	Case Acceleration #1	CA1
7	Case Acceleration #8	CA8
8	Case Acceleration #3	CA3
9	Case Acceleration #15	CA15
10	Case Acceleration #16	CA16
11	Case Acceleration #11	CA11
12	Spiral Bevel 1/Rev	BG1/Rev
13	60 per Rev - Synch Shaft	
14	Voice Identification	
Function - Propagation of Bevel Mesh Signals		

HLH TRANSMISSION NOISE REDUCTION TEST		
SEQUENCE NO. 3 TAPE SYSTEM B		
TRACK	PARAMETER	DESCRIPTION
1	Sun Probe Acceleration Upper PA4	SGPA4
2	Sun Probe Acceleration Lower PA2	SGPA2
3	Spiral Bevel Probe Accel.Upper PA7	BGPA7
4	Spiral Bevel Probe Accel.Lower PA5	BGPA5
5	Case Acceleration #4	CA4
6	Case Acceleration #11	CA11
7	Case Acceleration #15	CA15
8	STEP	
9	Case Acceleration #16	CA16
10	Case Acceleration #17	CA17
11	Case Acceleration #13	CA13
12	Spiral Bevel 1/Rev	BG1/Rev
13	60 per Rev - Synch Shaft	
14	Voice Identification	
Function - Propagation of Bevel Mesh Signal		

HLH TRANSMISSION NOISE REDUCTION TEST		
SEQUENCE NO. 4 TAPE SYSTEM A		
TRACK	PARAMETER	DESCRIPTION
1	Case Acceleration #1	CA1
2	Microphone #4	M4
3	Case Acceleration #3	CA3
4	STEP	
5	Case Acceleration #4	CA4
6	Case Acceleration #11	CA11
7	Case Acceleration #12	CA12
8	Case Acceleration #13	CA13
9	Case Acceleration #14	CA14
10	Case Acceleration #15	CA15
11	Case Acceleration #16	CA16
12	Sun Gear 1/Rev	SG1/Rev
13	60 per Rev - Synch Shaft	
14	Voice Identification	
Function - Propagation of Planet Mesh Signals		

HLH TRANSMISSION NOISE REDUCTION TEST		
SEQUENCE NO. 4 TAPE SYSTEM B		
TRACK	PARAMETER	DESCRIPTION
1	Case Acceleration #13	CA13
2	Microphone #1	M1
3	Microphone #6 Dynamic, #8 Shake	M6 or 8
4	Microphone #2	M2
5	Microphone #4	M4
6	Microphone #5 (or 9 for Shake Test)	M5 or 9
7	Microphone #3	M3
8	Case Acceleration #8	CA8
9	STEP	
10	Case Acceleration #4	CA4
11	Case Acceleration #9	CA9
12	Case Acceleration #17	CA17
13	60 per Rev - Synch Shaft	
14	Voice Identification	
Function - Microphones		

HLH TRANSMISSION NOISE REDUCTION TEST		
SEQUENCE NO. 5 TAPE SYSTEM A		
TRACK	PARAMETER	DESCRIPTION
1	Sun Gear Acceleration RA1	SGRA1
2	Sun Gear Acceleration RA2	SGRA2
3	Spiral Bevel Torque T1	BGT1
4	Spiral Bevel Torque T2	BGT2
5	STEP	
6	Sun Gear Torque T1	SGT1
7	Sun Gear Torque T2	SGT2
8	Spiral Bevel Bending B1	BGB1
9	Spiral Bevel Bending B3	BGB3
10	Sun Gear Bending B1	SGB1
11	Sun Gear Bending B3	SGB3
12	Sun Gear 1/Rev	SG1/Rev
13	60 per Rev - Synch Shaft	
14	Voice Identification	
Function - Sun Gear and Spiral Bevel Torsional		

HLH TRANSMISSION NOISE REDUCTION TEST		
SEQUENCE NO. 5 TAPE SYSTEM B		
TRACK	PARAMETER	DESCRIPTION
1		
2		
3		
4	Sun Gear Torque T1	SGT1
5	Sun Gear Torque T2	SGT2
6		
7		
8	Sun Bending B1	SGB1
9	Sun Bending B3	SGB3
10	STEP	
11		
12		
13	60 per Rev - Synch Shaft	
14	Voice Identification	
Function - Visual Display (use with Sequence 1A)		

HLH TRANSMISSION NOISE REDUCTION TEST		
SEQUENCE NO. 101 TAPE SYSTEM A		
TRACK	PARAMETER	DESCRIPTION
1	STEP	
2	Case Acceleration #13	CA13
3	Sun Gear Probe Acceleration	SGPA4
4	Sun Gear Probe Acceleration	SGPA2
5	Spiral Bevel Probe Acceleration	BGPA7
6	Spiral Bevel Probe Acceleration	BGPA5
7	Case Acceleration #11 UP	CA11V
8	Case Acceleration #11 OUT	CA11N
9	Case Acceleration #15 UP	CA15V
10	Case Acceleration #15 OUT	CA15N
11	Spiral Bevel Torque T2	BGT2
12	Spiral Bevel 1/Rev	BG1/Rev
13	60 per Rev - Synch Shaft	
14	Voice Identification	
Function - Propagation of Bevel Mesh Signals		

HLH TRANSMISSION NOISE REDUCTION TEST

SEQUENCE NO. 101 TAPE SYSTEM B

TRACK	PARAMETER	DESCRIPTION
1	STEP	
2	Case Acceleration #22	CA22
3	Case Acceleration #23	CA23
4	Case Acceleration #10UP	CA10N
5	Case Acceleration #10 OUT	CA10H
6	Case Acceleration #11 UP	CA11V
7	Case Acceleration #11 OUT	CA11N
8	Case Acceleration #5	CA5
9	Case Acceleration #24	CA24
10	Case Acceleration #7	CA7
11	Sun Gear 1/Rev	SG1/Rev
12	Spiral Bevel 1/Rev	BG1/Rev
13	60 per Rev - Synch Shaft	
14	Voice Identification	

Function - Propagation of Upper Case Signals

HLH TRANSMISSION NOISE REDUCTION TEST		
SEQUENCE NO. 102 TAPE SYSTEM A		
TRACK	PARAMETER	DESCRIPTION
1	Case Acceleration #5	CA5
2	STEP	
3	Sun Gear Probe Acceleration	SGPA4
4	Sun Gear Probe Acceleration	SGPA2
5	Spiral Bevel Probe Acceleration	BGPA7
6	Spiral Bevel Probe Acceleration	BGPA5
7	Case Acceleration #7	CA7
8	Case Acceleration #11 OUT	CA11N
9	Case Acceleration #10 UP	CA10N
10	Case Acceleration #15 OUT	CA15 N
11	Spiral Bevel Torque T2	BGT2
12	Sun Gear 1/Rev	SG1/Rev
13	60 per Rev - Synch Shaft	
14	Voice Identification	
Function - Property of Sun Gear Signals		

HLH TRANSMISSION NOISE REDUCTION TEST

SEQUENCE NO. 102 TAPE SYSTEM B

TRACK	PARAMETER	DESCRIPTION
1	Microphones #1	M1
2	STEP	
3	Microphone #17	M17
4	Microphone #14	M14
5	Microphone #15	M15
6	Microphone #5	M5
7	Microphone #16	M16
8	Case Acceleration #5	CA5
9	Case Acceleration #24	CA24
10	Case Acceleration #7	CA7
11	Sun Gear 1/Rev	SG1/Rev
12	Spiral Bevel 1/Rev	BG1/Rev
13	60 per Rev - Synch Shaft	
14	Voice Identification	

Function - Microphones

HLH TRANSMISSION NOISE REDUCTION TEST		
SEQUENCE NO. 103 TAPE SYSTEM A		
TRACK	PARAMETER	DESCRIPTION
1	Sun Gear Probe Acceleration	SGPA4
2	Sun Gear Probe Acceleration	SGPA2
3	STEP	
4	Spiral Bevel Probe Acceleration	BGPA7
5	Spiral Bevel Probe Acceleration	BGPA5
6	Case Acceleration #11	CA11
7	Case Acceleration #12	CA12
8	Case Acceleration #13	CA13
9	Case Acceleration #14	CA14
10	Case Acceleration #15	CA15
11		
12	Spiral Bevel 1/Rev	BG1/Rev
13	60 per Rev - Synch Shaft	
14	Voice Identification	
Function - Propagation of Bevel Mesh Signals		

HLH TRANSMISSION NOISE REDUCTION TEST		
SEQUENCE NO. 103 TAPE SYSTEM B		
TRACK	PARAMETER	DESCRIPTION
1	Sun Probe Acceleration	SGPA4
2	Sun Probe Acceleration	SGPA2
3	Spiral Bevel Probe Acceleration	BGPA7
4	Spiral Bevel Probe Acceleration	BGPA5
5	Case Acceleration #5	CA5
6	Case Acceleration #6	CA6
7	Case Acceleration #19	CA19
8	STEP	
9	Case Acceleration #7	CA7
10	Case Acceleration #10	CA10
11	Sun Gear Torque T2	SGT2
12	Spiral Bevel 1/Rev	BG1/Rev
13	60 per Rev - Synch Shaft	
14	Voice Identification	
Function - Propagation of Bevel Mesh Signals		

HLH TRANSMISSION NOISE REDUCTION TEST		
SEQUENCE NO. 104 TAPE SYSTEM A		
TRACK	PARAMETER	DESCRIPTION
1	Case Acceleration #10	CA10
2	Case Acceleration #19	CA19
3	Case Acceleration #20	CA20
4	STEP	
5	Case Acceleration #21	CA21
6	Case Acceleration #11	CA11
7	Case Acceleration #12	CA12
8	Case Acceleration #13	CA13
9	Case Acceleration #14	CA14
10	Case Acceleration #15	CA15
11	Sun Gear 1/Rev	SG1/Rev
12	Spiral Bevel 1/Rev	BG1/Rev
13	60 per Rev - Synch Shaft	
14	Voice Identification	
Function - Propagation of Ring Gear Signals		

HLH TRANSMISSION NOISE REDUCTION TEST

SEQUENCE NO. 104 TAPE SYSTEM B

TRACK	PARAMETER	DESCRIPTION
1	Microphone #5	M5
2	Microphone #6A	M6A
3	Microphone #7	M7
4	Microphone #10	M10
5	Microphone #11	M11
6	Microphone #13	M13
7	Case Acceleration #19	CA19
8	Case Acceleration #13	CA13
9	STEP	
10	Case Acceleration #10	CA10
11	Sun Gear 1/Rev	SG1/Rev
12	Bevel 1/Rev	BG1/Rev
13	60 per Rev - Synch Shaft	
14	Voice Identification	

Function - Microphones

HLH TRANSMISSION NOISE REDUCTION TEST

SEQUENCE NO. 201 TAPE SYSTEM A

TRACK	PARAMETER	DESCRIPTION
1	STEP	
2	Case Acceleration #2	CA2
3	Sun Gear Probe Acceleration	SGPA4
4	Sun Gear Probe Acceleration	SGPA2
5	Spiral Bevel Probe Acceleration	BGPA7
6	Spiral Bevel Probe Acceleration	BGPA5
7	Case Acceleration #3	CA3
8	Case Acceleration #26	CA26
9	Case Acceleration #27	CA27
10	Case Acceleration #16N	CA16N
11	Sun Gear 1/Rev	SG1/Rev
12	Spiral Bevel 1/Rev	BG1/Rev
13	60 per Rev - Synch Shaft	
14	Voice Identification	

Function - Propagation of Signals - 4th Dynamic Test

HLH TRANSMISSION NOISE REDUCTION TEST		
SEQUENCE NO. 201 TAPE SYSTEM B		
TRACK	PARAMETER	DESCRIPTION
1	STEP	
2	Case Acceleration #16N	CA16N
3	Microphone 16	M16
4	Microphone 18	M18
5	Microphone 21	M21
6	Case Acceleration #16H	CA16H
7	Case Acceleration #8H	CA8H
8	Case Acceleration #8N	CA8N
9	Case Acceleration #7	CA7
10	Case Acceleration #25	CA25
11	Sun Gear 1/Rev	SG1/Rev
12	Bevel 1/Rev	BG1/Rev
13	60 per Rev - Synch Shaft	
14	Voice Identification	
Function - Microphones & Case - 4th Dynamic Test		

HLH TRANSMISSION NOISE REDUCTION TEST

SEQUENCE NO. 202 TAPE SYSTEM A

TRACK	PARAMETER	DESCRIPTION
1	Case Acceleration #8N	CA8N
2	STEP	
3	Sun Gear Probe Acceleration	SGPA4
4	Sun Gear Probe Acceleration	SGPA2
5	Spiral Bevel Probe Acceleration	BGPA7
6	Spiral Bevel Probe Acceleration	BGPA5
7	Case Acceleration #7	CA7
8	Case Acceleration #25	CA25
9	Case Acceleration #17	CA17
10	Case Acceleration #18	CA18
11	Sun Gear 1/Rev	SG1/Rev
12	Spiral Bevel 1/Rev	BG1/Rev
13	60 per Rev - Synch Shaft	
14	Voice Identification	

Function - Propagation of Signals - 4th Dynamic Test

HLH TRANSMISSION NOISE REDUCTION TEST		
SEQUENCE NO. 202 TAPE SYSTEM B		
TRACK	PARAMETER	DESCRIPTION
1	Microphone #1	M1
2	STEP	
3	Microphone #16	M16
4	Microphone #18	M18
5	Microphone #21	M21
6	Microphone #20	M20
7	Microphone #19	M19
8	Case Acceleration #3	CA3
9	Case Acceleration #26	CA26
10	Case Acceleration #27	CA27
11	Sun Gear 1/Rev	SG1/Rev
12	Spiral Bevel L/Rev	BG1/Rev
13	60 per Rev - Synch Shaft	
14	Voice Identification	
Function - Microphones & Sump - 4th Dynamic Test		

APPENDIX B

DRIVE SYSTEM NOISE REDUCTION SENSOR SENSITIVITIES

Dynamic Test #1

SENSOR	SETTING	SENSITIVITY	COMMENTS*
		(RMS)	
PA-1	1.42	10 MV/g(PK)	
PA-2	1.52	10 "	
PA-3	8.65	2 "	
PA-4	8.10	2 "	
PA-5	1.42	10 "	
PA-6	1.43	10 "	
PA-7	2.96	5 "	
PA-8	2.96	5 "	
		(RMS)	
CA-1	89.7	3.3 MV/g(PK)	
CA-3	29.7	10 "	
CA-4	51.6	3.3 "	
CA-9	55.9	5 "	
CA-16	58.2	5 "	
CA-17	74.3	3.3 "	
CA-8	16.7	10 "	
CA-11	35.3	5 "	
CA-12	65.0	2.5 "	
CA-13	48.6	3.3 "	
CA-15	54.7	5 "	
CA-14	23.1	3.3 "	
BGT_1	4	165 µin./RCal	
BGT_2	8	165 "	
BGT_1	4	165 "	
BGT_2	4	165 "	
BGT_3	4	165 "	
BGT_4	4	165	
SGT_1	2	165 µin./RCal	
SGT_2	2	165 "	
SGB_1	2	165 "	
SGB_2	2	165 "	
SGB_3	2	165 "	
SGB_4	2	165 "	

*Comment Made only if Channel Output is Defective

(Continued)

Dynamic System Noise Reduction Sensor Sensitivities(cont'd)

Dynamic Test #1 (Continued)

SENSOR	SETTING	SENSITIVITY	COMMENTS*
M_1		136 db/Volt	
M_2		"	
M_3		"	
M_4		"	
M_5		"	
M_6		"	
		(RMS)	
PP_1	500	1.38 MV/ μin.(PP)	
PP_2	500	1.23 "	
PP_3	1000	.45 "	
PP_4	1000	.49 "	
PP_5	250	2.0 "	
PP_6	500	.93 "	
PP_7	250	2.13 "	
PP_8	250	1.82 "	

*Comment Made only if Channel Output is Defective

****

Dynamic System Noise Reduction Sensor Sensitivities (cont'd)

Dynamic Test #2

SENSOR	SETTING	SENSITIVITY (RMS)	COMMENTS*
PA-1	1.42	10 MV/g (PK)	
PA-2	1.52	10 "	
PA-3	8.65	2 "	
PA-4	8.10	2 "	
PA-5	1.42	10 "	
PA-6	1.43	10 "	No Signal Output
PA-7	2.96	5 "	
PA-8	2.96	5 "	
CA-7	89.7	3.3 MV/g (PK)	Saturated Output
CA-6	29.7	10 "	
CA-5	51.6	3.3 "	
CA-19	84.39	3.3 "	
CA-10	58.2	5 "	
CA-20	74.3	3.3 "	
CA-21	50.2	3.3 "	
CA-11	35.3	5 "	
CA-12	65.0	2.5 "	
CA-13	48.6	3.3 "	
CA-15	54.7	5 "	
CA-14	23.1	3.3 "	
BGT_1	4	165 µin./RCal	
BGT_2	8	165 "	
BGB_1	4	165 "	Spiking Output-Badly
BGB_2	4	165 "	
BGB_3	4	165 "	Spiking Output-Slightly
BGB_4	4	165 "	
SGT1	2	165 µin./RCal	
SGT2	2	165 "	Spiking Output-Slightly
SGB1	2	165 "	
SGB_2	2	165 "	
SGB_3	2	165 "	Spiking Output-Badly
SGB_4	2	165 "	Spiking Output-Slightly

(Continued)

Dynamic System Noise Reduction Sensor Sensitivities(cont'd)

Dynamic Test #2 (continued)

SENSOR	SETTING	SENSITIVITY	COMMENTS*
M_1		136 db/Volt	
M_2		136 "	
M_3		136 "	
M_4		136 "	
M_5		136 "	
M_6		136 "	
		(RMS)	
PP_1	500	1.38 MV/ µin.(P.P.)	
PP_2	500	1.28 "	
PP_3	1000	.45 "	
PP_4	1000	.49 "	
PP_5	250	2. "	
PP_6	500	.93 "	
PP_7	250	2.13 "	
PP_8	250	1.82 "	

****

Dynamic System Noise Reduction Sensor Sensitivities(cont'd)

Dynamic Test #3

SENSOR	SETTING	SENSITIVITY	COMMENTS*
		(RMS)	
PA-1	1.42	10 MV/g (PK)	
PA-2	1.52	10 "	
PA-3	8.65	2 "	
PA-4	8.10	2 "	
PA-5	1.42	10 "	
PA-6	1.43	10 "	No Signal Output
PA-7	2.96	5 "	
PA-8	2.96	5 "	
		(RMS)	
CA-22	55.9	5 MV/g (PK)	
CA-10up	89.7	3.3 "	
CA-24	59.4	5 "	
CA-5	51.6	3.3 "	
CA-10out	58.2	5 "	
CA-23	74.3	3.3 "	
CA-11up	16.7	10 "	
CA-11out	35.3	5 "	
CA-15up	65.0	2.5 "	
CA-13	48.6	3.3 "	
CA-15out	81.9	3.3 "	
CA-7	77.6	1 "	
BGT_1	4	165 µin./RCal	Spiking Output-Slightly
BGT_2	8	165 "	Spiking Output-Badly
BGB1	4	165 "	Output Completely Bad
BGB_2	4	165 "	Output Completely Bad
BGB_3	4	165 "	Spiking Output-Slightly
BGB_4	4	165 "	Output Completely Bad
SGT_1	2	165 µin./RCal	
SGT_2	2	165 "	Spiking Output-Slightly
SGB_1	2	165 "	
SGB_2	2	165 "	
SGB_3	2	165 "	Spiking Output-Badly
SGB_4	2	165 "	Spiking Output-Slightly

(Continued)

Dynamic System Noise Reduction Sensor Sensitivities (cont'd)

Dynamic Test #3 (Continued)

SENSOR	SETTING	SENSITIVITY	COMMENTS*
M1		136 db/Volt	
M2		136 "	
M3		136 "	
M4		136 "	
M5		136 "	
M6		136 "	
		(RMS)	
PP-1	500	1.38 MV/μin.(P.P.)	
PP-2	500	1.28 "	
PP-3	1000	.45 "	
PP-4	1000	.49 "	
PP-5	250	2. "	
PP-6	500	.93 "	
PP-7	250	2.13 "	
PP-8	250	1.82 "	

****

Dynamic System Noise Reduction Sensor Sensitivities (cont'd)

Dynamic Test #4

SENSOR	SETTING	SENSITIVITY	COMMENTS*
		(RMS)	
PA-1	1.42	10 MV/g (PK)	
PA-2	1.52	10 "	
PA-3	8.65	2 "	
PA-4	8.10	2 "	
PA-5	1.42	10 "	
PA-6	1.43	10 "	No Signal Output
PA-7	2.96	5 "	
PA-8	2.96	5 "	
		(RMS)	
CA-26	55.9	5 MV/g (PK)	
CA-2	89.7	3.3 "	
CA-3	59.4	5 "	
CA-18	51.6	3.3 "	
CA-27	58.2	5 "	
CA-17	98.8	2.5 "	
CA-8Long.N	33.4	5 "	
CA-8Lat.H	35.3	5 "	
CA-16Long.N	65.0	2.5 "	
CA-25	81.0	2.5 "	
CA-16Lat.H	27.3	10 "	
CA-7	77.6	1 "	
BGT_1	4	165 µin./RCal	N.B.-All Bridges are Bad at this Point
BGT_2	8	165 "	
BGB_1	4	165 "	
BGB_2	4	165 "	
BGB_3	4	165 "	
BGB_4	4	165 "	
SGT_1	2	165 µin./RCal	
SGT_2	2	165 "	
SGB_1	2	165 "	
SGB_2	2	165 "	
SGB_3	2	165 "	
SGB_4	2	165 "	
M_1		136 db/Volt	
M_2		136 "	
M_3		136 "	
M_4		136 "	
M_5		136 "	
M_6		136 "	

(Continued)

Dynamic System Noise Reduction Sensor Sensitivities (cont'd)

Dynamic Test #4 (continued)

SENSOR	SETTING	SENSITIVITY (RMS)	COMMENTS*
PP-1	500	1.38 MV/ µin.(PK)	
PP-2	500	1.28 "	
PP-3	1000	.45 "	
PP-4	1000	.49 "	
PP-5	250	2. "	
PP-6	500	.93 "	
PP-7	250	2.13 "	
PP-8	250	1.82 "	

****

APPENDIX C
RUN LOG AND TAPE LOG

SHAKE TEST
Run Log and Tape Log

TYPE OF RUN				SHAKER FREQUENCY ~ Hz	SHAKE SEQUENCE NUMBER	TAPE LOG NUMBER
TORQUE	ACCEL.	DECEL.	STABILITY			
40%			X	1563	1	6-G-1
			X	3615	1	
			X		2	
			X		3	
			X	3615	4	
			X	1563	2	
			X		3	
40%			X	1563	4	6-G-1
60%	X				1	6-G-2
	X				2	
	X				3	
	X				4	
			X	1563	1	
			X		2	
			X		3	
			X	1563	4	
			X	3615	1	
			X		2	
			X		3	
60%			X	3615	4	6-G-2
80%	X				1	6-G-3
	X				2	
	X				3	
	X				4	
			X	1563	1	
			X		2	
			X		3	
			X	1563	4	
			X	3615	1	
			X		2	
			X		3	
80%			X	3615	4	6-G-3

(Continued)

SHAKE TEST (Continued)

TYPE OF RUN				SHAKER FREQUENCY ~ Hz	SHAKE SEQUENCE NUMBER	TAPE LOG NUMBER
TORQUE	ACCEL.	DECEL.	STABILITY			
90%	X				1	6-G-4
	X				2	
	X				3	
	X				4	
			X	1563	1	
			X		2	
			X		3	
			X	1563	4	
			X	3615	1	
			X		2	
			X		3	
90%			X	3615	4	6-G-4
100%	X				1	6-G-5
	X				2	
	X				3	
	X				4	
			X	1563	1	
			X		2	
			X		3	
			X	1563	4	
			X	3615	1	
			X		2	
			X		3	
100%			X	3615	4	6-G-5

TEST CELL STATIC TORQUE CALIBRATION

TORQUE	SHAKE SEQ. NO.	TAPE LOG NUMBER
0%	2	6-G-6
20%		
40%		
60%		
80%		
90%		
100%		
0%		
90%		
100%	2	6-G-6

DYNAMIC TEST NUMBER 1
Run Log and Tape Log

TORQUE	ACCEL.	DECEL.	rpm	SEQUENCE NUMBER	TYPE OF RUN	TAPE LOG NUMBER
80%			7460	1	Stab.rpm	6-G-7
↓			↓	2	↑	↓
				3		
				4		
				5		
				1		
				2		
				3		
				4		
			7460	5	Stab.rpm	
		X	7.5→3K	1	Sweep	
	X		3→7.5K	1	↓	
		X	7.5→3K	5		
	X		3→7.5K	5		
		X	7.5→3K	2		
80%	X		3→7.5K	2	Sweep	6-G-7
80%		X	7.5→3K	3	Sweep	6-G-8
↓	X		3→7.5K	3	↓	↓
		X	7.5→3K	4		
	X		3→7.5K	4		
80%		X	7.5→3K	1	Sweep	6-G-8
80%			3400	1,2,3,4,5	Stab.rpm	6-G-9
↓			3600	↓	↓	↓
			3800			
			4200			
			4400			
			5600			
80%			5800	1,2,3,4,5	Stab.rpm	6-G-9
80%			5900	1,2,3,4,5	Stab.rpm	6-G-10
↓			6000	↓	↓	↓
			6100			
			6200			
			6300			
			6400			
80%			6600	1,2,3,4,5	Stab.rpm	6-G-10

(Continued)

Dynamic Test Number 1 (Continued)

TORQUE	ACCEL.	DECEL	rpm	SEQUENCE NUMBER	TYPE OF RUN	TAPE LOG NUMBER
80%			6800	1,2,3,4,5	Stab.rpm	6-G-11
			7000			
			7200			
			7460	1,2,3,4,5		
		X	7.5→3K	4		
80%	X		3→7.5K	4		
60%		X	7.5→3K	5A,1B	Stab.rpm	6-G-11
60%		X	7.5→3K	1	Sweep	6-G-12
	X		3→7.5K	1		
		X	7.5→3K	2		
	X		3→7.5K	2		
		X	7.5→3K	3		
	X		3→7.5K	3		
		X	7.5→3K	4		
	X		3→7.5K	4		
		X	7.5→3K	5		
60%	X		3→7.5K	5		
40%		X	7.5→3K	1		
40%	X		3→7.5K	1	Sweep	6-G-12
40%		X	7.5→3K	2	Sweep	6-G-13
	X		3→7.5K	2		
		X	7.5→3K	3		
	X		3→7.5K	3		
		X	7.5→3K	4		
	X		3→7.5K	4		
		X	7.5→3K	5		
40%	X		3→7.5K	5		
100%		X	7.5→3K	1		
	X		3→7.5K	1		
		X	7.5→3K	2		
100%	X		3→7.5K	2	Sweep	6-G-13
100%		X	7.5→3K	3	Sweep	6-G-14
	X		3→7.5K	3		
		X	7.5→3K	4		
	X		3→7.5K	4		
		X	7.5→3K	5		
100%	X		3→7.5K	5		
90%		X	7.5→3K	1		
	X		3→7.5K	1		
		X	7.5→3K	2		
	X		3→7.5K	2		
		X	7.5→3K	3		
90%	X		3→7.5K	3	Sweep	6-G-14

(Continued)

Dynamic Test Number 1 (Continued)

TORQUE	ACCEL.	DFCEL	rpm	SEQUENCE NUMBER	TYPE OF TUN	TAPE LOG NUMBER
90%		X	7.5→3K	4	Sweep	6-G-15
	X		3→7.5K	4		
		X	7.5→3K	5		
90%	X		3→7.5K	5	Sweep	6-G-15
60%			5600	1,2,3,4,5	Stab.rpm	6-G-16
			5800			
			6000			
			6200			
			6400			
			6600			
60%			6800	1,2,3,4,5	Stab.rpm	6-G-16
60%			6800	5	Stab.rpm	6-G-17
			7000	1,2,3,4,5		
			7200			
60%			7460	1,2,3,4,5		
40%			5600	1,5		
			5800			
			6000			
			6200			
			6400			
			6600			
			6800			
			7000			
			7200			
40%			7460	1,5	Stab.rpm	6-G-17
100%			5600	1,5	Stab.rpm	6-G-18
			5800			
			6000			
			6200			
			6400			
			6600			
			6800			
			7000			
			7200			
100%			7460			
90%			5600			
			5800			
			6000			
			6200			
			6400			
			6600			
			6800	1,5		
90%			7000	1	Stab.rpm	6-G-18

(Continued)

Dynamic Test Number 1 (Continued)

TORQUE	ACCEL.	DECEL.	rpm	SEQUENCE NUMBER	TYPE OF RUN	TAPE LOG NUMBER
90%			7000	5	Stab.rpm	6-G-19
			7200	1,5	Stab.rpm	
			7460	1,5	Stab.rpm	
		X	7.5→3K	5A	Sweep	
90%		X	7.5→3K	1B	Sweep	
40%			5600	2,3,4	Stab.rpm	
			5800			
			6000			
			6200			
			6400			
			6600			
			6800			
			7000			
			7200			
40%			7460	2,3,4	Stab.rpm	6-G-19
40%			7460	2,3,4	Stab.rpm	6-G-20
100%			5600			
			5800			
			6000			
			6200			
			6400			
			6600			
			6800			
			7000			
			7200			
100%			7460	2,3,4	Stab.rpm	6-G-20
90%			5600	2,3,4	Stab.rpm	6-G-21
			5800			
			6000			
			6200			
			6400			
			6600			
			6800			
			7000			
			7200			
			7460	2,3,4		
			5600	1B		
			5800			
			6000			
			6200			
			6400			
90%			6600	1B	Stab.rpm	6-G-21

(Continued)

Dynamic Test Number 1 (Continued)

TORQUE	ACCEL.	DECEL.	rpm	SEQUENCE NUMBER	TYPE OF RUN	TAPE LOG NUMBER
100%			5600	1B	Stab.rpm	6-G-22
			5800			
			6000			
			6200			
			6400			
			6600			
			6800			
			7000			
			7200			
100%			7460			
			5800			
			5900			
			6000			
			6100	1B		
			6600	2B, 3B, 4B		
			6800			
			7000			
			7200			
			7460	2B, 3B, 4B	Stab. rpm	6-G-22
80%		X	7.5→3K	3B	Stab.rpm	6-G-23
	X		3→7.5K	3B		
		X	7.5→3K	4B		
	X		3→7.5K	4B		
80%		X	7.5→3K	1B	Stab.rpm	6-G-23

*****

DYNAMIC TEST NUMBER 2

Run Log and Tape Log

TORQUE	ACCEL.	DECEL.	rpm	SEQUENCE NUMBER	TYPE OF RUN	TAPE LOG NUMBER
80%		X	7.5→3K	103	Sweep	6-G-24
	X		3→7.5K	103		
		X	7.5→3K	104		
	X		3→7.5K	104	Sweep	
			5600	103/104	Stab.rpm	
			5800			
			6000			
			6200			
			6400			
			6600			
			6800			
			7000			
80%			7460	103/104	Stab.rpm	6-G-24
60%		X	7.5→3K	103	Sweep	6-G-25
	X		3→7.5K	103		
		X	7.5→3K	104		
	X		3→7.5K	104	Sweep	
			5600	103/104	Stab.rpm	
			5800			
			6000			
			6200			
			6400			
			6600			
			6800			
			7000			
			7200			
60%			7460	103/104	Stab.rpm	6-G-25
40%		X	7.5→3K	103	Sweep	6-G-26
	X		3→7.5K	103		
		X	7.5→3K	104		
	X		3→7.5K	104	Sweep	
			5600	103/104	Stab.rpm	
			5800			
			6000			
			6200			
			6400			
			6600			
			6800			
			7000			
			7200			
40%			7460	103/104	Stab.rpm	6-G-26

(Continued)

Dynamic Test Number 2 (Continued)

TORQUE	ACCEL.	DECEL.	rpm	SEQUENCE NUMBER	TYPE OF RUN	TAPE LOG NUMBER
100%		X	7.5→3K	103	Sweep	6-G-27
	X		3→7.5K	103		
		X	7.5→3K	104		
	X		3→7.5K	104	Sweep	
			5600	103/104	Stab.rpm	
			5800			
			6000			
			6200			
			6400			
			6600			
			6800			
			7000			
			7200			
100%			7460	103/104	Stab.rpm	6-G-27
90%		X	7.5→3K	103	Sweep	6-G-28
	X		3→7.5K	103		
		X	7.5→3K	104		
	X		3→7.5K	104	Sweep	
			5600	103/104	Stab.rpm	
			5800			
			6000			
			6200			
			6400			
			6600			
			6800			
			7000			
			7200			
90%			7460	103/104	Stab.rpm	6-G-28

****

DYNAMIC TEST NUMBER 3

Run Log and Tape Log

TORQUE	ACCEL.	DECEL.	rpm	SEQUENCE NUMBER	TYPE OF RUN	TAPE LOG NUMBER
80%		X	7.5→3K	101	Sweep	6-G-29
	X		3→7.5K	101		
		X	7.5→3K	102		
	X		3→7.5K	102	Sweep	
			5600	101/102	Stab.rpm	
			5800			
			6000			
			6200			
			6400			
			6600			
			6800			
			7000			
			7200			
80%			7460	101/102	Stab.rpm	6-G-29
60%		X	7.5→3K	101	Sweep	6-G-30
	X		3→7.5K	101		
		X	7.5→3K	102		
	X		3→7.5K	102	Sweep	
			5600	101/102	Stab.rpm	
			5800			
			6000			
			6200			
			6400			
			6600			
			6800			
			7000			
			7200			
60%			7460	101/102	Stab.rpm	6-G-30
40%		X	7.5→3K	101	Sweep	6-G-31
	X		3→7.5K	101		
		X	7.5→3K	102		
	X		3→7.5K	102	Sweep	
			5600	101/102	Stab.rpm	
			5800			
			6000			
			6200			
			6400			
			6600			
			6800			
			7000			
			7200			
40%			7460	101/102	Stab.rpm	6-G-31

Dynamic Test Number 3 (Continued)

TORQUE	ACCEL.	DECEL.	rpm	SEQUENCE NUMBER	TYPE OF RUN	TAPE LOG NUMBER
100%		X	7.5→3K	101	Sweep	6-G-32
	X		3→7.5K	101		
		X	7.5→3K	102		
	X		3→7.5K	102	Sweep	
			5600	101/102	Stab.rpm	
			5800			
			6000			
			6200			
			6400			
			6600			
			6800			
			7000			
			7200			
100%			7460	101/102	Stab.rpm	6-G-32
90%		X	7.5→3K	101	Sweep	6-G-33
	X		3→7.5K	101		
		X	7.5→3K	102		
	X		3→7.5K	102	Sweep	
			5600	101/102	Stab.rpm	
			5800			
			6000			
			6200			
			6400			
			6600			
			6800			
			7000			
			7200			
90%			7460	101/102	Stab.rpm	6-G-33

****

DYNAMIC TEST NUMBER 4

Run Log and Tape Log

TORQUE	ACCEL.	DECEL	rpm	SEQUENCE NUMBER	TYPE OF RUN	TAPE LOG NUMBER
80%		X	7.5→3K	201	Sweep	6-G-34
	X		3→7.5K	201		
		X	7.5→3K	202		
	X		3→7.5K	202	Sweep	
			5600	201/202	Stab.rpm	
			5800			
			6000			
			6200			
			6400			
			6600			
			7000			
			7200			
			7460			
80%			7600	201/202	Stab.rpm	6-G-34
60%		X	7.5→3K	201	Sweep	6-G-35
	X		3→7.5K	201		
		X	7.5→3K	202		
	X		3→7.5K	202	Sweep	
			5600	201/202	Stab.rpm	
			5800			
			6000			
			6200			
			6400			
			6600			
			6800			
			7000			
			7200			
			7460			
60%			7600	201/202	Stab.rpm	6-G-35
40%		X	7.5→3K	201	Sweep	6-G-36
	X		3→7.5K	201		
		X	7.5→3K	202		
	X		3→7.5K	202	Sweep	
			5600	201/202	Stab.rpm	
			5800			
			6000			
			6200			
			6400			
			6600			
			6800			
			7000			
			7200			
			7460			
40%			7600	201/202	Stab.rpm	6-G-36

(Continued)

Dynamic Test Number 4 (Continued)

TORQUE	ACCEL.	DECEL.	rpm	SEQUENCE NUMBER	TYPE OF RUN	TAPE LOG NUMBER
100%		X	7.5→3K	201	Sweep	6-G-37
	X		3→7.5K	201		
		X	7.5→3K	202		
	X		3→7.5K	202	Sweep	
			5600	201/202	Stab.rpm	
			5800			
			6000			
			6200			
			6400			
			6600			
			6800			
			7000			
			7200			
			7460			
100%			7600	201/202	Stab.rpm	6-G-37
90%		X	7.5→3K	201	Sweep	6-G-38
	X		3→7.5K	201		
		X	7.5→3K	202		
	X		3→7.5K	202	Sweep	
			5600	201/202	Stab.rpm	
			5800			
			6000			
			6200			
			6400			
			6600			
			6800			
			7000			
			7200			
			7460			
90%			7600	201/202	Stab.rpm	6-G-38

(Continued)

Dynamic Test Number 4 (Continued)

TORQUE	ACCEL. 3--7.6K	DECEL. 7.6--3K	rpm	SEQUENCE NUMBER	LIFT	DRAG	PM	TAPE LOG NO.
80%		X		201	20,000	0	0	6-G-39
	X			201				
		X		202				
	X			202		0		
		X		201		2,000		
	X			201				
		X		202				
	X			202	20,000			
		X		201	0			
	X			201				
		X		202				
	X			202		2,000		
		X		201		0		
	X			201				
		X		202				
80%	X			202	0	0	0	6-G-39
80%			7460	201/202	20,000	0	0	6-G-40
						2,000		
						2,000		
80%			7460	201/202	20,000	0	0	6-G-40

****

LIST OF SYMBOLS

A	Surface Area, sq cm
$[C]$	Damping Matrix
DFR	Damped Forced Response
D-82	Unified Structural Analysis or Damped Forced Response Computer Program
E_{cal}	Voltage Calibration Signal
F_S, F_C	Sine or Cosine Components of the Exciting Loads, lb, in.-lb
G	g-Loading (Acceleration)
GEARO (R-33)	Gear Mesh Excitation Computer Program
$[K]$	Stiffness Matrix of Structure
P	Acoustic Power, watts
$[M]$	Mass Matrix
M_P	Contact Ratio
R_{cal}	Resistance Calibration
r	Resultant Vibratory Amplitude, in., rad
SPL	Sound Pressure Level
t	Time, sec
TORRP (R-32)	Torsional Response Computer Program
W	Displacement Amplitude, cm
X	Displacement (in.) or Rotation (rad)
X_S, X_C	Sine or Cosine Components of the Displacement (or Rotation) of the Mode of One Structural Element, in., rad
α	Energy Conversion Factor
β	Environment Factor
Δ	Increment of Change
ω	Frequency, Hz
Ω	Frequency, rad/sec